RES | THE SCHOOL *for* RENEWABLE ENERGY SCIENCE

Corrosion in the Kalina cycle

An investigation into corrosion problems at the Kalina cycle geothermal power plant in Húsavík, Iceland

Peter Whittaker

UNIVERSITY OF ICELAND

University of Akureyri

CORROSION IN THE KALINA CYCLE

An investigation into corrosion problems at the Kalina cycle geothermal power plant in Húsavík, Iceland

Peter Whittaker

A 30 credit units Master´s thesis

Supervisors:
Ásbjörn Einarsson
Gestur Bardarson
Sigurpáll Asgeirsson

A Master's thesis done at
RES │ the School for Renewable Energy Science
in affiliation with
University of Iceland &
the University of Akureyri

Akureyri, February 2009

Corrosion in the Kalina cycle

An investigation into corrosion problems at the Kalina cycle geothermal power plant in Húsavík, Iceland

A 30 credit units Master's thesis

RES │ the School for Renewable Energy Science
Solborg at Nordurslod
IS600 Akureyri, Iceland
telephone: + 354 464 0100
www.res.is

Printed in 14/05/2009
at Stell Printing in Akureyri, Iceland

ABSTRACT

An overview of the utilization of geothermal energy in Húsavík Iceland is given. Corrosion is discussed in a theoretical manner, with references to the literature for examples of different mechanisms of corrosion. Samples taken from the Húsavík power plant were analyzed by SEM and X-ray EDS, the theory behind this method is discussed and the results are given. Ultimately the investigation into why there were corrosion problems was inconclusive but instructive. Hypotheses discussed in the conclusion, with ways to further investigate them, include: dissolution of micro-constituents in the ammonia environment, galvanic corrosion, stray current corrosion and erosion corrosion. Mild steel and aluminum seem to be inappropriate materials for Kalina cycle systems but several stainless steels (304, 316, nitronic 60 and duplex) as well as 6Al-4V titanium do not appear to suffer from corrosion.

AKNOWLEDGEMENTS

Gestur Bardarson at Exorka for his negotiations with Húsavík on behalf of the author.

Siguráll Asgeirsson at Exorka for helping to collect samples from the power plant and answering many questions about plant operations and the history of corrosion problems at the power plant in Húsavík.

Ásbjörn Einarsson for helping to make sense of the results and for his feedback on the thesis.

Birgir Johannesson at Nýsköpunarmiðstöð Íslands for operating the SEM and offering his advice and expertise in interpreting the results.

Thorstænn I. Sigfússon director of Nýsköpunarmiðstöð Íslands for subsidizing the SEM analysis.

Axel Björnsson and Hrefna Kristmannsdóttir for taking an interest and for helping to coordinate with the people listed above.

PREFACE

Kalina cycle systems offer a way to extract heat from low temperature sources for the production of electricity at higher efficiencies than Rankine cycles. They use a working fluid of ammonia and water, benefiting from the property of mixtures of boiling over a temperature range at constant pressure, to achieve better temperature matching in the boiler between the working fluid and heat source. This increases the utilization efficiency of the process. Furthermore, because the fluid passing through the turbine is mostly ammonia a small turbine cross sectional area is needed and the use of a smaller turbine can result in lower capital costs than for a similarly sized power plant running an organic Rankine cycle.

Very few Kalina cycle power plants have ever been built. The first built for the utilization of low temperature geothermal waters, opened in Húsavík, Iceland in the year 2000. From the start it was bedeviled by problems, many of them associated with corrosion of the turbine and nozzle vanes which caused the plant to shut down repeatedly and to operate at significantly lower efficiency and lower power output than was promised by the design. Ultimately the original turbine was replaced in 2004 and corrosion of the turbine ceased to be a problem. However the second turbine failed catastrophically in January of 2008 – the cause of the failure remains unexplained. From January 2008 until the present time, the Húsavík power plant has been out of operation and the future of the power plant is unclear.

Ultimately this thesis is an attempt to understand, at least partly, the early problems of the Kalina cycle power plant in Húsavík so that in the future the benefits of Kalina cycle power plants can be realized without the difficulties associated with the plant in Húsavík.

TABLE OF CONTENTS

LIST OF FIGURES

LIST OF TABLES

1 PURPOSE

A study of corrosion in and materials selection, for the Kalina cycle. The goal of this thesis is to discuss the corrosion problems that were present at the Húsavík power plant during its first four years of operation (June 2000 to August 2004), to determine possible causes for the corrosion and to suggest ways in which corrosion can be minimized in the design, construction and operation of Kalina cycle power plants.

Materials selection will be discussed, including: materials that are known from the literature to be incompatible with ammonia, materials that were used in the original (2000 to 2004) turbine in Húsavík that proved to be susceptible to corrosion and erosion, materials used in the later (2004 to 2008) turbine that did not show signs of corrosion or erosion. On the basis of the experience of the plant at Húsavík some materials will be recommended for use in future Kalina cycle power plants.

2 BACKGROUND

2.1 What is Kalina?

The Kalina cycle is a closed cycle for electrical generation similar to the Rankine cycle. The difference between Kalina and Rankine cycles is in the working fluid: Rankine cycles use a single species, pure fluid while Kalina uses a mixture of ammonia and water (Mlcak, 1996).

Many different Kalina cycle systems have been designed to produce electric power from a variety of heat sources. These sources include waste heat from industrial processes, heat from the gasification and combustion of municipal waste, bottoming cycles for gas and diesel engines as well as geothermal fluids.

Kalina cycle systems are designed to use lower temperature heat sources (<200 °C). At lower temperatures it can be difficult to extract useful work from the heat source and high efficiency systems are necessary. A typifying factor of all Kalina cycle systems is the use of heat exchanger network theory to recapture as much heat as possible from the turbine exhaust in order to preheat the working fluid prior to entry into the boiler.

2.2 Exergy

The motivation for a mixed working fluid is to obtain a closer temperature match in the boiler between the working fluid and the heat source. A pure fluid at a fixed boiler pressure will boil at a constant temperature. A mixture will begin boiling when the pure component saturation temperature of the more volatile component is reached and continue to boil at increasing temperature until the pure component saturation temperature of the heavier component is reached. This is shown in Figure 1. In between the two temperature extremes (the saturation temperatures of the pure components) the mixture will have different compositions in the vapor and liquid phase, with the more volatile component being enriched in the vapor phase and the heavier component being enriched in the liquid phase (the boiler acts as a single distillation stage).

This “temperature glide” upon boiling behavior is desirable because heat transferred across a finite temperature difference is an irreversible change; it generates entropy and as a result less work can be done with the heat. Minimizing the temperature difference across which heat is transferred reduces the magnitude of the irreversibility and leads to higher utilization efficiency.

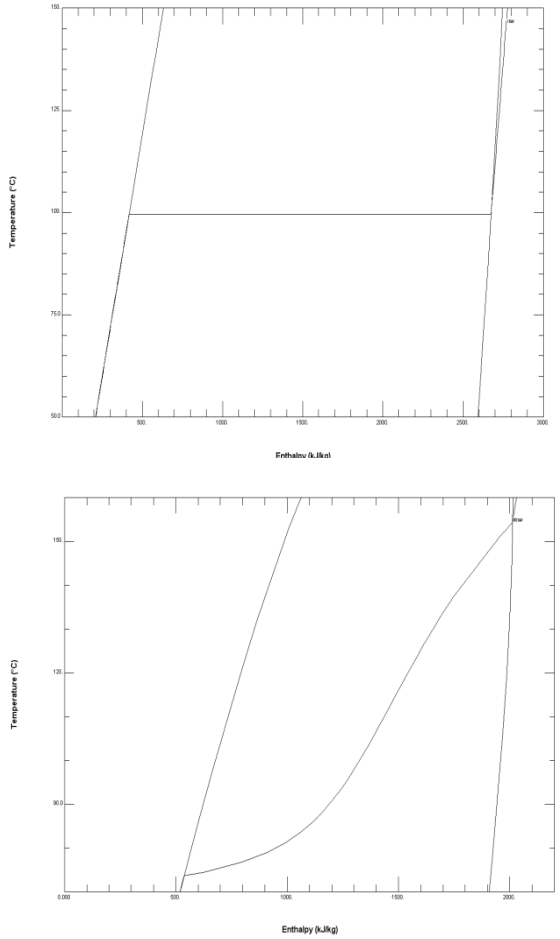

Figure 1. Temperature – Enthalpy diagrams for water at 1 bar pressure on the left and 85% ammonia-water at 30 bar pressure on the right. Water, a pure fluid boils at constant temperature, while an ammonia-water mixture boils over a wide temperature range.

One way to keep track of the availability of a heat source to do work and to find parts of a system that destroy this availability is with a function called exergy. It can be defined in different ways but in this thesis it is defined as follows:

Equation 1

$$e = h - h_0 - T_0(s - s_0)$$

The exergy (e) is equal to the difference between the enthalpy (h) of the heat source being considered and the enthalpy of material of the same composition as the heat source but at a reference state, minus the difference in entropy (s) from the actual state to the reference state multiplied by the absolute temperature (T) of the reference state. The lowercase letters symbolize specific properties (either on a per mole or on a per mass basis - mass is used in this thesis). The reference state, sometimes called the dead state, is one in equilibrium with the local environment; it is a state from which no more work can be obtained.

Kalina cycles have been studied on the basis of exergy analysis and energy utilization diagrams and found to be very well optimized with regards to temperature matching (Wall, Chuang, & Ishida, 1989). The same methods were used in conjunction with ASPEN Plus process simulation software, to show that in a conventional Rankine cycle system, most of

the exergy losses in the system were due to poor temperature matching in the boiler. In the study it was shown that exergy losses in the boiler and other heat exchangers were significantly reduced in Kalina cycle systems (Srinophakun, Laowithayangkul, & Ishida, 2000).

Pertaining to heat transfer, the design of heat exchanger networking was studied and shown to have a significant effect on efficiency. Kalina cycle systems were held up as an example of good heat exchanger network design (Ibrahim, 1996).

2.3 Background of Geothermal Utilization in Húsavík

The use of geothermal heat in northern Iceland has a long history. At the Hveravellir geothermal field vegetable cultivation in the hot soil began in the late 1800's and later it became a center for green house production of vegetables (Georgsson, Sæmundsson, & Hjartarson, 2005).

In the town of Húsavík the first use of geothermal waters came in 1960 when the town swimming pool was first connected with one of the local hot springs. At the same time the idea of using geothermal heat for district heating was considered, and between 1960 and 1965 five wells were drilled for this purpose with temperatures in the range 80 – 110 °C. However the water proved to be too high in salt concentration for direct use.

In 1969 a feasibility report was prepared by Fjarhitun Consulting Engineers concerning district heating possibilities; it concluded that the best option was to use water from Hveravellir, 20 km south-east of Húsavík. The water at Hveravellir flows under artesian pressure and because the town of Húsavík is 100 meters lower in elevation, no pumping would be required.

In 1970 an asbestos reinforced concrete pipeline was laid between Hveravellir and Húsavík. At first only surface waters were collected from the hot springs but in1974 the first well was drilled to a depth of 450 meters. This well was capable of producing 40 liters per second and the temperature at depth was 128 °C. Because of the use of the concrete pipeline, the water could not be taken from the reservoir and delivered to the town under pressure; instead it was flashed at the wellhead and then piped to Húsavík. This resulted in the loss of about 2.2 kilograms per second of steam and a considerable amount of heat being wasted. Additionally water running in the pipeline lost another 15 degrees in temperature through heat losses to the environment, reaching the town at 85 °C. (Hjartarson, 2002)

Increasing demand for hot water during the 1990's lead to the drilling of a new well in 1998, capable of producing 60 liters per second at a temperature of 124 °C. At the same time a renovation of the entire district heating system was undertaken with plans to increase the utilization of the geothermal energy through a cascaded approach to usage. This included installing a new, insulated DN400 steel pipeline to carry the geothermal waters from Hveravellir to Húsavík under pressure and the construction of a geothermal power plant on outskirts of town.

The town received three bids for binary cycle power plants: two for conventional organic Rankine cycles (ORC) assumed a power production of 1.5 MW net and the Kalina cycle system promised 2 MW net. Because a Kalina cycle had only been used to operate a few demonstration projects at that time, the Icelandic engineering company VGK was asked to evaluate the proposals and after their review, it was decided to buy the Kalina power plant. The total cost of the renovation of the district heating system and building the power plant was about 12 million EUR, of which 663 thousand was granted to the project through the fourth framework program of the European Union. About two-thirds of the total cost was spent on the pipeline and district heating and one-third on the power plant.

Water enters the pipeline form Hveravellir at 124 °C, reaches the power plant at 121 °C and is cooled to 80 °C in transferring heat to the working fluid of the power plant. That 80 °C water is then used for district heating and industrial uses such as the drying of wood and fish. At still lower temperatures water can be used to supply hot tap water and to heat the town pool. The water used to cool the power plant is warmed to about 22 °C and can be used for fish farming. This integrated use of water at differing temperatures is referred to as a cascaded system and is shown in Figure 2 (Hjartarson, Maack, & Jóhannesson, Húsavík Energy Multiple use of geothermal energy, 2003).

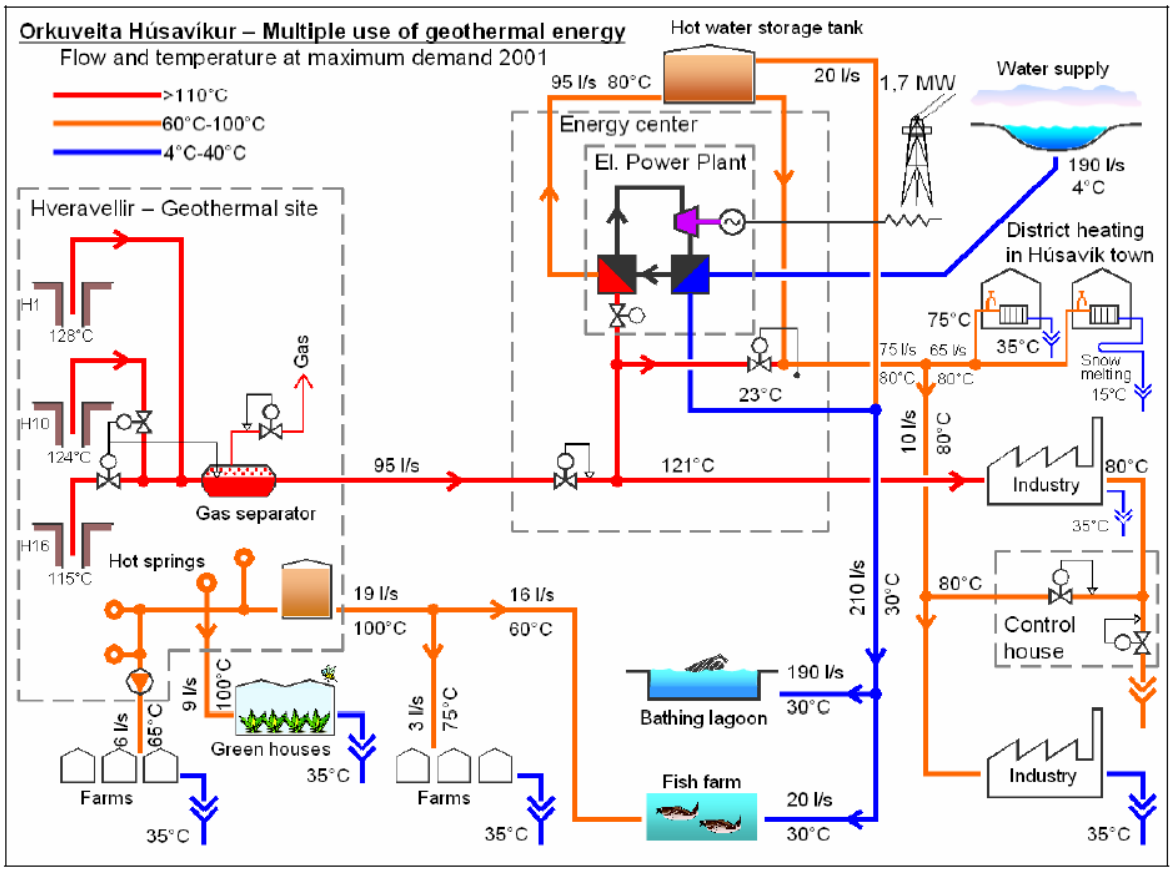

Figure 2. A diagram showing the cascaded use of hot geothermal waters by the town of Húsavík. From the paper Húsavík Energy Multiple use of geothermal energy by Hjartarson et al.2003.

2.4 Walkthrough of the Kalina Power Plant

The layout of the Húsavík plant is given in Figure 3. Hot geofluid enters the boiler at 121 °C and transfers heat to the working fluid. The geofluid then exits the power plant at 80 °C for use by industry and district heating. The ammonia – water working fluid is raised to a temperature of 116-118 °C at a pressure of about 30 bar.

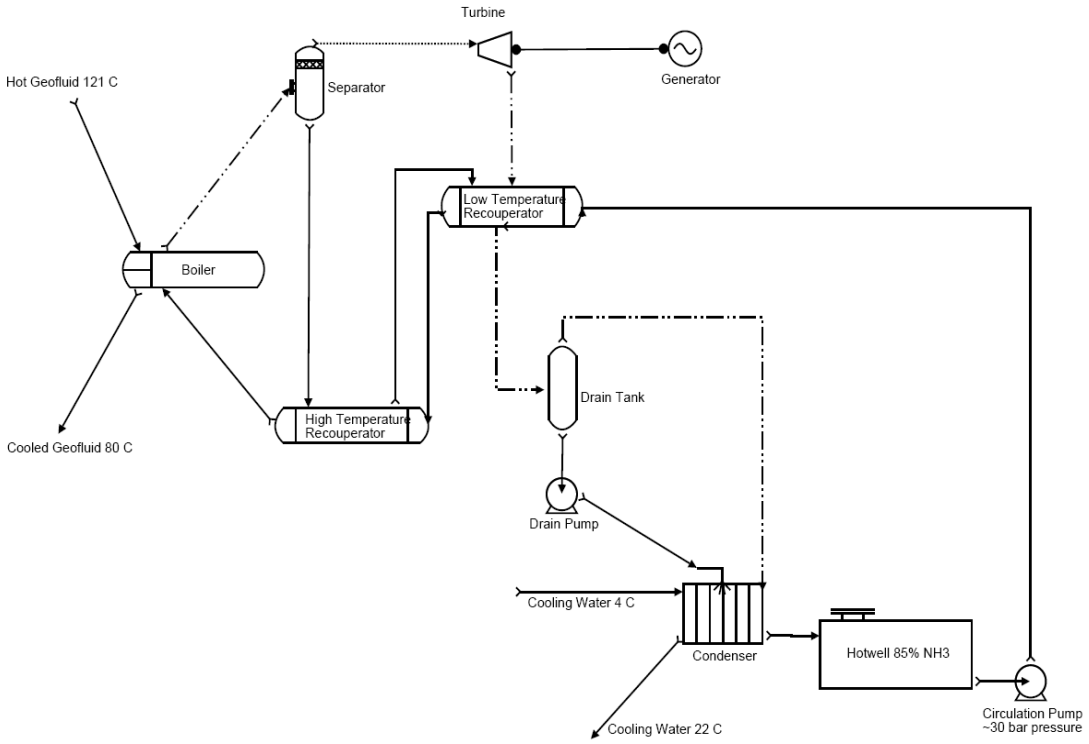

Figure 3. Schematic of the Kalina cycle used in the Húsavík power plant.

As can be seen from the phase diagram (Figure 4), at this temperature and pressure two phases exist. The two phase fluid goes into the separator, where the denser liquid leaves through the bottom, while the less dense vapor leaves though the top. The vapor phase, which is over 96% ammonia and 77 % of the total mass flow, enters the turbine while the hot liquid goes to the high temperature recuperator. Both streams reunite and partially mix in the low temperature recuperator. From there they flow to the drainage tank where they separate again. The wet vapor flows into the plate and frame condenser unit, where it is sprayed with the drainage tank bottoms. Spraying promotes good contacting between the liquid and vapor phases which is important because in addition to condensing, some of the vapor can also absorb (dissolve) into the liquid phase which allows the condenser to operate at slightly below the condensation pressure of ammonia at the outlet temperature. The cooling water enters at 4-5 °C and exits at 22-25 °C depending on mass flow rate. The warmed cooling water can then be used for fish farming and the excess is discharged to a bathing lagoon. The working fluid flows from the condenser to a holding tank (hotwell) before being recirculated at 30 bar pressure, being warmed first in the low temperature recuperator and then the high temperature recuperator and finally returning to the boiler, completing the cycle.

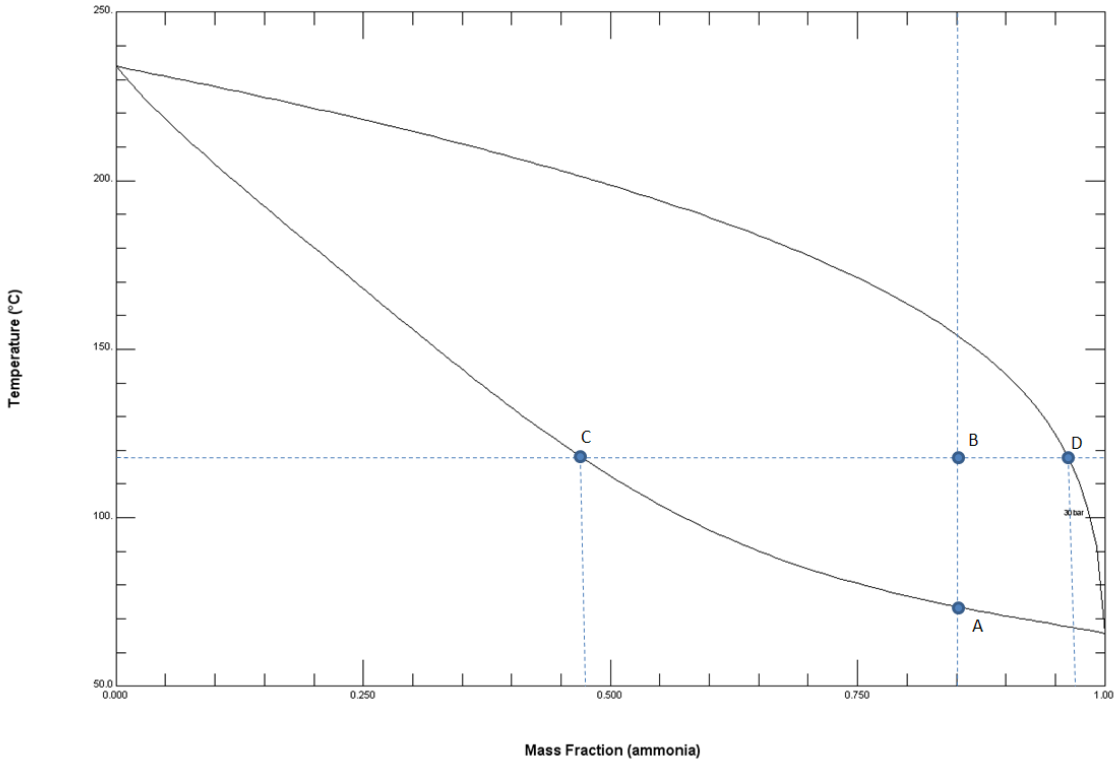

Figure 4. Phase diagram for 85% ammonia-water. The working fluid starts to boil at point A and overall composition remains constant along segment AB, but at 118 °C the vapor phase (point D) has a composition of more than 96% ammonia while the liquid phase (point C) is 47% ammonia. The mass fraction of the vapor is given by the lever rule: BC/CD = 77% vapor.

2.5 Operational History of the Húsavík Geothermal Power Plant operating on the Kalina cycle

The Húsavík power plant was commissioned in June of 2000. It was purchased and is owned by Húsavík Energy (Orkuveita Húsavíkur); the plant seller was EXERGY. The plant was designed to produce 2 MW_e net but never achieved more than 1760 kW_e. This was attributed to higher back pressure in the condenser than was anticipated in the design. The liquid-vapor feed separator did not function correctly and the flow into the turbine had lower quality than the design specification. The turbine wheel, vanes, shroud rings and housing were made of Cr-Mo steel alloys.

Corrosion/erosion problems were evident almost from the start of operation. At that time liquid entrained in the vapor stream was considered the most likely cause. The flow rate in to the turbine was reduced to limit wear and the separator was redesigned. During this time the plant operated at 1400 kW_e. Early in 2001, at the same time the flow rate was being reduced, materials testing began. Some of the wear on the turbine did not seem consistent with erosion due to liquid entrainment and the goal was to determine if other materials might be better suited to the ammonia/water environment. In these tests 316 stainless steel was found to perform best among the materials tested.

In October of 2001, the separator was replaced and in November of that year, the turbine reinstalled having been refurbished by the manufacturer (KK & K). The new separator was found to produce a vapor stream that met with the quality specifications of the turbine. The turbine was next inspected in March 2002 and it was apparent that changing the separator had not improved the corrosion/erosion problems.

By September of 2002 sections of the turbine shroud ring had begun to break off and fall into the turbine because of the corrosion. Also at this time the second stage nozzles were seen to be significantly damaged by both corrosion and erosion. The turbine was sent back to the manufacturer for repair.

One of the causes of erosion in the turbine seemed to be corrosion products forming between the turbine housing and the first stage nozzle vanes. These corrosion products would then break off and ricochet between the turbine, nozzles and shroud ring causing erosion damage. To remedy this problem a ring made of 316 stainless steel was installed between the first stage nozzles and the turbine housing. This material was chosen based on the earlier materials tests.

In November of 2002 the turbine was reassembled. KK & K had not made any repairs to the second stage nozzles. At this time, due to the extensive wear on the turbine and nozzles, the Húsavík power plant could produce only 1200 kW_e.

In April of 2003 the shroud ring for the second stage of the turbine fell into the turbine wheel, necessitating significant repairs to both the nozzles and turbine blades. Turbine manufacturer KK & K declined to do the repair work and Húsavík Energy did the work themselves, welding and shaping 316 stainless steel to the nozzles and turbine wheel. These repairs were quite successful, allowing the plant to produce 1670 kW_e net.

In August 2004 a GE-Rotoflow (GE-R) turbine was installed, replacing the KK & K turbine. The design of the GE-R turbine was different from the old KK & K turbine. The KK & K had been a 2 stage turbine made of Cr-MO steel alloy; the GE-R was a single stage turbo expander with a 6Al-4V titanium turbine wheel, nitronic 60 nozzle vanes and a 304 stainless steel housing. The GE-R turbine had no problems with corrosion between August 2004 and January 2008, however the nozzle vanes were damaged by impacting particles of corrosion products from elsewhere in the plant.

In January 2008 the GE-R turbine suffered a catastrophic failure. A part of the turbine wheel itself broke off and significantly damaged the turbine blades, shaft, nozzle vanes and housing. There were no signs of corrosion on the turbine and this failure is still unexplained. (Ásgeirsson, 2008)

2.6 Environment of the corrosion

The formation of black magnetite scaling (confirmed by XRD) is present on all the low alloy steel in the plant with the exception of the KK & K turbine, turbine housing and the first meter or two of the turbine exhaust pipe. In the turbine section material loss was significant. The appearance of the turbine and other affected surfaces is described below.

In the pipe leading from the separator to the turbine scaling is present. The temperature in this pipe was 115-118 °C and the pressure was ~30 bar. Coming from the separator the working fluid was almost totally vapor. The composition of the working fluid found from

the phase diagram (Figure 4) was 96% ammonia vapor in equilibrium with 47% ammonia by weight in the first drops of condensate formed.

In the turbine exhaust pipe, material loss and no scaling are present for the first one to two meters, after which magnetite scaling resumes (the exhaust pipe was unavailable for inspection and lengths are an estimate based on personal communications with a plant manager (Ásgeirsson, 2008)). The temperature was ~55 °C and the pressure was ~6 bar. Coming out of the turbine the working fluid was about 6-7% liquid. The liquid composition would have been about 43% ammonia while the vapor would have been 99% ammonia.

In the turbine itself the working fluid was changing between these two equilibria.

The pH of the condensate has not been measured. Some data could be found for the relationship between ammonia concentration in water and pH at 25 °C (Agency for toxic substance and disease registry)

Table 1. Relationship between concentration of NH_3 in water and pH

Concentration (M)	pH
0.01	10.6
0.1	11.1
1	11.6

The data shows a logarithmic relationship between concentration and pH. A logarithmic equation fitting this data is

Equation 2

$$pH = 0.5 * \log_{10} C_{NH_3} + 11.6$$

Where the concentration is in molarity. In the environment of the turbine and exhaust the ammonia mass fraction is about 45%, which results in a molarity of about 20 M. Using the above equation, this computes to a pH of about 12.3 at 25 °C. It is known that dissociation increases with temperature so the pH will be slightly higher than this in the operational environment.

One of the puzzling details is what, if anything, could have been changing in the turbine exhaust to create a region in which there was material loss and no scaling and a region of scaling and no material loss.

2.7 Previous Investigations of the Corrosion

In December of 2002 electrical potentials and currents within the generator, turbine and gear set were measured. At the same time magnetic fields around the turbine were measured. Eight points corresponding to magnetic south poles were identified but no corresponding north poles were found. The conclusion at that time was that the currents and voltages detected were not related to corrosion/erosion. No conclusions were reached with regard to the magnetic field. (Ögmundsson, 2003)

Siemens made a report on the turbine in July of 2004. The report draws no conclusions but makes several observations among them:

- Insufficient data on materials in this environment
- Increased erosion after the new, better working, separator was installed
- Most valves had leaks
- Turbine erosion is independent of flow velocity – rate is chemically dominated
- Erosion is attributable to erosion/corrosion process

The Siemens report concludes with the observation that switching to metals that form a passive layer might correct the observed corrosion/erosion problem but these materials would be more susceptible to stress crack corrosion. (Siemens, 2004)

2.8 Qualitative Description of the Corrosion at Húsavík

On the KK & K turbine wheel itself, the corrosion – erosion produced a dull grey, powdery appearance. Feeling the surface of the turbine wheel with a finger tip or the tip of a sharp knife, it is like very fine grit sand paper and it seems that the surface is made up of tiny pits and fine nodules. The surface can be scored with an x-acto knife. Scraping the surface with the same sort of knife, corrosion products seem to be absent or present only in a very thin film. Placing a piece of white paper below the turbine to catch scrapings, almost nothing comes off the surface. Luster is restored upon scraping but this seems to have as much or more to do with flattening the surface out than with removing any corrosion products.

The turbine nozzles have a similar surface texture to the turbine wheel and the second stage nozzle vanes have ragged, cracked edges.

The inlet to the turbine housing looks totally different. It is covered by a uniform, matte black layer of corrosion products. It feels smooth to the touch. It cannot be scored or scratched with a knife to an appreciable degree. Scraping with a knife, very little of the black material comes off; what does come off clings to the blade of the knife in a clump and smears across white paper. After being in contact with the paper for several days a yellow stain appears on the paper around the smears of corrosion product.

The retainment ring has both effects present. Parts of the ring are grey and have the texture of the turbine wheel; other areas, particularly areas that were covered and not directly exposed to the flowing working fluid, are covered in the black corrosion products. There are places on the retainment ring that were covered by washers or by a flange that show crevice or filiform corrosion.

The turbine exhaust pipe was not available for inspection but is described by a plant manager as having been affected in the same way as the turbine wheel: uniform, dull grey color, no noticeable build-up of corrosion products, slightly rough texture.

Channeling was not observed in either the turbine housing or the turbine exhaust pipe. Channeling might have been expected if the metal was dissolving in the working fluid condensate.

The turbine wheel was attached to the shaft by a large nickel plated nut. The nickel plating has acquired a golden patina but is smooth. In places it has flaked off of the nut and the underlying region is dull grey.

In April of 2003 a 316 stainless steel shroud ring was installed on the turbine and 316 stainless steel nuts were used to replace older nickel plated nuts on the retainment ring. These have a gold patina but otherwise show no signs of corrosion.

The GE-R turbine wheel was unavailable for inspection.

The nitronic 60 nozzle vanes are brown and smooth on the back, dull silver on the front surface that directed the working fluid vapor. The front surface has been marred by many small impacts. The tip is bent and cupped slightly. The sides have a wear pattern consistent with rubbing against the wheel on which the vanes were mounted.

The vane control wheel on which the vanes are mounted is colored brown to black and is smooth. It has wear patterns corresponding to the vanes.

The duplex steel pins that restrict the range of motion of the vanes by riding in a slot of the wheel are lustrous and smooth except on the sides were they have been scraped flat against the sides of the slots in the vane control wheel.

The inside of the 304 stainless steel turbine housing is colored grey with brown-red stains. It has a rough uneven texture but this is probably associated with casting and finishing rather than corrosion or erosion. The brown-red material can be scraped off with a knife; it is only a very thin layer. The underlying metal cannot be scored. The bottom of the turbine housing looks darker and an oily film can be both seen and felt.

3 THEORY OF CORROSION

3.1 Thermodynamics of corrosion

Corrosion is a result of thermodynamics; most metals have a lower free energy as oxides than as pure metals at standard temperature and pressure. Corrosion is the oxidation of a metal and often has negative effects on the mechanical properties of the metal affected. From a chemical standpoint oxidation occurs when the metal looses electrons in a reaction (often but not necessarily a reaction with oxygen). Charge neutrality dictates that if electrons are being lost in one reaction they must be consumed in another coupled reaction. A material is reduced by participating in a reaction in which it gains electrons. Because oxidation and reduction are coupled they are often described as half reactions, with one producing electrons and the other consuming them.

Electrical work (w) happens when charged particles are moved across an electrical potential. Electrical work is defined as being equal to the amount of electrical charge (Q measured in coulombs) moved multiplied by the potential (E measured in volts) through which it is moved. In electrochemistry it is convenient for the unit of charge to be equal to the charge on an electron (e^-) and to count the number of charges being moved in moles (z). The Faraday constant is used to convert charge form moles of electrons to coulombs of charge (F = 96,485 C/mol). Therefore

Equation 3

$$w = -zFE$$

This is analogous to classical mechanics in which work can be described by moving mass (m) in a gravitational potential field (g)

Equation 4

$$w = \Delta PE = mg\Delta h$$

In chemical thermodynamics the driving force for a reaction is the change in Gibbs free energy (G). This is equal to the electrical work done by an electrochemical cell

Equation 5

$$\Delta G = -zFE = w$$

Gibbs free energy is a function of temperature and pressure (or concentration) and changes in the function are calculated relative to reference state. For standard conditions (273.15 K and 1 atmosphere or 1 mole per liter concentration) both Gibbs energy (ΔG°) and chemical potential (E°) are tabulated for many reactions

Equation 6

$$\Delta G^\circ = -zFE^\circ$$

The Nernst equation relates the actual change in Gibbs free energy for a reaction to the standard state value by a correction factor

Equation 7

$$\Delta G = \Delta G^\circ + RT \ln Q$$

Where R is the universal gas constant (8.314 J/mol-K), T is the actual temperature (in K) and Q comes from the balanced reaction equation. If

Equation 8

$$aA + bB \leftrightarrow mM + nN$$

Then

Equation 9

$$Q = \frac{\alpha_M^m * \alpha_N^n}{\alpha_A^a * \alpha_B^b}$$

Where lower case letters symbolize the stoichiometric coefficients of the reaction, capitol letters represent the species involved and α is the activity of the subscripted species. Often a good approximation for the activity is given by the partial pressure or concentration of a species. Pure solids, in equilibrium with liquids or gases, always have an activity of one.

Equation 5 and Equation 6 can be combined with the Nernst equation (Equation 7) to give a form that is useful for electrochemical calculations

Equation 10

$$E = E^\circ - \frac{RT}{zF} \ln Q$$

The chemical potential of a cell can be calculated from the potential of the two half cells against a reference electrode.

Equation 11

$$E^\circ_{cell} = E^\circ_{cathode} - E^\circ_{anode}$$

Many different reference electrodes exist, including the silver chloride electrode ($AgCl + e^- = Ag + Cl^-$), the calomel electrode ($Hg_2Cl_2 + 2e^- = 2\ Hg + 2\ Cl^-$) and the copper sulfate electrode ($Cu^{+2} + 2\ e^- = Cu$ in sulfate solution). Most tabulated values, however, are in reference to the standard hydrogen electrode, or SHE ($2\ H^+ + 2\ e^- = H_2$ on a platinum surface). In practice it does not matter which reference electrode is used, so long as the same reference is used to measure both half cells.

3.2 Corrosion kinetics

Thermodynamics dictates which direction a reaction will go in but not how fast. Kinetics is concerned with the rate of the reaction and therefore the current (rate of charge transfer) in the corrosion cell.

The rate of the reaction can be affected in three places: on the surface of the metal, in the "double layer" of the electrolyte and in the transfer of charge between the anode and cathode.

3.2.1 The activation over potential

On the surface of a metal there exists an equilibrium between oxidation and reduction of the metal and its ions

Equation 12

$$M \leftrightarrow M^{z+} + ze^{-}$$

The current generated by the flow of electrons at the metal surface is called the exchange current (i_0) or if normalized by dividing by the surface area, the exchange current density (j_0). If the rate of the forward reaction is equal to the rate of the reverse reaction, then the reaction is completely reversible and the magnitude of the exchange current density is zero. If the rate of the forward reaction is greater than the rate of the reverse reaction then the surface is acting as an anode and the metal is oxidized; conversely if the rate of the reverse reaction is predominant then the surface is cathodic and the metal ions are being reduced. In either case electrons are moving, either out from or to the metal surface and j_0 is no longer zero.

Returning briefly to thermodynamics, one way to picture the reaction described by Equation 12 is to imagine the energy needed to accomplish the change, either to separate the electrons from the metal ions or to reform the metal from the electrons and ions. The energy required for this is called the activation energy; a simple drawing of this is shown in (Figure 5). In the reversible reaction, the energy of the metal ions plus electrons is equal to the energy of the metal surface and the activation energy (ΔG^{*}) is equal in either direction. In order for the surface to become anodic, the energy of the products must be less than the energy of the reactant and the activation energy of the forward reaction ($\Delta G^{\dagger}$) must be less than the activation energy of the reverse reaction ($\Delta G^{\ddagger}$). The opposite is true when the surface is cathodic.

It was shown above that energy could be related to electrical potential (Equation 5). The activation over potential (η_{act}) is the energy needed to move the reaction at the surface (Equation 12) away from the reversible equilibrium in either the anodic or cathodic direction. It is possible that for a given current density the activation over potential at the cathode (η_{cath}) will be different from the anode (η_{anode}) but it is difficult to measure the two activations over potentials separately, and reasonable results can be obtained by assuming that a single over potential applies at both surfaces.

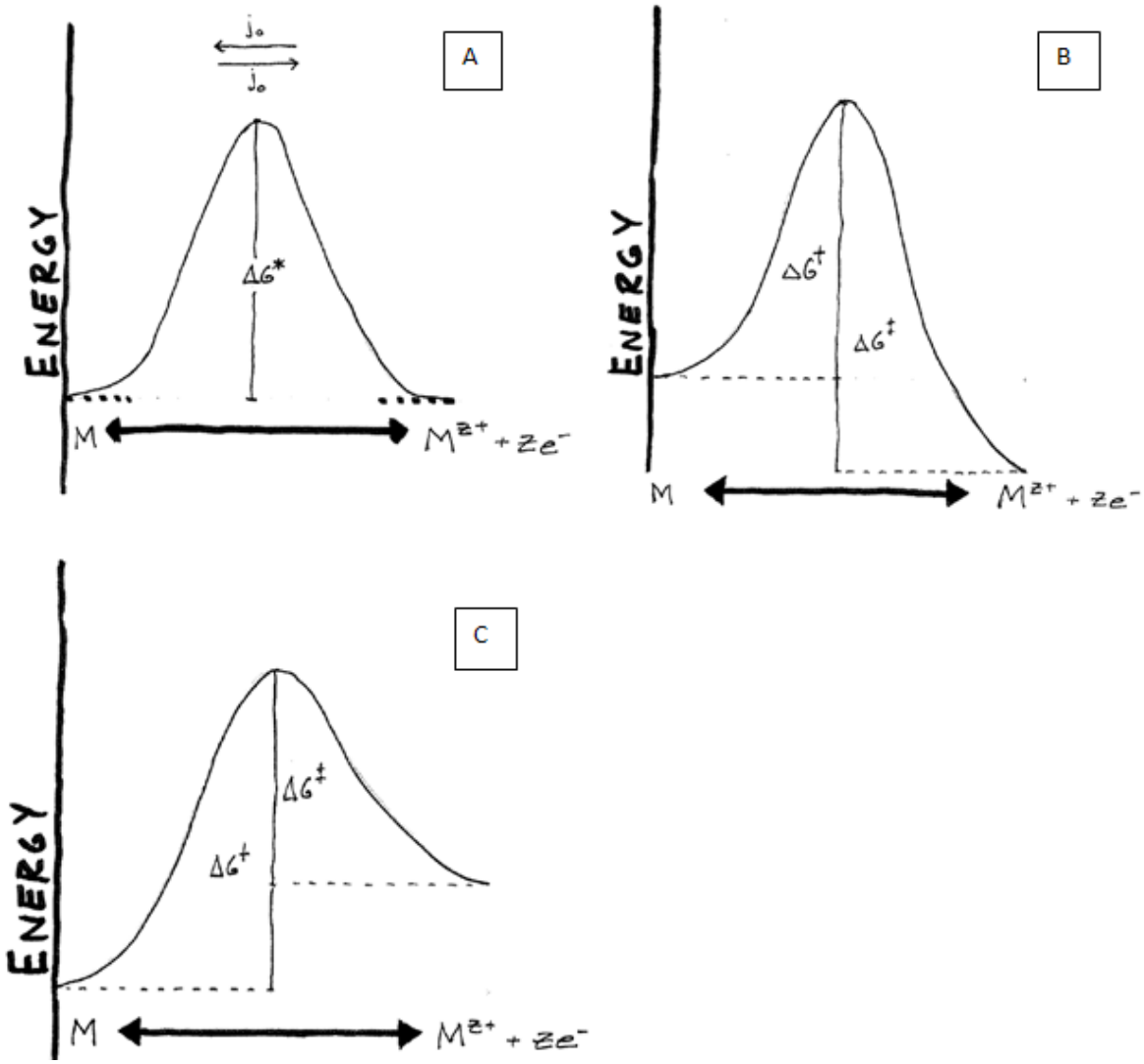

Figure 5. Activation energy curve cartoons. In A the reversible equilibrium is shown, the activation energy barrier is the same for both oxidation and reduction reactions. In B the anodic reaction is favored by having a lower energy barrier than the cathodic reaction. In C the cathodic reaction is favored by having a lower energy barrier than the anodic reaction.

The net current density can be related to the activation over potential and the exchange current density by the Butler-Volmer equation

Equation 13

$$j_{net} = |j_{anode}| - |j_{cath}| = j_0 \left\{ exp\left[\frac{\beta z F \eta_{act}}{RT}\right] - exp\left[\frac{-(1-\beta) z F \eta_{act}}{RT}\right] \right\}$$

Here β is a symmetry factor related to the shape of the activation energy curve (Figure 5). It can take values from 0 to 1 but it is also difficult to measure and a value of 0.5 is usually appropriate.

For near reversible conditions (small η_{act}) both the anodic and cathodic current densities are of similar magnitude and a plot of current against activation over potential produces a curve. As the over potential increase in magnitude either the anodic or cathodic current

will become negligibly small and one of the two exponentials can be omitted from Equation 13.

When cathodic current is negligible

Equation 14

$$j = |j_{anode}| = j_0 \left\{ exp \left[\frac{-\beta z F \eta_{act}}{RT} \right] \right\}$$

And when anodic current is negligible

Equation 15

$$j = |j_{cath}| = j_0 \left\{ exp \left[\frac{(1-\beta) z F \eta_{act}}{RT} \right] \right\}$$

Taking logarithms

Equation 16

$$\ln j = \ln j_0 + \left[\frac{-\beta z F \eta_{act}}{RT} \right]$$

For the anode and

Equation 17

$$\ln j = \ln j_0 + \left[\frac{1 - \beta z F \eta_{act}}{RT} \right]$$

For the cathode. Solving algebraically for the activation over potential at the anode

Equation 18

$$\eta_{act} = \left[\frac{RT}{\beta z F} \right] \ln j + \left[\frac{-RT}{\beta z F} \right] \ln j_0$$

And for the cathode

Equation 19

$$\eta_{act} = \left[\frac{-RT}{(1-\beta) z F} \right] \ln j + \left[\frac{RT}{(1-\beta) z F} \right] \ln j_0$$

These are one form of the Tafel equations. They take the linear form

Equation 20

$$\eta = a + b \ln j_0$$

Or

Equation 21

$$\eta = a + b \log j_0$$

Where a and b are both constants; b is called the Tafel slope.

In a real corrosion cell the reaction(s) of interest will generally not be oxidation of the metal at the anode and reduction of the same metal at the cathode. While the metal will still be oxidized at the anode, generally another species present in the electrolyte will be reduced at the cathode. The actual potential of the surface will then be a mix of the

potentials for both reactions and the current density will depend on the intersection of lines given by the Tafel equations. An Evans diagram shows this mixed potential phenomenon (Figure 6).

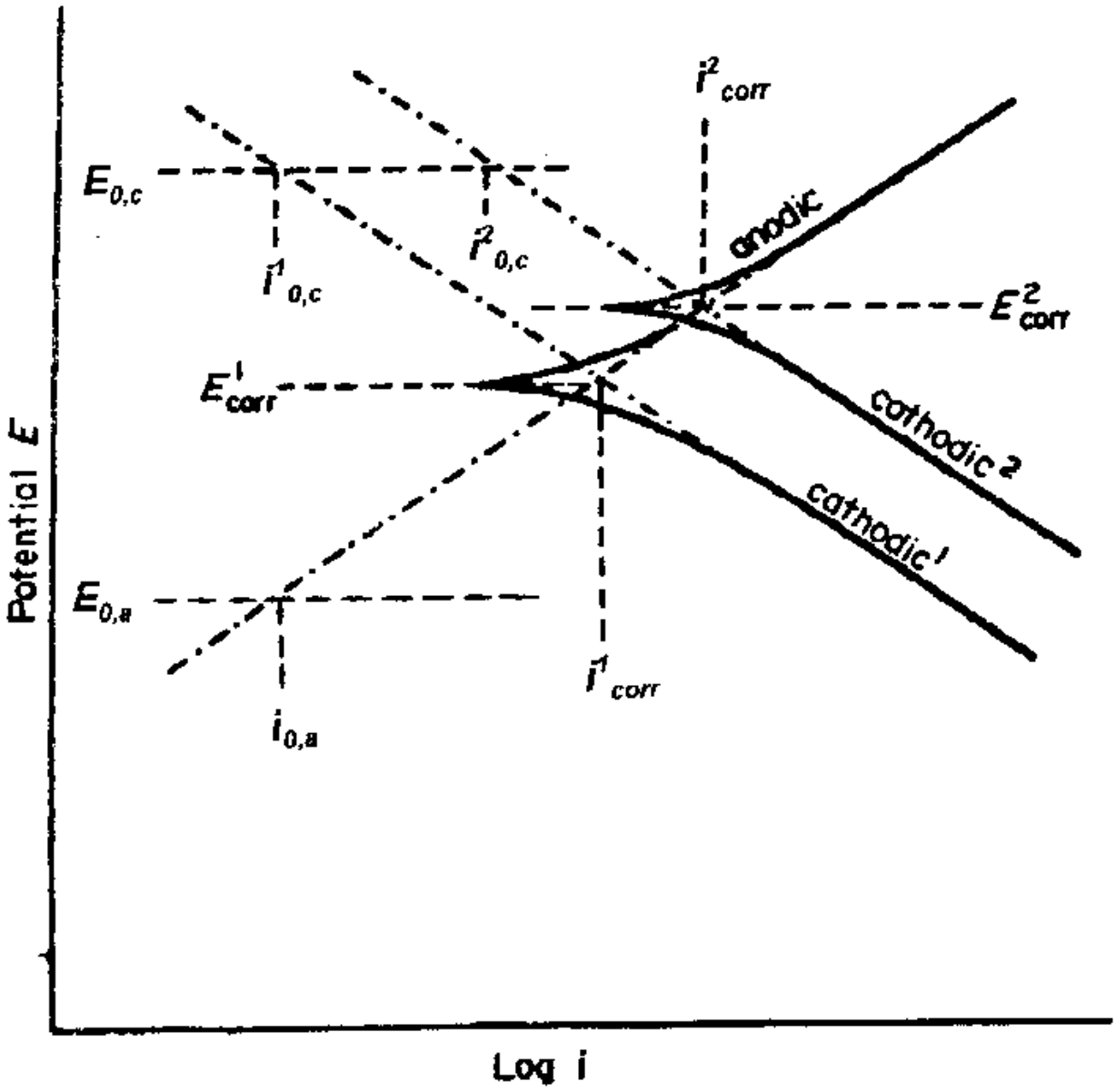

Figure 6. An Evans diagram showing the mixed potential for separate anodic and cathodic reactions. The actual corrosion cell potential and current will occur where the anodic branch of reaction 1 intersects the cathodic branch of reaction 2. (Kruger, 2001)

Things that can affect the activation over potential include:

- Material - some metals are particularly catalytic for the cathodic reaction
- Surface roughness – the over potential is higher on smooth surfaces than on rough ones
- Temperature – higher temperature provides more energy to the reacting species and effectively decreases the activation barrier

3.2.2 The concentration over potential

In addition to the energy required to move the reaction away from the reversible equilibrium (η_{act}) another factor that can affect the rate of a corrosion reaction is the rate of diffusion of metal ions from the anode into the bulk electrolyte and ions to be reduced from the bulk electrolyte to the cathode. Excess metal ions at the surface of the anode would represent a positively charged layer that would inhibit the formation of more cations – however this is not usually observed. More often the diffusion limitation occurs at the cathode, particularly if the species being reduced is either slow to diffuse or exists in the bulk electrolyte only in low concentrations. Both slow diffusion and low concentration can apply when the reduction reaction involves dissolved oxygen. For instance the cathodic reaction

Equation 22

$$O_2 + 2H_2O + 4e^- \leftrightarrow 4OH^-$$

Is rate dependent on oxygen being able to diffuse to the cathode. Diffusion rates can be modeled by Fick's first law

Equation 23

$$J_i = -D_i \frac{dC_i}{dx}$$

Where J_i is the flux of species i, D_i is the diffusivity of species i in the electrolyte solution and the derivative term is the concentration gradient of i between the bulk solution concentration and the surface concentration. The region across which this gradient applied is called the concentration boundary layer and is on the order of a few microns thick for aqueous solutions with the bulk solution in flow. In the limiting case, species i is consumed at the surface as fast as it can diffuse and the concentration gradient goes linearly from zero at the surface to the bulk concentration (C_b) across the boundary layer.

The flux (J in mol/s-cm^2) can be related to the current density (j in amps/cm^2) by the Faraday constant and the charge transfer coefficient.

Equation 24

$$J_i = \frac{j}{nF}$$

Combining Equation 23 with Equation 24 and assuming that the surface concentration for species i is zero gives the equation for the surface concentration limited current density (j_L)

Equation 25

$$j_L = -nFD_i \frac{C_c}{\delta}$$

Where δ is the concentration boundary layer thickness. The over potential needed to overcome concentration limitations is found from

Equation 26

$$\eta_{conc} = \frac{RT}{nF} \ln\left(1 - \frac{j}{j_L}\right)$$

3.2.3 The ohmic over potential

Metals are good electronic conductors and when the anodic site is close to the cathodic site, ionic conduction in the electrolyte is not a source of significant resistance. On the other hand in some forms of corrosion the anode and cathode may not be close together; for instance in galvanic corrosion, in which the potential is created by two different kinds of metal making an electrical connection. In such a case the anode and cathode could be separated by a significant difference and the resistivity of the electrolyte might create a significant over potential with the effect on current density given by Ohms law

$$\frac{V}{l} = j\rho$$

Written in this way, V/l is the electric field between the two electrodes and ρ is the resistivity of the electrolyte.

3.3 Corrosion of different metals and potential –pH diagrams

Potential-pH diagrams (Pourbaix diagrams) show the equilibrium relationships that exist between a metal, its ions in solution and its corrosion products as a function of potential and pH. This shows under what environmental conditions the metal will be stable, when it would be expected to form a passivating film of corrosion products and when corrosion would be expected to proceed unabated because the corrosion products are themselves soluble.

Potential-pH diagrams are shown for iron, aluminum, nickel and titanium in water at 25 °C in the following subsections.

3.3.1 Corrosion of iron

A potential-pH diagram for iron is shown in Figure 7 – low alloy steels will have the same behavior (Ahmed, 2006). It can be seen that in acid solutions at higher potentials the corrosion products are soluble and therefore cannot offer any protection from further corrosion. At neutral to high pH ranges the corrosion products, like magnetite, hematite and iron (II) hydroxide form a passive layer preventing or greatly reducing the rate of corrosion. At high pH and low potential versus SHE iron (II) hydroxide can be reduced to $HFeO_2^-$ which is soluble and offers no protection from further corrosion.

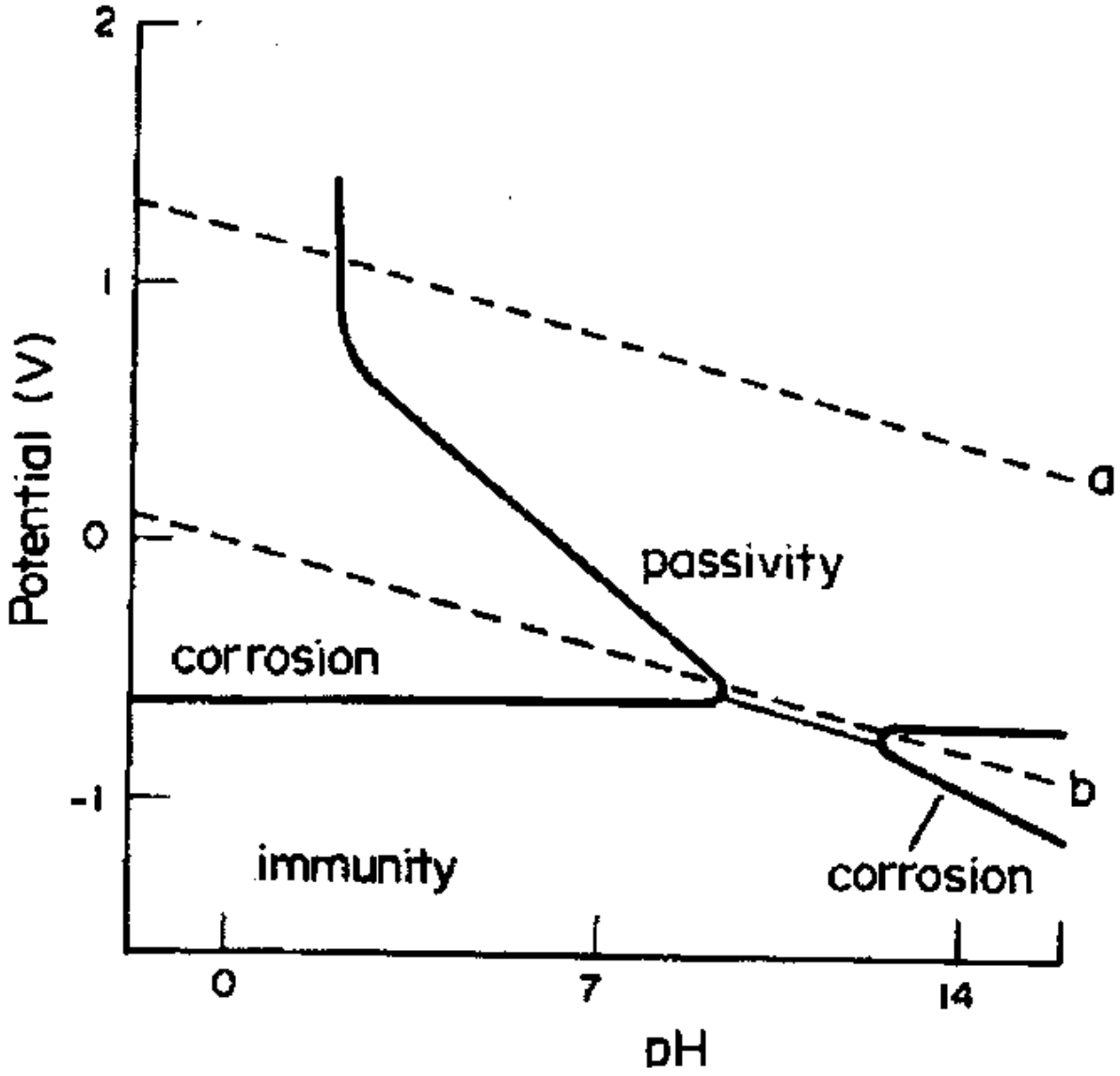

Figure 7. A potential-pH diagram for iron or steel at 25 °C. In acid solutions Fe^{2+} and Fe^{3+} ions form at the anode and dissolve into the electrolyte offering no protection. At high pH $HFeO_2^-$ can form and dissolve into the electrolyte.

In ammonia it is possible to form iron amides but they are only short lived intermediates to the formation of iron (II) hydroxide which is insoluble (Birk, 2001).

3.3.2 Corrosion of aluminum

From the potential-pH diagram of aluminum (Figure 8) it can be seen that at both acidic and basic pHs the corrosion products of aluminum are soluble. This diagram also shows the effect of ionic concentration in solution on solubility. This affect is far greater under basic conditions than under acidic conditions.

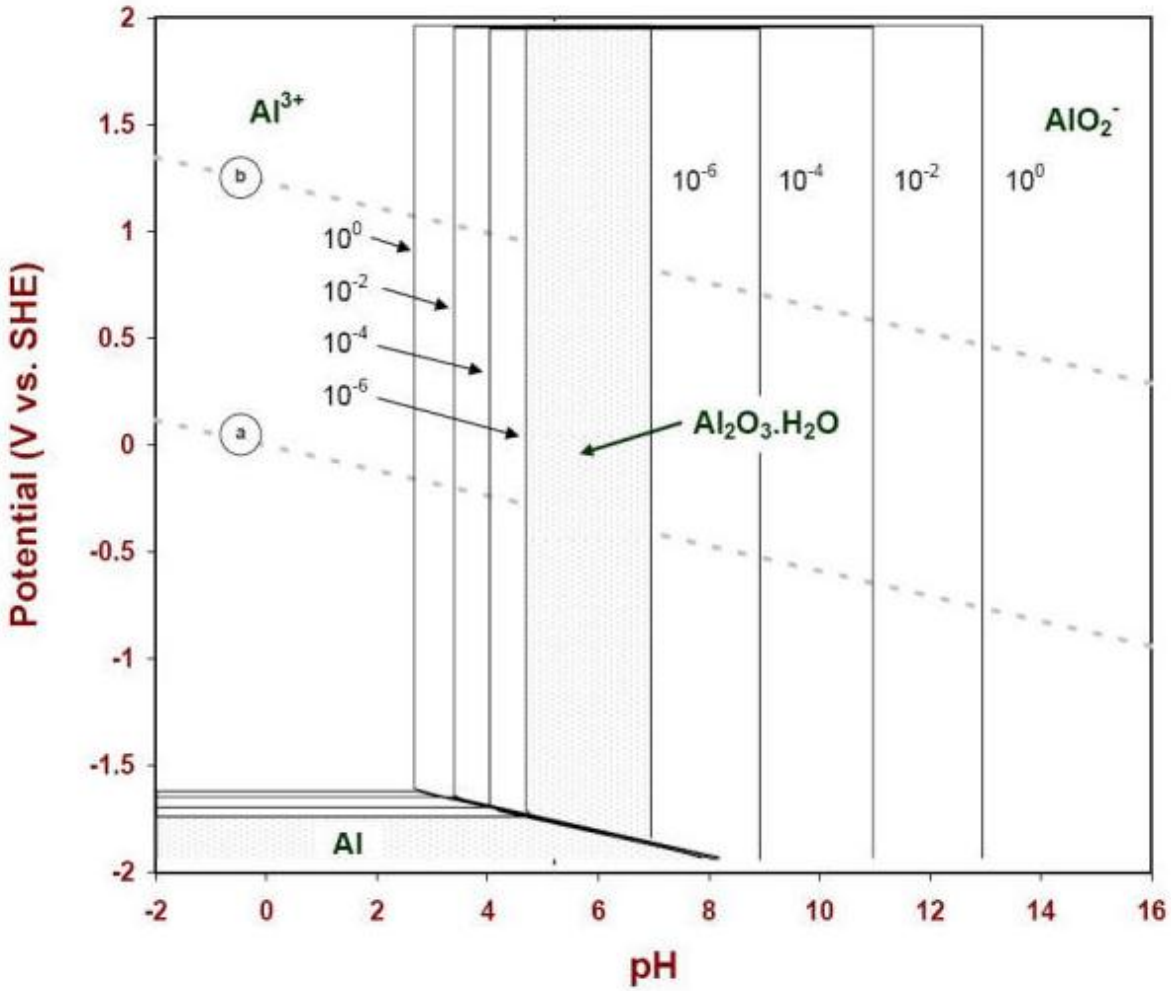

Figure 8. Potential-pH diagram of aluminum showing the affects of concentration of ions in solution on the solubility of the corrosion product. (Roberge, Aluminum E-pH diagram)

As with iron, the formation of amide complexes is possible but short lived. Aluminum in ammonia solution usually forms $Al(OH)_3$ which at high pH can form the soluble product $Al(OH)_4^-$ (Birk, 2001).

3.3.3 Corrosion of nickel

Nickel was not observed to be corroding in the turbine. Nickel was present as a coating plated onto steel nuts. Ordinarily the corrosion potential of nickel is cathodic to that of iron or low alloy steel (Roberge, 2008) and so it is likely that a galvanic couple would have formed with the nickel being cathodically protected. It is found that in ammonia nickel can form the amide ion – hexammine nickel (II) ($Ni(NH_3)_6)^{2+}$) which is stable at high concentrations of ammonia, in equilibrium with solid nickel hydroxide (Birk, 2001). A potential-pH diagram, Figure 9, shows that nickel would be expected to corrode under oxidizing, acidic conditions but ordinarily would form a passive film under basic conditions.

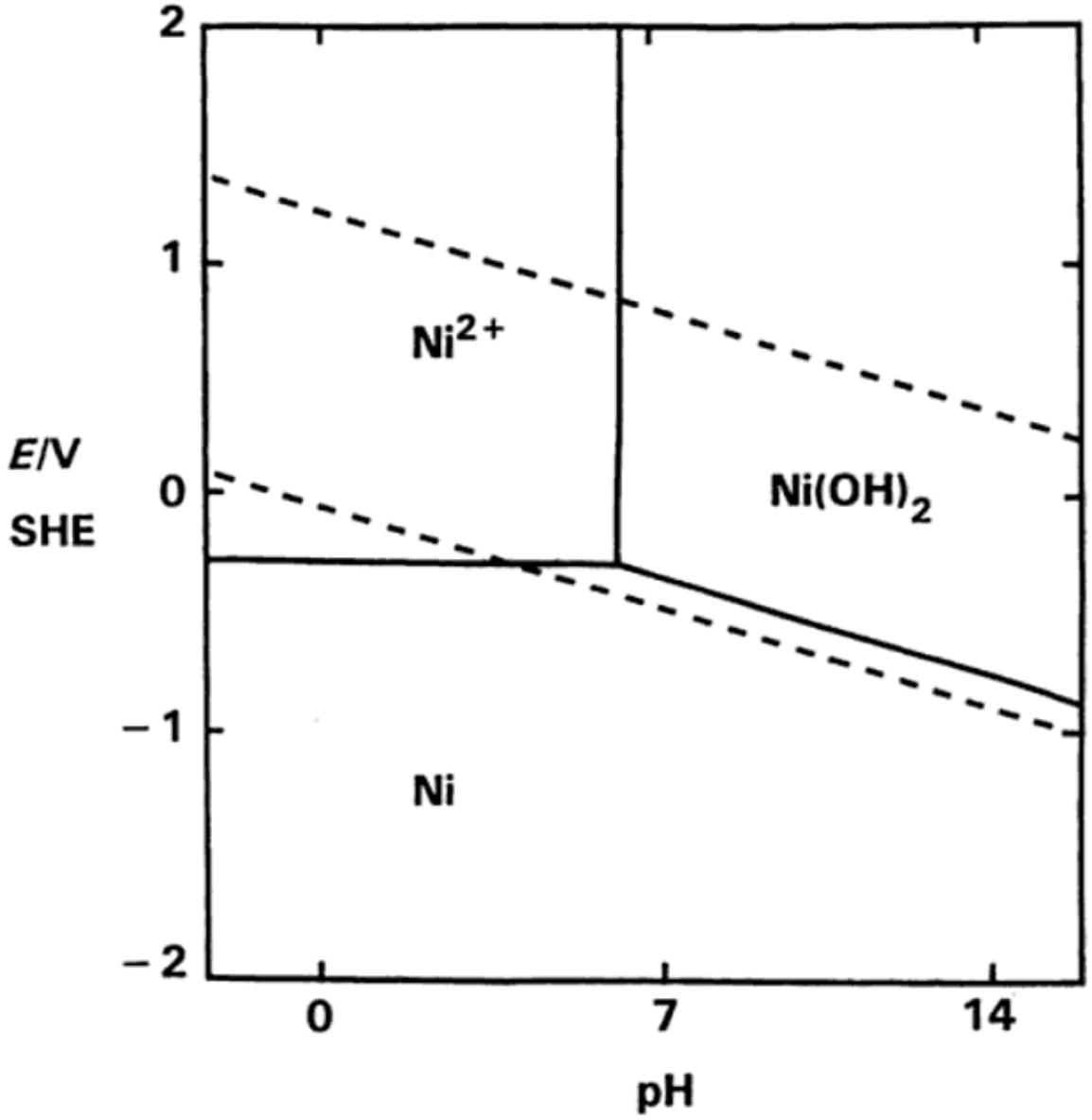

Figure 9. A potential-pH diagram for nickel showing corrosion potential in acidic solutions but not showing the equilibrium between aqueous hexamine nickel (II) and solid nickel hydroxide in ammonia solutions. (Talbot & Talbot, 1998)

3.3.4 Corrosion of titanium

Titanium is usually thought of as being quite stable because it rapidly forms an oxide film under a wide range of conditions. The potential-pH diagram (Figure 10) shows that only under very acidic and oxidizing conditions and in very basic conditions does the protective film of titanium become soluble. Titanium amines are known to form but information about their stability and equilibrium with other corrosion products could not be found.

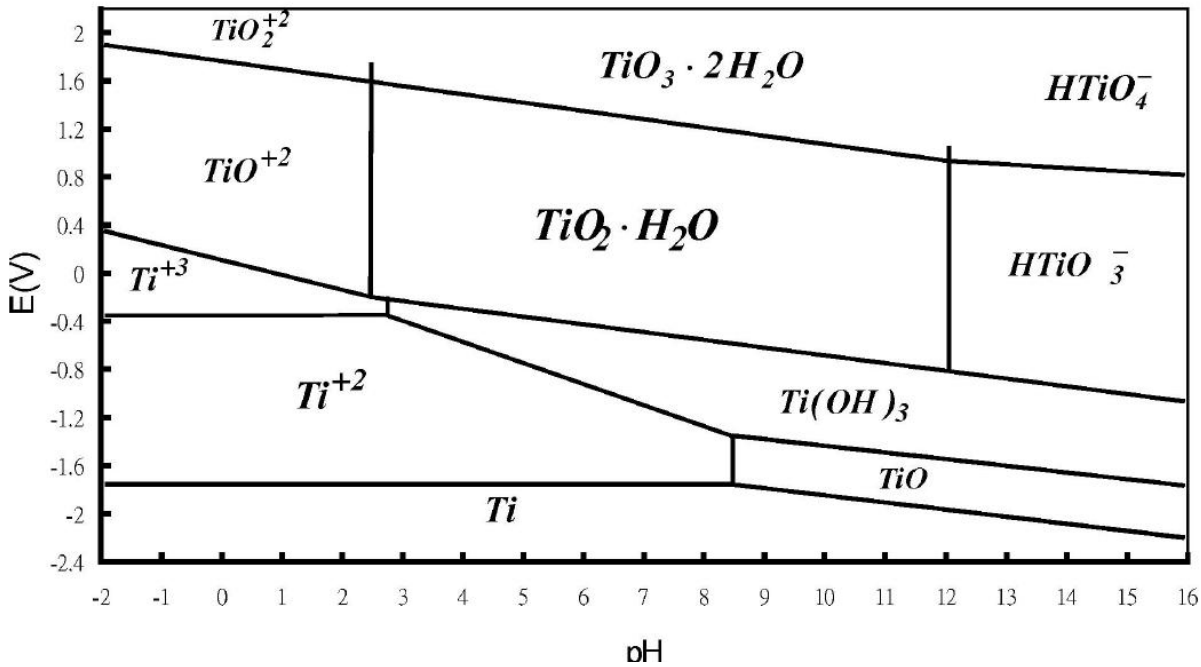

Figure 10. Potential-pH diagram for titanium. Passivating films form over a wide pH range (Chen, Chen, Chao, & Say, 2005).

3.4 Description of Corrosion Cells

As stated above, oxygen is not needed for oxidation to occur. In an acid solution for instance, metal atoms lose electrons to become ions in solution. At the same time electrons are consumed by hydrogen ions from the solution, adsorbed onto the metal surface, which come together with the electrons to form diatomic hydrogen. The site of the oxidation reaction is said to be anodic and the site of the reduction is cathodic. The reactions look like this:

Equation 27

$$At\ the\ anode\ M_{(s)} \xrightarrow{yields} M^{z+}{}_{(aq)} + ze^-$$

$$And\ at\ the\ cathode\ zH^+{}_{(aq)} + ze^- \xrightarrow{yields} \frac{z}{2} H_{2(g)}$$

Here z represents the number of electrons lost by the metal in the oxidation. It is also the valence number of the resulting ion, and in other electrochemical applications it is called the charge transfer number.

In a basic solution a possible cathodic reaction is

$$zH_2O + ze^- \xrightarrow{yields} zOH^- + \frac{z}{2} H_2$$

These reactions, along with the need to maintain charge neutrality, have two implications: first the electrons must be able to travel from the anode to the cathode, and second the metal ions must go into the same solution (and be mobile) as the hydrogen ions come out. Because metals are good conductors the electrons are easily transferred from anode to cathode. A liquid capable of transferring charge by the conduction of ions is called an

electrolyte (solid state electrolytes also exist but are beyond the scope of a discussion of corrosion). The electrolyte can be a bulk solution or a thin film of liquid.

These four things

- Anode
- Cathode
- Electronic connection
- Electrolytic connection

together form a closed circuit and a complete corrosion cell.

There are many types of corrosion and corrosion cells including, but not limited to

- Galvanic cells
- Concentration cells
- Electrolytic cells
- Uniform corrosion
- Selective dissolution
- Erosion-corrosion

Galvanic Cells

Galvanic cells develop when two different metals are touching (electronic connection) and in contact with a common electrolyte. If the oxidation potential of the two metals is different, the metal with the greater potential for corrosion will become the anode and the metal with the lesser potential will become the cathode. When metals are joined like this intentionally it is called cathodic protection, because the metal forming the cathode will be protected from corrosion by the sacrificial corrosion of the metal at the anode (it is also possible to obtain this same sort of protection by impressing an external voltage to the metal to be protected).

An important factor in galvanic corrosion and cathodic protection is the ratio of the areas of the anode and the cathode. A large cathode and a small anode will lead to concentrated oxidation over a very small area and rapid material failure; on the other hand a large anode and a small cathode results in slow corrosion of the anode over a large area – a favorable situation.

A special kind of galvanic cell can develop when the same metal (or multiple pieces of the same type of metal) has regions in which a surface film has developed which protects the underlying metal from further oxidation and other regions in which no such film exists. The filmed over region is cathodic with respect to the unfilmed region and the difference in oxidative potential can be as high as 0.3 volts. This is sometimes called a surface film cell (Roberge, Corrosion Engineering - Principles and Practice, 2008).

Concentration Cells

Concentration cells develop when there is a difference in the composition in the electrolyte between the anodic site and the cathodic site. Typical examples include crevice corrosion (in joints between two metals) and pitting (in a single piece of metal) in which an oxygen gradient is formed between the head of the corrosive pit (anode) and the tail (cathode). The anodic reaction consumes oxygen faster than oxygen in the bulk electrolyte can diffuse to

the anode. The cathode is essentially the entire surface of the metal outside of the pit or crevice.

Concentration cells are often found in corrosion in soil. If a metal object such as a pipe is buried in soil and part of the soil is then covered by paving, for instance. Both oxygen and moisture will be prevented from entering directly into the soil beneath the paving. In such cases oxygen starved areas of the underlying pipe will become anodic and the cathodic reaction can be the reduction of oxygen in water:

Equation 28

$$At\ the\ anode\ M_s \xrightarrow{yields} M^{z+}{}_{(aq)} + z\ e^-$$

$$And\ at\ the\ cathode\ O_{2(aq)} + 2H_2O_{(l)} + 4e^- \xrightarrow{yields} 4OH^-_{(aq)}$$

It is also possible that the pipe might be covered with soils of different compositions, in which case the concentration of ions in the electrolyte would differ along the length of the pipe and again a concentration cell would form to try to reduce this imbalance.

A pipe corroding in soil is only one example of where and how concentration cells can develop. Any situation in which a low rate of diffusion in the electrolyte leads to concentration imbalances can become a concentration type of corrosion cell. (Ahmed, 2006)

Electrolytic cells

An electrolytic cell is one in which external current creates a potential at the metal surface. This can happen intentionally in order to duplicate the effects of cathodic protection as was mentioned before or this can happen entirely by accident as is the case with stray current corrosion.

In stray current corrosion an electrical circuit, almost always DC, exists in which some of the current leaks out of the intended conductor and strays to a secondary, unintended conductor linked by an electrolytic contact, but not usually by an electronic contact. In order for the current flowing through the secondary conductor to complete the circuit, at some point it must pass out of the conductor, back through the electrolyte. The area where the stray current enters the secondary conductor becomes the cathode and is protected while the area from which the current leaves becomes an anode and is corroded (Ahmed, 2006).

Uniform Corrosion

In addition to the above mentioned localized forms of corrosion, there can also be uniform corrosion in which many local anodes and cathodes occur on the same metal surface, right next to each other. The anodes and cathodes can switch positions, leading to a uniform loss of metal from the surface. This form of corrosion has the highest loss of material related to it, but because the environmental factors involved are usually obvious it can be predicted (see the potential-pH diagrams) and is usually not a cause of failure in modern engineered systems.

(Roberge, 2008) and (Ahmed, 2006)

Selective dissolution (leaching)

In this form of corrosion one component in an alloy is dissolved selectively because of a difference in potentials among the constituents in the alloy – analogous to galvanic corrosion. The result is that one alloying compound will be significantly depleted at the surface and the mechanical properties of the metal at the surface will be altered. (Kruger, 2001)

Erosion-corrosion

Erosion due to flow across the surface disrupts or removes the passive layer. This leaves the exposed metal open to attack from any of the many forms of corrosion. (Kruger, 2001)

3.5 Ammonia corrosion in other industries

With the exception of the turbine, a Kalina cycle plant shares much in common with ammonia/water absorption heat pumps (chillers, refrigeration cycles and air conditioners). These heat pumps are mostly built of carbon or low alloy steel, like the Húsavík power plant. Two patents were found describing the use of new inhibitors to prevent corrosion in the ammonia environment (Agrawal & al., 1994) and (Mansfield & Sun, 2001).

The corrosion problems described in the two patents have some differences from the Kalina system. The patents are mostly concerned with corrosion at high temperatures (200+ °C) while the corrosion in the Kalina cycle happened between about 55 and 115 °C. Also the patents make no mention of evaporation or vapor liquid ratios, but in the Kalina cycle the corrosion seems to occur as the vapor is just starting to condense. The use of inhibitors is an interesting idea. The two described by the patents, sodium silicate and sodium chromate, would follow the liquid through the separator and therefore not be of use in the turbine. It is known in other industries that organic inhibitors can be used to protect boilers and these could follow the vapor stream in a Kalina process.

Looking at corrosion in ammonia and fertilizer plants was less fruitful.

Commercially ammonia is produced by the petrochemical industry in a process involving both high heat (up to 1200 °C) and high pressure (up to 200 bar). The main corrosion concern comes from the very high temperature, carbon monoxide attacking the passive films, H_2S corrosion and hydrogen embrittlment. Ammonia corrosion does not seem to be a significant problem for alloys chosen for use in such extreme conditions. The preferred alloys for the highest temperature sections of ammonia plants are those with both high chromium (20-25%) and high nickel (32-35%) such as the HP alloys and alloy 800. Elsewhere other stainless steels are used (Sukumaran Nair, 2001).

The failure of a pipe carrying high pressure ammonia in a fertilizer plant was analyzed but it was determined to be chloride induced pitting that had destroyed the pipe from the outside in. The fertilizer plant was located near the ocean and sea spray was getting onto the pipe (Sivaprasad, Narang, & Singh, 2006).

The failure of 304 stainless steel heat exchangers in a urea plant was investigated and some of the corrosion products were found to contain nitrogen – suggesting that the ammonia was complexing with the anodic products to form metal amides. However the root cause of the corrosion was determined to be galvanic coupling between the 304 SS and duplex steel parts that had been installed a few months before the failure occurred. A secondary factor in the corrosion was found to be the breakdown of the passive layer on the 304 SS in the presence of high temperature CO_2 in an anaerobic environment. It was suggested that only a single type of steel be used in the future and that 0.8% oxygen be added to the CO_2 to help maintain the passive film (Shaik, Rao, George, Anita, & Katack, 2003).

3.6 Corrosion Testing

The future of the Kalina power plant in Húsavík is uncertain at the time of this thesis. The plant has not produced electricity in over a year and a new turbine would need to be purchased and installed in order to make it operational. Even if they intend to reopen the power plant, Orkuveita Húsavíkur might not have an interest in corrosion testing. Their interest in the power plant is not as a research project or a learning experience, it is to generate electricity reliably and cheaply for the town of Húsavík.

Unquestionably corrosion damage was a significant cost during the first period of plant operation with the KK & K turbine (2000 to 2004). However during the second period of operation with the GE-Rotoflow expander (2004 to 2008) corrosion in the turbine section was not found to be a problem. During this second period the only significant repair that needed to be made to the turbine section was to the nozzle vanes, which were damaged by erosion. It has been speculated elsewhere in this thesis that corrosion fatigue could have played a role in the catastrophic failure of the titanium expander wheel, however this is only speculation and no examination of the expander wheel was carried out to substantiate the hypothesis.

Therefore on the basis of nearly four years of operation without corrosion problems Orkuveita Húsavíkur, if they choose to purchase a new turbine and reopen the power plant, is very likely to choose a turbine made of the same materials as the GE-R and do no further corrosion testing.

On the other hand the company, Exorka, which provided advice on this thesis and which would like to build and operate its own Kalina cycle power plants in the future is motivated to continue materials testing to find an optimum between corrosion resistance of materials and price.

Because corrosion is environmentally specific and because the environment of interest (two phase flow, pressure up to 30 or 35 bar, temperature up to 120 °C) would be difficult to replicate in a laboratory setting the range of useful experimental testing is restricted to measurements that could be carried out in situ in a pilot plant or full scale plant environment.

One possibility is linear polarization resistance testing. A rugged probe with three electrodes (working, reference and counter electrodes) can be introduced directly into the flow in the regions of interest. The electrodes on the probe are made out of the material of interest. The probe can be monitored by computer, gives data in real time and the data is easy to interpret. By leaving the probe installed for an extended period of time (weeks or months) time dependence of the corrosion rate could be investigated.

One difficulty to linear polarization resistance testing might be in mimicking the electrical conduction in the electrolyte. Most probes seem to be designed to be immersed in a liquid electrolyte and in the turbine section the working fluid is mostly vapor, with only a film of liquid existing on the surface of the metal.

Another method of corrosion testing likely to be used by Exorka in the evaluation of materials is coupon weight loss testing. In this method sample pieces of the material of interest are placed into the operational environment and after set periods of time they are removed, cleaned of corrosion products and weighed. The accuracy of weight loss testing is dependent upon properly removing the corrosion products from the test coupons. ASTM G1 provides some guidelines for the removal of corrosion products without damage to the base metal. Accuracy can be increased by using flat plates for testing, thereby maximizing the ratio of surface area on which corrosion can take place to volume.

Record keeping is essential to any corrosion monitoring or materials testing plan. Prior to this thesis some materials tests were made at the Kalina plant in Húsavík and some of the test samples were analyzed as part of this thesis, however not all of the samples could be found – a titanium sample and an inconel sample had been mislaid. Materials testing loses much of its value if the test coupons and results are not available for future investigations.

3.7 Failure of the titanium turbo-expander wheel

In January of 2008 the titanium turbo-expander wheel from of the GE-Rotoflow turbine, installed in 2004, failed catastrophically. The damaged section of the wheel can be seen in Figure 11.

Figure 11. In January 2008 a piece of the titanium wheel broke loose, forcing the shutdown of the power plant. This material failure has not been explained.

Neither the wheel nor any written reports about the failure were available for this thesis. Hearsay has focused on three hypotheses:

1. An error in the manufacturing process resulted in a defect (sometimes speculated to have been an "oxide inclusion") in the body of the wheel.
2. The wheel was correctly made but the frequency of rotation of the wheel corresponded to a harmonic oscillatory frequency (sometimes called an "Eigen frequency) which resulted in vibrational stresses greater than the wheel was designed for.
3. Some sort of pressure instability across the expander which resulted in pressure oscillations or pulses between the high pressure and low pressure sides of the expander.

Is it possible that corrosion could have been a contributing factor to the failure?

Maybe. No material loss was ever observed from the titanium expander and based on that and the potential-pH diagram for titanium (Figure 10) it is reasonable to assume that the titanium was in a passive region. A thin oxide layer had formed on the surface protecting the metal from further corrosion. Corrosion fatigue can occur in metals protected by a passive layer under certain stress conditions, namely repeated or cyclical stressing at stress levels well below the tensile strength of the metal.

There are several theories for crack initiation and propagation

- Stress concentration at the base of pits
- Stress distorted regions of metal acting anodicly to undistorted regions

- Passive film rupture by either cracking of the surface film under stress or attack by aggressive ions
- Adsorption of chemical species at the crack tip (hydrogen embrittlement)

Whatever the mechanism, there appears to be some minimal stress value that must be exceeded for corrosion fatigue to set in. It can be a slow process, often taking years before the cracks propagate to a length that causes fracture.

Any of the 3 speculations on the cause of failure could be compatible with and aggravated by corrosion fatigue. A defect in the metal, if it was near the surface, could have been a point of crack initiation. Either vibration at harmonic frequencies or pressure pulsing could have provided a cyclic stress sufficient to cause the formation of microscopic cracks in the surface film and to help propagate those cracks.

Without having the expander wheel to examine it is impossible to say if corrosion fatigue was a factor in the failure. Usually if corrosion fatigue is occurring, multiple cracks will form. This could be investigated through surface inspection, possibly with the aid of a microscope, by ultrasonic inspection or by taking a cross section of the wheel and polishing it and examining it under magnification – corrosion fatigue is typified by triangular non-branching cracks.

4 THEORY OF FE SEM

A conventional optical microscope uses reflected incident photons focused through a series of glass lenses to magnify a surface. An electron microscope on the other hand uses a focused beam of electrons, scanned over a sample, to generate an image.

To do this an electron microscope must have several parts: an electron source to generate the primary electron beam, electromagnetic lenses to focus the electron beam and a secondary electron detector to collect electrons generated at the surface of the sample by interactions between the primary electrons in the beam and the sample. Electron microscopes operate at reduced (vacuum) pressures in order to avoid interaction between the electron beam or the electron source and gas molecules. (Chumbley)

The electron source can be either thermionic or field effect.

A thermionic source uses a filament with a sharp "hair pin" bend in it. The filament is commonly made of tungsten but is sometimes made of other materials. The filament is heated and a negative voltage on the order of 100 kV is applied (making it a cathode). A grid (Wehnelt cylinder) near the filament is positively charged with respect to the filament by a few hundred volts. Below this is an electrically grounded ring that acts as the anode. The combination of the electric field acting on the tight curve of the filament and the elevated temperature is sufficient to strip electrons from the filament. The Wehnelt cylinder helps to focus the electrons toward the hole in the anode and the large electrical potential between the cathode and anode accelerate the electrons to a high velocity proportional to the magnitude of the electric field. The electrons pass through the anode and down the column.

Field emission is a newer and more expensive method of generating the primary electron beam. The filament is not heated in a field emission electron source but instead a single crystal tungsten needle is placed at the tip of the hairpin filament. The tip of the needle must be on the order of ten of nanometers across. The electrical field is similar to that of a thermionic generator but the area the field acts upon (the tip of the needle) is much smaller. The advantage of using field emission is that the source is much "brighter" than for thermionic emission, where brightness is defined as

Equation 29

$$B = \frac{j}{\pi\beta^2}$$

Where B is brightness and has units of amps per meter squared per steradian, j is current density having units of amps per meter squared and β is angle of convergence for the electron beam. The small tip results in a higher current density. Disadvantages include higher cost and the need to maintain harder vacuum than with a thermionic electron source (Electron Guns, 2000).

After passing through the anode the electrons are focused by three electromagnetic lenses. First the condenser lens focuses the electrons into a beam. The beam is deflected by changing the magnetic field of the scanning coils (thereby scanning the beam across the sample surface). Lastly the beam is brought into tight focus on the sample by the objective lens. These electromagnetic lenses act on the electrons through the Lorentz force, described by the equation

Equation 30

$$\boldsymbol{F} = q[\boldsymbol{E} + (\boldsymbol{v} \times \boldsymbol{B})]$$

Where bold face indicates a vector quantity, F is force in newtons, q is the charge on the electron, E is the electric field in volts per meter, v is the instantaneous velocity of the electron in meters per second and B is the electric field in teslas. Electrons moving down the column axis will be subject only to axial forces; off axis electrons will be pushed into spiraling down around the axis by interaction with the magnetic field.

Secondary electrons are generated by inelastic interactions between the primary electron beam and valence electrons on the atoms of the sample. The primary electron collides with the valence electron, imparting enough energy to cause the valence electron to leave its orbit. Secondary electrons generally have very low energy (~5 eV) compared to the primary electrons (~10 keV). Because of the low energy of secondary electrons they cannot penetrate very far through the sample. Maximum escape depth is dependant on material (insulators have a greater escape depth than metals) but in either case most secondary electrons come from the uppermost 2-5 nm of the sample surface. (Secondary Electrons)

The secondary electron detector collects these particles from the spots on the sample at which the primary beam is focused. The number and energy of the electrons coming from different spots on the sample are converted into a voltage by the secondary electron detector. This voltage is then converted to a grey scale to produce the image of the sample.

Other particles in addition to secondary electrons can be generated by interactions between the sample and the primary electron beam. Among these are x-ray photons which can be detected by an energy dispersive spectroscopy (EDS) X-ray detector.

The electrons from the primary beam can generate X-rays in two ways: by interacting with the nucleus of atoms or by interacting with inner shell of electrons in the atoms of the sample. In the former case, the primary electron is slowed and loses energy in the form of a photon. In the later case the primary electron collides with one of the inner most (K-shell) electrons of a sample atom, giving up enough energy to force the electron out of the lowest energy well (the K-shell) and into an outer shell – when this happens another electron in the same atom will give up energy in the form of a photon in order to move into the K-shell and re-establish the lowest energy configuration for the electron shell. In the case of primary electron – nucleus interactions, photons of many different energy levels may be given off. This is called bremsstrahlung radiation and it forms a continuous background signal for the X-ray detector. K-shell emission on the other hand produces higher energy X-rays and, as first observed by Henry Moseley, the energy of the K-shell emission is specific to each element – making it possible to use EDS to analyze the composition of a sample. (Wittke, 2006) and (Making X-rays, 2000)

5 PROCEDURE

On January 13th, 2009 samples were taken from the Húsavík power plant for analysis by SEM. The samples are shown in Figure 12.

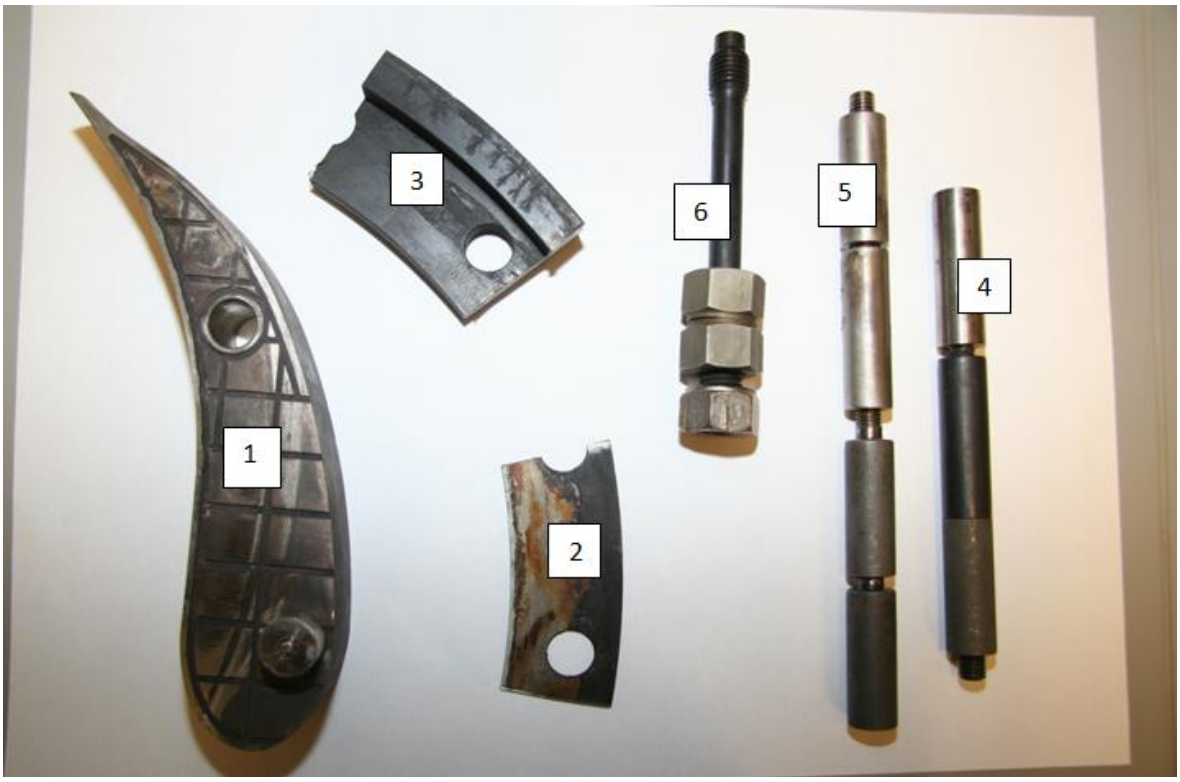

Figure 12. Samples taken from the Húsavík power plant on Jaunary 13th 2009.

The samples taken were:

1. Nozzle vane from the newer GE-Rotoflow turbine made of nitronic 60. The nozzle ring is designed to allow the nozzle vanes to open and close, the hole in the vane is for a pivot pin; the pin, still in the vane, slides in a slot, controlling the angle of the vane. The pin and the side of the nozzle vane shown in the picture exhibit mechanical damage from sliding against the nozzle ring. The surface of the nozzle has been repaired, with new material welded in along both edges. The new material is Castolin XHD 6805. Dents can be seen in the unrepaired middle of the nozzle surface. It was a part of the plant during the period 2004 to 2008.
2. Spacer ring from the original KK & K turbine. The plant manager made this to fit between the nozzle ring and the turbine housing to prevent corrosion products from breaking free of the turbine housing and impacting on the turbine. This ring is made of 316 stainless steel. The grey area has been etched away by some sort of erosion or corrosion-erosion process. It was a part of the plant during the period 2002 to 2004.
3. Retaining ring from the original KK & K turbine. On the surface exposed to the ammonia-water fluid the black areas were cover by washers and protected while the grey area was eroded-corroded. Since being removed from the turbine housing (2004), it has undergone further corrosion (the red-brown rusty areas). Erosion can

be seen in several of the black areas where the ring did not seal well and the fluid got under the washers or under the flange and filiform corrosion took place. This is the same material that the turbine casing was made from (1% Cr alloy steel). This was a part of the plant between 2000 and 2004.

4. Test cylinders I. These test pieces were inserted into the stream of flow in 2001 or 2002 for 2 – 3 weeks. The lustrous cylinder is 316 stainless steel; there is perhaps some minor corrosion between the grooves. The black cylinder is a carbon steel placed on the high-pressure side of the turbine. The dull grey cylinder is the same carbon steel material but it was exposed to the environment of the low-pressure side of the turbine.
5. Test cylinders II. These pieces were tested at a later time than those described by 4 but before 2004. The shiny cylinders are stainless steels; the dark ones are two different alloys with chrome or nickel and chrome. There were additional cylinders tested at the same time as these, made of titanium and inconel but these cylinders have been lost.
6. Nuts and a bolt. The shiny silver nut was part of the original KK & K turbine and is plated with nickel (2000 – 2004). The 2 nuts with a yellow or gold coloration were replacement nuts for the KK & K turbine made from 316 stainless steel (sometime after 2000 to 2004) – at the time the KK & K turbine was removed from the plant these nuts are reported to have been silver and shiny. It is possible that exposure to the working fluid in the turbine conditioned the exposed surface of the nuts to be susceptible to secondary corrosive attack after they were removed from the turbine environment. The bolt was part of the original KK & K turbine, only one end of the bolt (the end pictured with the nuts on it) seems to have actually been exposed and it has the grey color and fine roughness similar to the turbine wheel itself.

On January 21st, 2009 the samples were taken to the Innovation Center Iceland (Nýsköpunarmiðstöð Íslands) for analysis by FE-SEM. Because of time constraints not all of the samples could be analyzed and standards were not used. The samples selected for analysis were #2 the stainless steel spacer ring with eroded channels, #3 the retaining ring with filiform corrosion, #4 the carbon steel cylinders from the low and high pressure sides of the turbine but not the 316 stainless steel cylinder and #1 the duplex steel pin from the nozzle vane (the vane itself was too big for the microscope). The microscope was operated by Birgir Johannesson, of the Innovation Center Iceland.

5.1.1 Description of the Instrument

The instrument used was a LEO Supra-25 field emission scanning electron microscope with an acceleration voltage between 0.5 and 30 kV. Constituent analysis was done with an Oxford Instruments EDS X-ray detector.

5.1.2 Sample Preparation

It was observed that sample #2, the first to be analyzed, did not stick to the carbon tape normally used to immobilize samples in the vacuum chamber of the microscope. The sample was wiped with the solvent “inhibisol” and blown dry with compressed air in an attempt to remove any oily film that might have formed from handling the sample. This did not improve the ability of the tape to stick to the sample. All other samples were similarly unable to be taped, however they were not wiped with inhibisol.

In order to get an analysis of the metal itself, a corner of sample #3 was filed down to bare metal before being placed in the sample chamber of the microscope.

6 SEM ANALYSIS AND RESULTS

6.1.1 Sample 2

Four regions of sample #2 (Figure 13), a 316 stainless steel spacer ring, were inspected and analyzed. They are numbered as shown in the picture: area 1 the black corrosion products, area 2 the metal of the eroded channel, area 3 brown corrosion products and area 4 a rough area in the eroded channel.

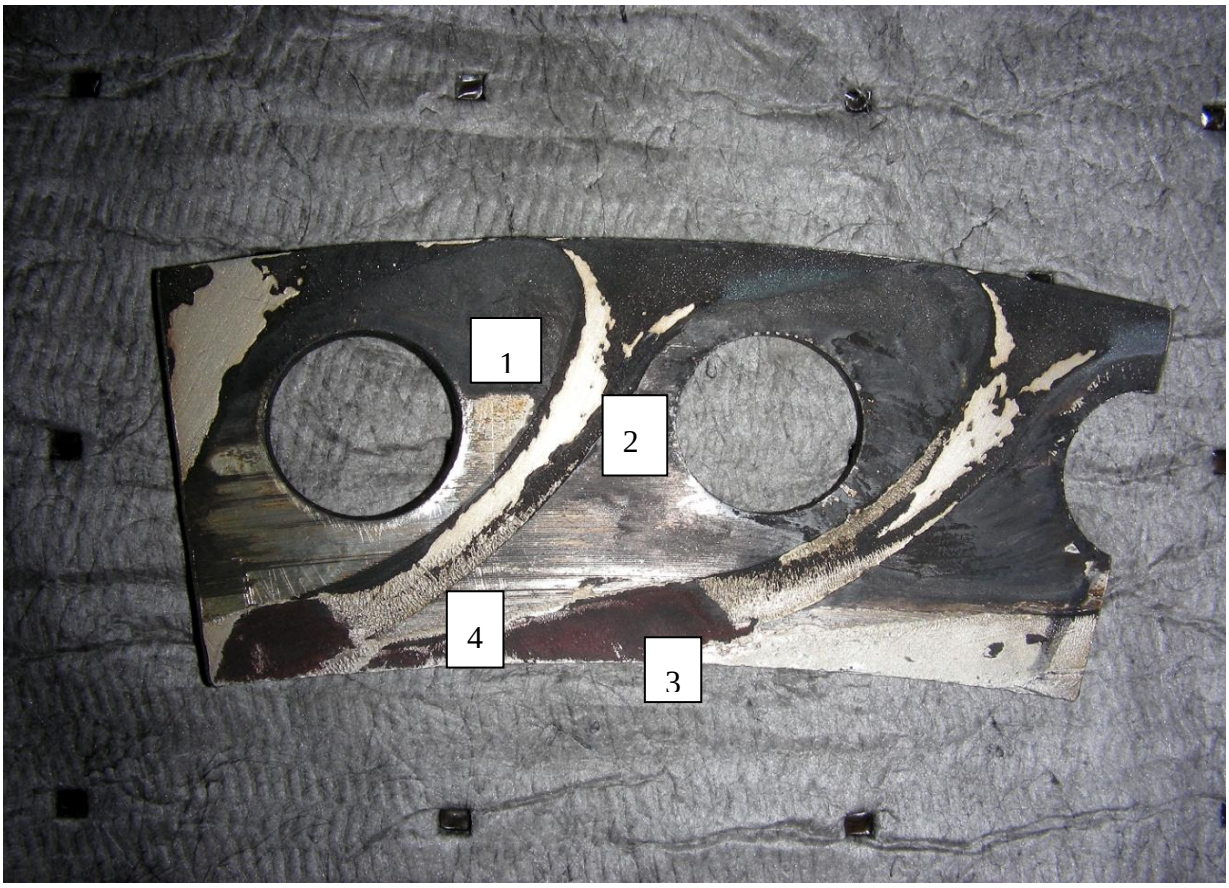

Figure 13. Sample number 2, analyzed by SEM. Four regions were inspected. 1. The black corrosion products. 2. A smooth section of the eroded channel. 3. Brown/red corrosion products. 4. A roughly textured region in the channel.

Sample 2, area 1 analysis and results

Area one consists of black corrosion products and was covered by one of the first stage nozzle vanes. Micrographs of area 1 are shown in Figure 147. In image A it can be seen that the surface is made up of roughly cubic crystals of varying sizes. Image B shows that not all of the crystals are cubic. The crystal shown has a rough, broken look to it and the angles of the crystal in the center of the picture and the one to its right are greater than 90°, though that may just be the effect of the crystals forming at an odd angle relative to the plane of the micrograph. Image C shows cubic crystals growing from a darker back ground.

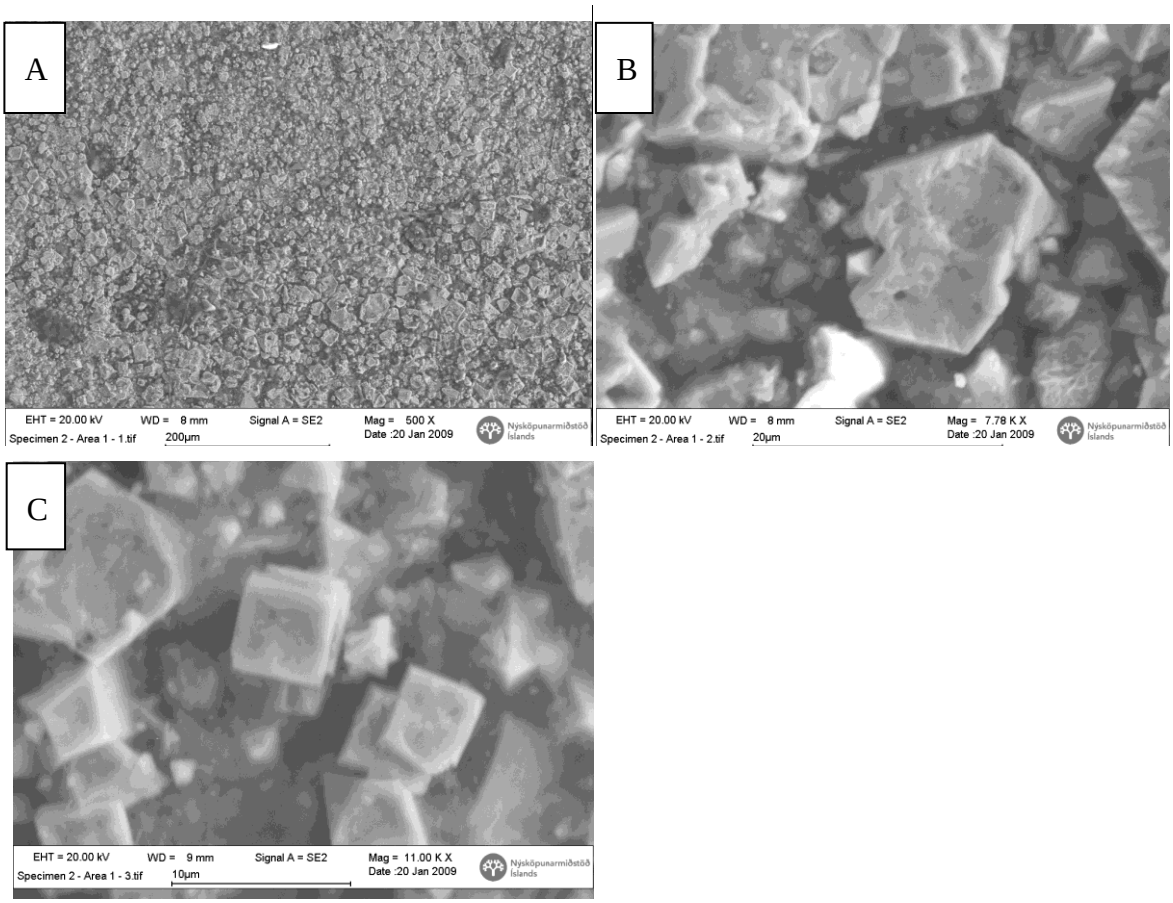

Figure 14. Micrographs of area 1 of sample 2. Micrograph A is an overview of surface at 500X magnification. Micrograph B is a close up of one of an irregularly shaped crystal at 7 780X magnification. Micrograph C is a close up of cubic crystals at 11 000X magnification.

Two EDS X-ray analyses were made of area 1 of sample 2 and EDS analyses were also made for the crystals shown in images B and C. The results are presented in tables in Table 2 and Table 3. Sample number 2 is made from 316 stainless steel and the composition of that steel is included in the tables for comparison.

The two spectra of area one are in agreement, with only small differences notable in the overall amounts of carbon and iron.

The spectra of the crystals also are consistent with one another.

Table 2. Composition of sample 2, area 1.

	Area 1, Analysis 1		*Area 1, Analysis 2*		*316 Stainless Steel*
Element	Weight%	Atomic%	Weight%	Atomic%	Weight%
C K	36.22	57.17	34.59	55.77	0.08
O K	23.5	27.85	23.65	28.62	
Na K	0.24	0.2	0.24	0.2	
Mg K	0.28	0.22	0.18	0.14	
Al K	0.97	0.68	0.86	0.62	
Si K	1.36	0.92	1.13	0.78	0.75
S K	0.17	0.1	0.11	0.06	0.03
Cl K	0.14	0.08	0.09	0.05	
Ca K	0.51	0.24	0.42	0.2	
Cr K	4.5	1.64	4.92	1.83	16 to 18
Mn K	0.5	0.17	0.53	0.19	2
Fe K	31.61	10.73	33.03	11.45	balance
Ni K			0.26	0.09	10 to 14
Mo L					2 to 3
P K					0.045
Totals	100		100		100

Table 3. Composition of crystals on sample 2, area 1.

	Crystal B		*Crystal C*		*316 Stainless Steel*
Element	Weight%	Atomic%	Weight%	Atomic%	Weight%
C K	11.34	25.13	9.9	22.96	0.08
O K	27.3	45.4	25.58	44.52	
Na K					
Mg K					
Al K					
Si K			0.19	0.19	0.75
S K					0.03
Cl K					
Ca K					
Cr K	6.37	3.26	6.5	3.48	16 to 18
Mn K	0.54	0.26	0.94	0.47	2
Fe K	54.45	25.95	56.89	28.37	balance
Ni K					10 to 14
Mo L					2 to 3
P K					0.045
Totals	100		100		100

Discussion of sample 2, area 1 analysis and results

Comparing the results of the EDS X-ray analysis of area 1 (Table 2) with the analysis of individual crystals on the surface of the area (Table 3) it can be seen that the crystal composition is different from the back ground composition. The crystals are predominantly made up of iron oxides and chromium oxides while the background has considerably more carbon and minor constituents. The lower amounts of chromium and manganese and the complete absence of nickel from the corrosion products suggests that they may have formed not from the stainless steel ring but more likely from the nozzle vane that contacted the ring in that location. The high concentration of carbon will be discussed at the end of the SEM section of the thesis.

The location of the corrosion products under the vane shows that liquid must have penetrated into this area (or that vapor penetrated the area and condensed there). This is not surprising as grooves from machining can be seen on the surface of the spacer ring and it would have been difficult or impossible to get an impermeable seal. Such a confined space would promote crevice corrosion. The vanes themselves were unavailable for inspection, but the grooves in the spacer ring did not appear to have been damaged by corrosion, supporting the theory that the corrosion products came from the vane. It is possible that by being in physical contact with the 316 stainless steel and the fluid intrusion, a galvanic cell was created which would have accelerated the corrosion of the vane.

Sample 2, area 2 analysis and results

Area 2, of sample 2, is a channel in the surface of the 316 stainless steel ring. The areas outside the channel were covered by the first stage nozzle vanes, while the area of the channel was directly exposed to the fluid coming from the separator as it entered the turbine. To the naked eye it appears to be bare metal. A micrograph of area 2 is shown in Figure 15.

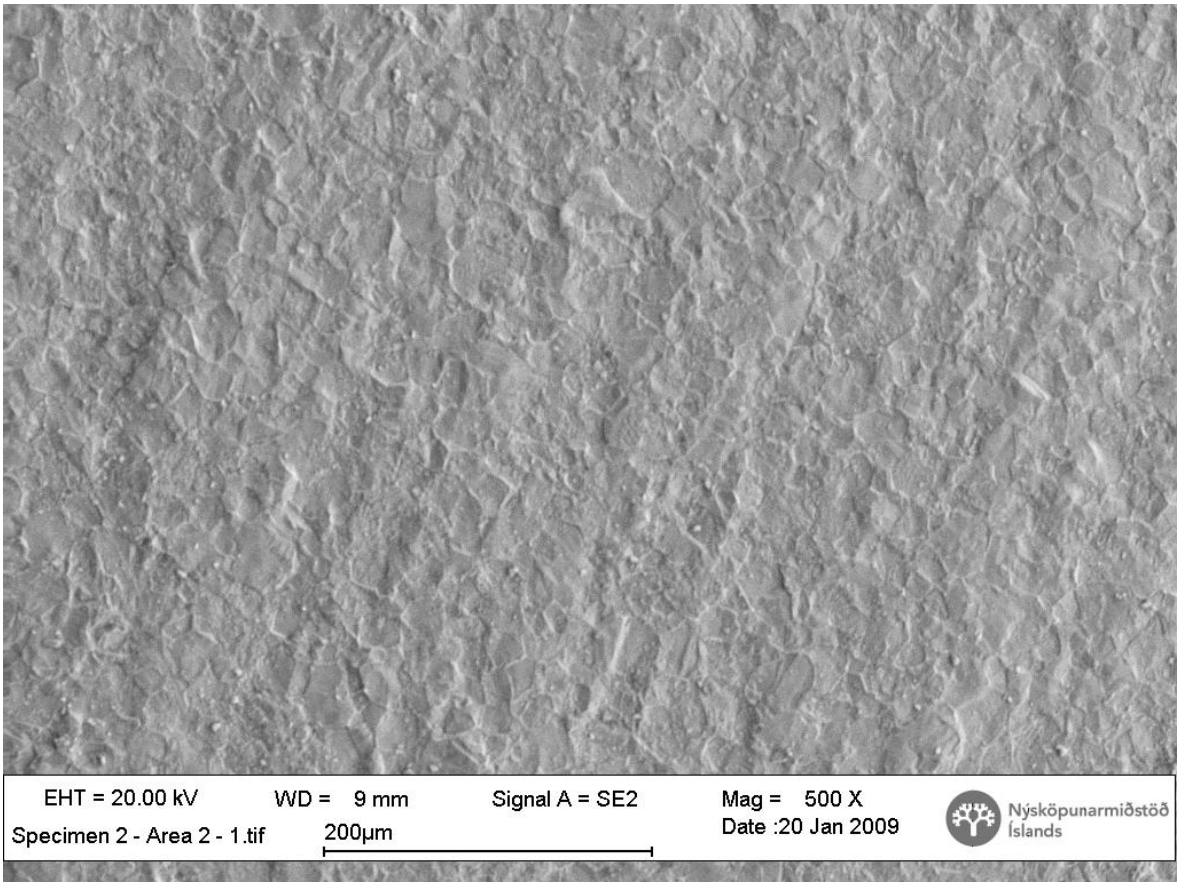

Figure 15. Sample 2, area 2 at 500X magnification. No corrosion products are visible.

Under 500X magnification no corrosion products or structures could be seen and it was assumed that this was the true surface of the metal, covered by no more than a thin oxide film. Two EDS X-ray analyses were performed and are presented in Table 4.

Table 4. Results of X-ray emission analysis of sample 2, area 2.

	Area 2, Analysis 1		*Area 2, Analysis 2*		*316 Stainless Steel*
Element	Weight%	Atomic%	Weight%	Atomic%	Weight%
C K	13.46	36.73	13.45	37.24	0.08
O K	8.42	17.24	7.41	15.41	
Na K					
Mg K					
Al K					
Si K	0.48	0.56	0.51	0.6	0.75
S K					0.03
Cl K					
Ca K					
Cr K	16.15	10.18	16.09	10.3	16 to 18
Mn K	1.14	0.68	1.29	0.78	2
Fe K	49.01	28.75	49.75	29.63	balance
Ni K	9.18	5.12	9.37	5.31	10 to 14
Mo L	2.16	0.74	2.12	0.74	2 to 3
P K					0.045
Totals	100		100		100

Discussion of sample 2, area 2 analysis and results

The spectra of area 2 are nearly the same, demonstrating repeatability. Comparing the results of the analysis of sample 2, area 2 to the reference composition of 316 stainless steel, it can be seen that they are nearly identical in the major constituents. This confirms the assumption that this area is bare metal with no more than an oxidized film on the surface. It is noted however that the amount of carbon is unexpectedly high.

Sample 2, area 3 analysis and results

Area 3 is a formation of black and brown corrosion products near the inner edge of the ring at the terminus of one of the channels between the nozzle vanes. A micrograph is shown in Figure 16. At 500X magnification the surface looks very porous, like a sponge. It does not look like the crystalline structures from sample 2, area 1 (Figure 14).

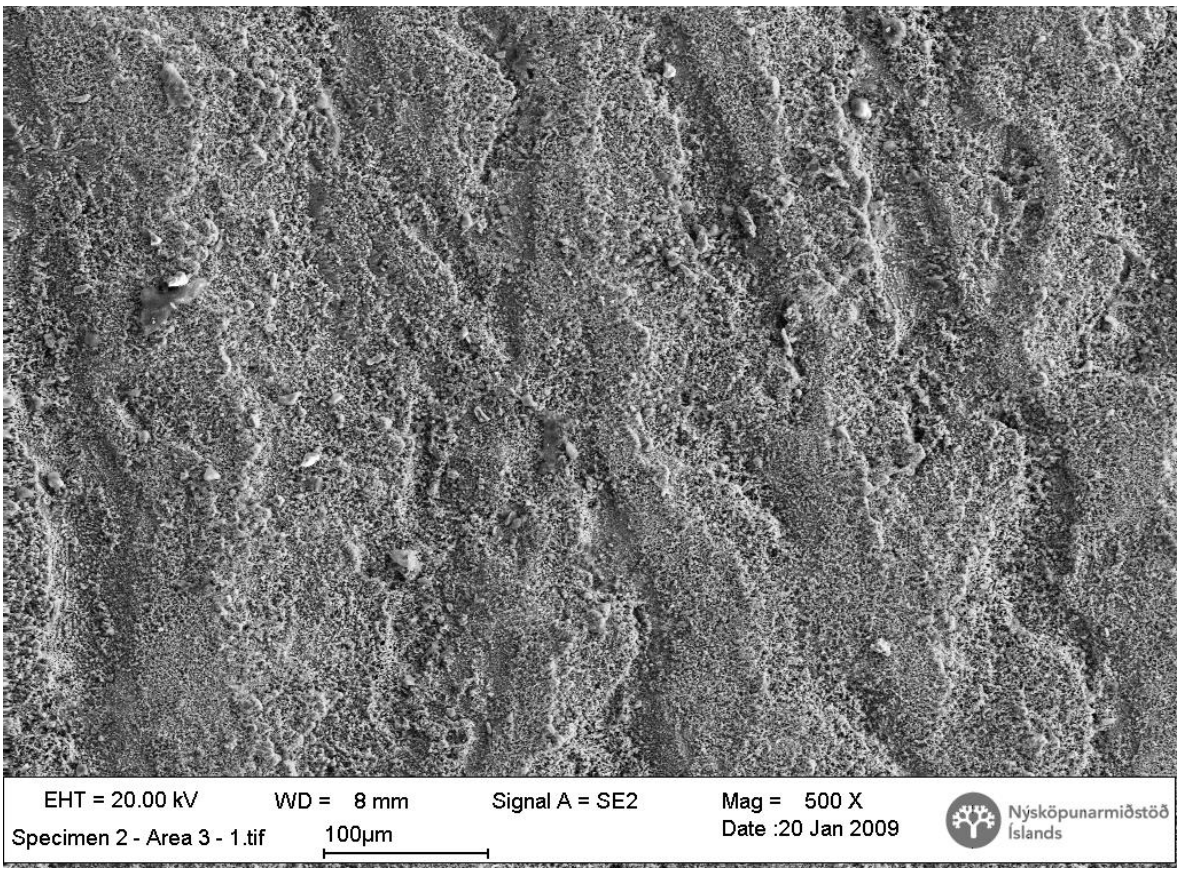

Figure 16. Sample 2, area 3, brown and black corrosion products at the inner edge of the ring.

An EDS X-ray analysis was made of this region and is presented in Table 4. For ease of comparison, spectrum one of area one is repeated in the table and the composition of 316 stainless steel is given. Due to time constraints only a single analysis was made of the composition of area 3.

Discussion of sample 2, area 3 analysis and results

The corrosion products of area 3 are different than the corrosion products of area 1. They do not have the same crystal structure as can be seen from the micrographs and they have a different composition as can be seen from the table above. Area 3 has considerably more iron and manganese as well as having nickel while it has lesser (or undetectable) amounts of the minor constituents that are found in area 1. Because of the location of area 3 (at the end of a channel, like area 2) it is possible that material that is scoured from the channel is being deposited at area 2 and it is a mixture of the products from area 1 and the steel removed from area 2. This supposition is supported by the much lower Fe/O ratio.

Table 5. Analysis of sample 2, area 3. A spectrum of sample 2, area 1 is included so that comparison can be made between the corrosion products. The composition of 316 stainless steel is also included for comparison.

	Analysis of Area 3		*Area 1, Analysis 1*		*316 Stainless Steel*
Element	Weight%	Atomic%	Weight%	Atomic%	Weight%
C K	13.95	29.41	36.22	57.17	0.08
O K	27.57	43.65	23.5	27.85	
Na K			0.24	0.2	
Mg K			0.28	0.22	
Al K	0.25	0.24	0.97	0.68	
Si K	0.33	0.3	1.36	0.92	0.75
S K			0.17	0.1	0.03
Cl K			0.14	0.08	
Ca K	0.19	0.12	0.51	0.24	
Cr K	3.76	1.83	4.5	1.64	16 to 18
Mn K	1.13	0.52	0.5	0.17	2
Fe K	51.95	23.56	31.61	10.73	balance
Ni K	0.87	0.37			10 to 14
Mo L					2 to 3
P K					0.045
Totals	100		100		100

Sample 2, area 4 analysis and results

Area 4 lies in the same channel as area 2 but closer to the end of the channel. Area 4 is in between area 2 and corrosion products at the end of the channel (like area 3), making it a possible transitionary region between what happens in the beginning and middle of the channel (erosion) and what happens at the end (material deposition). Upon visual inspection, area 4 looks rough but is does not appear to be covered by corrosion products.

Four micrographs were taken of area 4. Three are shown in Figure 17 and one on the page after (Figure 18). In figure A the overall structure of the area is given. At 107X magnification ridges and channels can be seen and a forest of fine structures cover parts of the ridges. Figure B is a close-up on the "forest" of one of the ridges at 2000X magnification. Figure C shows scale formations in between the ridges at 3000X magnification.

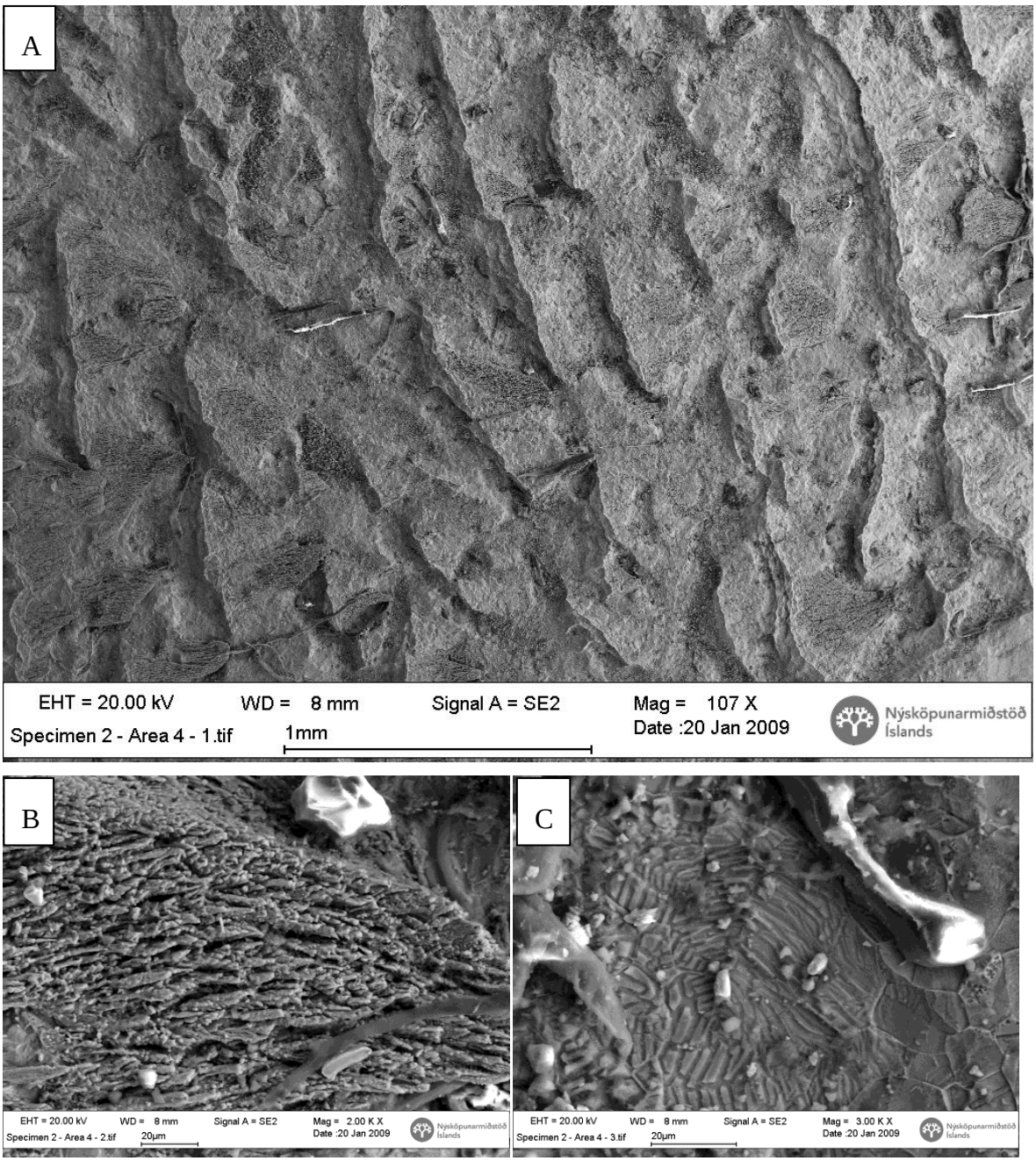

Figure 17. Sample 2, area 4. A. The overall surface structure of the area. B. Close-up of a "forest structure" at the edge of one of the ridges. C. Oxide scale on the surface of 316 stainless steel.

On the next page is a picture of the scaling at 10 780X magnification (Figure 18). It can be seen that the scale is on the order of 1 or 2 microns thick.

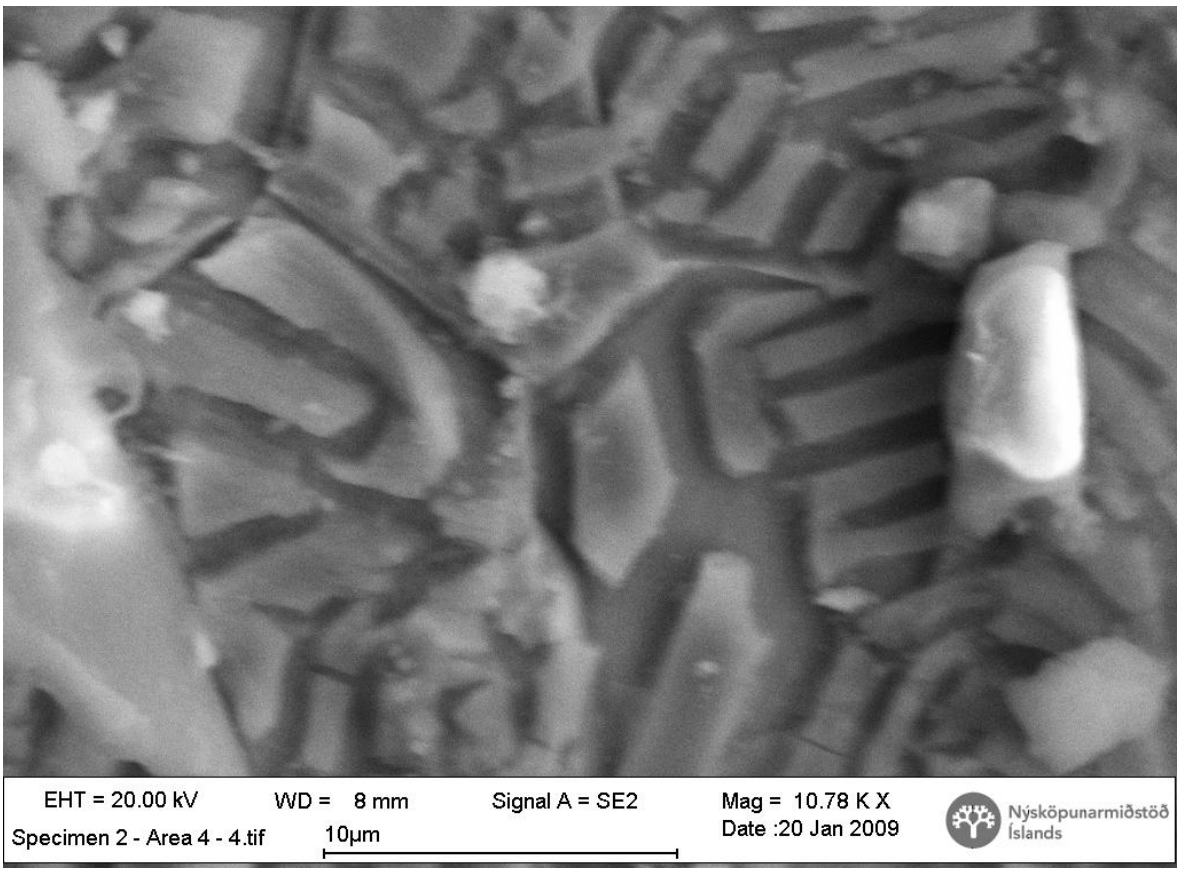

Figure 18. Scaling on sample 2, area 4. The grains or crystals are less than 10 microns across and only 1 or 2 microns thick.

EDS X-ray analyses were made of the forest of structures (Figure 17 B) and of an individual grain of the scaling material (Figure 18). The results of the analysis are presented on the following page. The most striking contrast between the forest structure and the scale is that in the former iron is clearly the dominant cation while in the latter iron is balanced by chromium and nickel.

Discussion of sample 2, area 4 analysis and results

In the literature ((Grabke, Muller-Lorenz, Straus, & al, 1998), (Liu, Tang, Jonsson, & al, 2006)) it can be found that stainless steels obtain much of their ability to resist corrosion from the formation of impermeable, chromium rich, oxide films at the surface. These films are on the order of 100 - 200 nanometers thick. On top of these films can grow larger, non-protective crystals on the order of a few microns in size. Study of both the protective thin film and the larger non-protective grains has shown them both to be enriched in chromium and deficient in iron with respect to the bulk metal composition. It seems likely that it is these larger non-protective grains that are seen in the figure above.

In the forest region, the iron content is similar to what was found in area 3, supporting the speculation that the environment changes going down the channels from primarily erosive

(area 2) to deposition at the end (area 3). The way the forest is all bent in the same direction maybe demonstrative of the direction of flow.

Table 6. Surface composition of sample 2, area 4.

	"Forest" Analysis		*Scale Analysis*		*316 Stainless Steel*
Element	Weight%	Atomic%	Weight%	Atomic%	Weight%
C K	16.91	34.39	16.61	33.49	0.08
O K	26.36	40.23	26.78	40.52	
Na K	0.36	0.38	0.57	0.6	
Mg K					
Al K	0.26	0.23			
Si K	0.25	0.21	0.32	0.27	0.75
S K			0.59	0.45	0.03
Cl K	0.16	0.11	0.78	0.53	
Ca K	0.13	0.08			
Cr K	1.97	0.92	21.13	9.84	16 to 18
Mn K	0.3	0.13	0.85	0.38	2
Fe K	53.31	23.31	27.38	11.87	balance
Ni K			4.98	2.05	10 to 14
Mo L					2 to 3
P K					0.045
Totals	100		100		100

6.1.2 Discussion of Sample 2

Both the micrographs and the compositional analysis seem to be consistent with the idea that the channels on the 316 stainless steel ring were formed primarily through erosion. The corrosion products in area 1 seem to be inconsistent with the composition of the steel suggesting that the corrosion was on the contacting nozzle vane or that the corrosion products were transported from elsewhere in the power plant.

That within the span of 3 or 4 centimeters (the length of the channels) the effect of flow on the steel could change from erosion (area 2) through some transition zone (area 4) to deposition (area 3) is a testament to the complex flow path taken by the fluid entering the turbine.

6.1.3 Sample 3

Sample 3 is a part of the retaining ring that held the nozzle ring in place. One face of the retaining ring was shielded from the fluid by being pressed up against the nozzle ring. The opposite side, though out of the main flow path, was exposed. The shielded side is coated by black corrosion products that look like the same material as is on sample 2 at area 1. The exposed side of the retaining ring is grey and rough like the turbine wheel, the nozzles, the inside of the turbine housing (after the nozzles) and the turbine exhaust. It is made out of mild steel, believed to be about 1% chromium but the precise composition is unknown.

The exposed side of the retaining ring is pictured in Figure 19. The black circles are where washers shielded the ring from contact with flowing fluid. The black circles are noticeably raised from the grey surface, showing that material has been lost from the exposed areas. It can be seen that under some of the washers, significant crevice corrosion took place as channels are etched into the steel and are circled in red.

Figure 19. The exposed side of the retaining ring, from which sample 3 was cut. Evidence of crevice corrosion is circled in red.

Sample 3 is pictured in Figure 20. There were 4 areas examined on sample 3, all of which are on the shielded side of the ring. Areas 1 and 3 are sites of filiform corrosion on opposite ends of the channel. Area 2 is on the lower side of a step that was etched into the ring. The upper side of the step (with the filiform corrosion) was held tight against the nozzle ring while the lower part of the step, while protected by the geometry of the turbine from the flow path, was uncovered. Area 4 is a corner of the sample that was filed down to bare metal to get an analysis of the composition of the ring, which is believed to be made of the same material as the turbine housing.

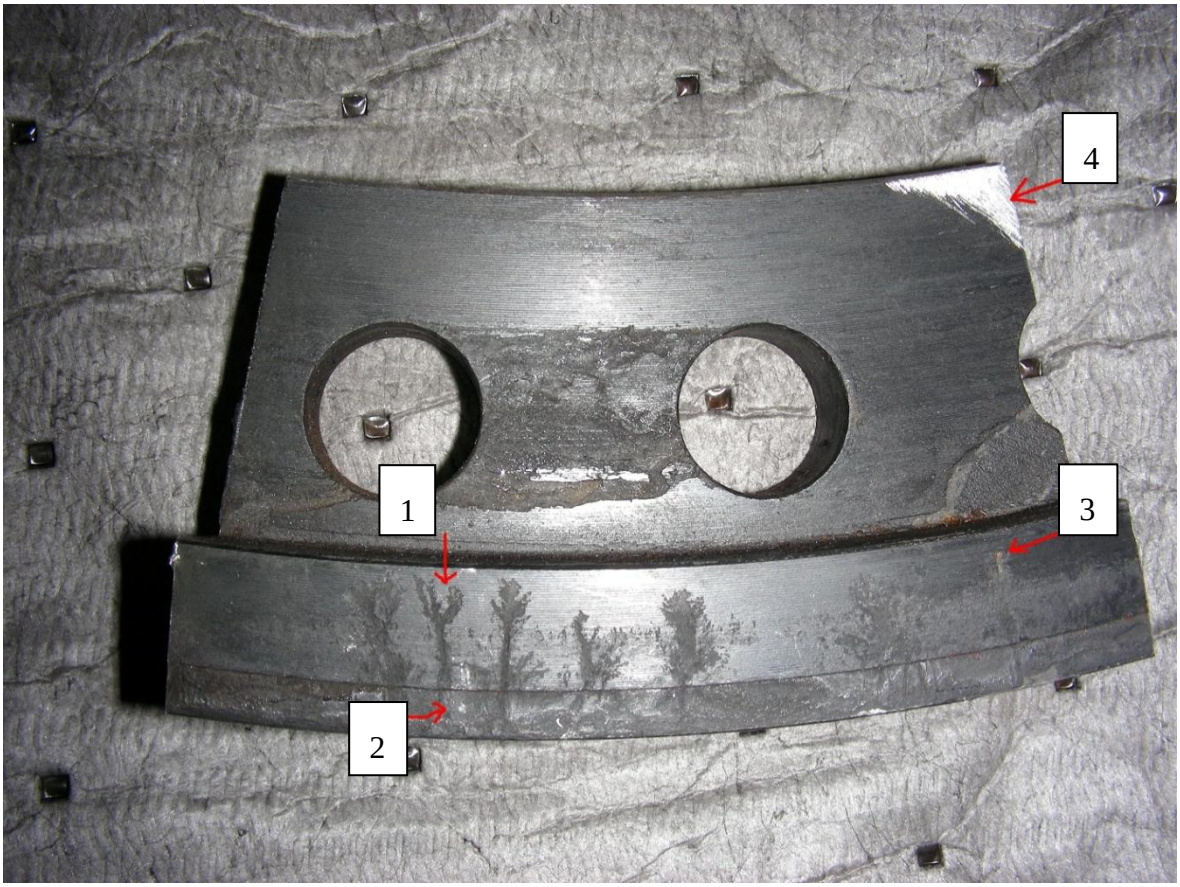

Figure 20. Sample 3. Area 1 is a filiform corrosion channel. Area 2 is a point in the region below the step. Area 3 is the tip of another filiform corrosion channel. Area 4 is bare metal, exposed by filing the sample before putting it into the SEM.

Sample 3, area 1 analysis and results

Five micrographs were taken of area 1, a filiform corrosion channel; they are shown in the following page and labeled A through E (Figure 2114). The step, etched into sample 3, can be seen at the botton of image A. It can bee seen from the image that the filiform channeling begins from this step and that below the step the corrosion was more uniform. Image B shows grooving in the bottom of the main channel of area 1. Image C shows channels branching off of the main channel. Branching like this is typical of filiform corrosion and distigushes it from other types of crevice corrosion. Images D and E show the end of one of the channels, it can be seen that pitting of the metal takes place in advance of connection to the channel.

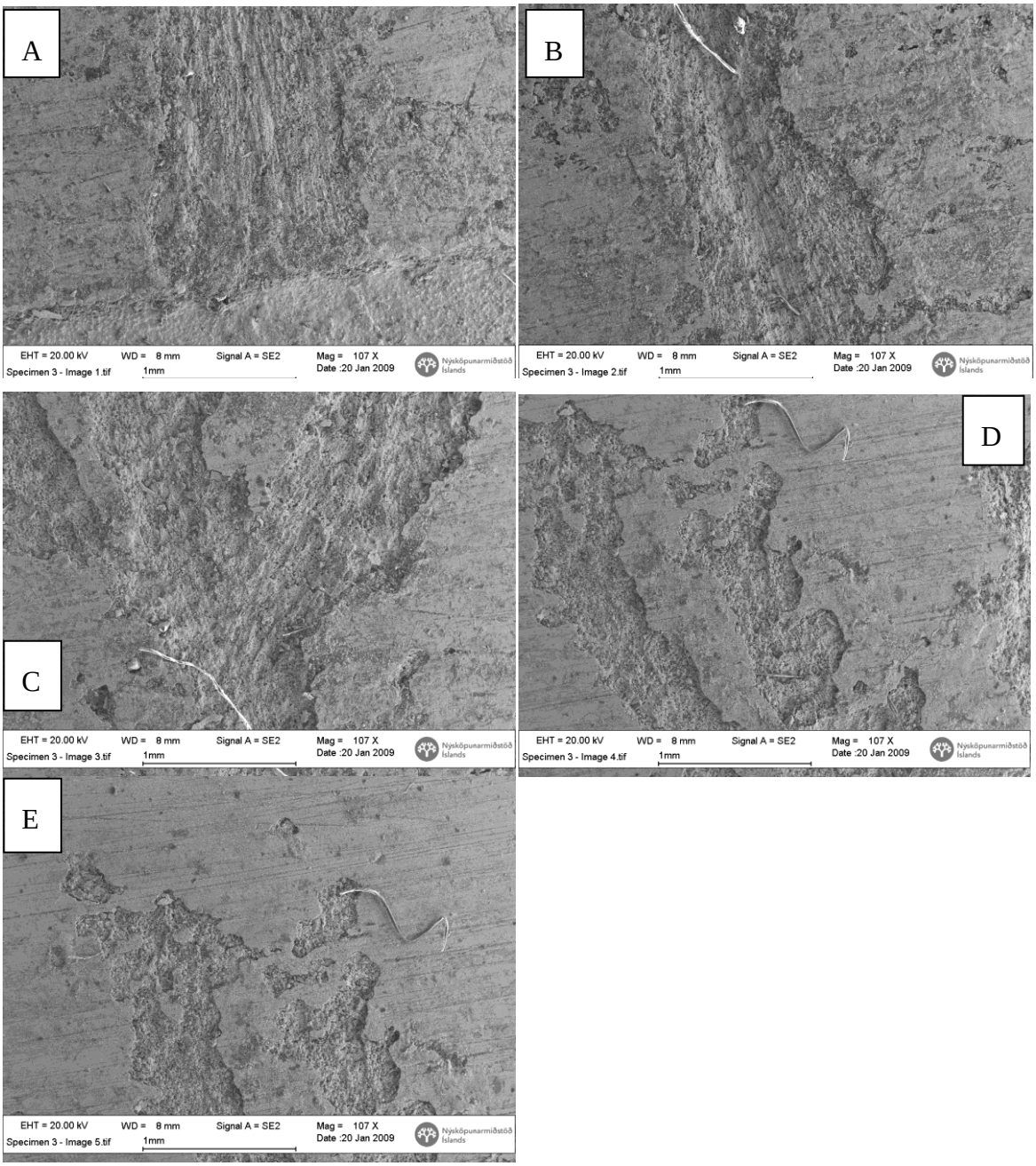

Figure 21. Micrographs of sample 3, area 1 at 107X magnification. A. The beginning of the filiform channel, the step can be seen at the bottom of the image. B. The main channel of area 1. C. Branching form the main channel, which typifies filiform corrosion. D. The end of one of the channels of area 1. E. The end of a channel in area 1, in which it can be seen that pits form in advance of the main channel.

Four EDS X-ray analyses were made of area 1: two from the bottom of the main channel (one near the tail and one near the mid-point), one from a pit at the head of the channel and one from a region off to the side of the filiform corrosion channel, covered in dense black corrosion products similar to area 1 of sample 2. The results of the analysis are presented in Table 7.

Table 7. Composition of surface attacked by filiform corrosion: sample 3, area 1.

	Channel Analysis 1		*Channel Analysis 2*		*Pit Analysis*		*Outside Channel*	
Element	Weight%	Atomic%	Weight%	Atomic%	Weight%	Atomic%	Weight%	Atomic%
C K	38.62	60.65	40.28	62.82	44.32	67.68	32.7	56.02
O K	21.29	25.11	19	22.25	16.5	18.92	20.48	26.34
Na K			0.19	0.15				
Mg K	0.16	0.13	0.23	0.18	0.15	0.11		
Al K	0.55	0.38	1.91	1.33	0.28	0.19	0.2	0.16
Si K	0.91	0.61	0.79	0.53	0.46	0.3	0.34	0.25
S K	0.2	0.12	0.18	0.1	0.44	0.25	0.2	0.13
Cl K			0.12	0.06			0.12	0.07
Ca K	0.38	0.18	0.32	0.15	0.34	0.15	0.12	0.06
Cr K	0.82	0.3	1.03	0.37	2.73	0.96	2.99	1.18
Mn K			0.2	0.07	0.63	0.21	0.34	0.13
Fe K	37.07	12.52	35.74	11.99	34.15	11.22	42.5	15.66
Ni K								
Mo L								
P K								
Totals	100		100		100		100	

Discussion of sample 3, area 1 analysis and results

The images (Figure 20. Sample 3. Area 1 is a filiform corrosion channel. Area 2 is a point in the region below the step. Area 3 is the tip of another filiform corrosion channel. Area 4 is bare metal, exposed by filing the sample before putting it into the SEM.Figure 21) show that area 1 has been attacked by filiform corrosion. EDS analysis shows that the amount of oxygen is the same or is degreasing going from the tail (first analysis) of the channel to the middle (second analysis) and is definitely lower in the pit. This might be consistent with the traditional idea of an oxygen driven concentration cell as a driving mechanism for filiform corrosion, however there should be little or no dissolved oxygen in the system. The trend for silicon is the same as for oxygen. The amount of chromium increases from the tail to the pit at the head and is highest in the unattacked region. The amount of chromium in the pit and on the surface outside the filiform channel is strange if this steel is indeed 1% chromium by weight. It is possible that this chromium came from the shroud ring, which contained about 12% chromium.

Sample 3, area 2 analysis and results

Area 2 is below the step structure on sample 3. The region above the step was pressed tight against the nozzle ring assembly and the region below the step was out of the path of flow but exposed. A micrograph of area 2, showing the step at the top of the image is shown below (Figure 225).

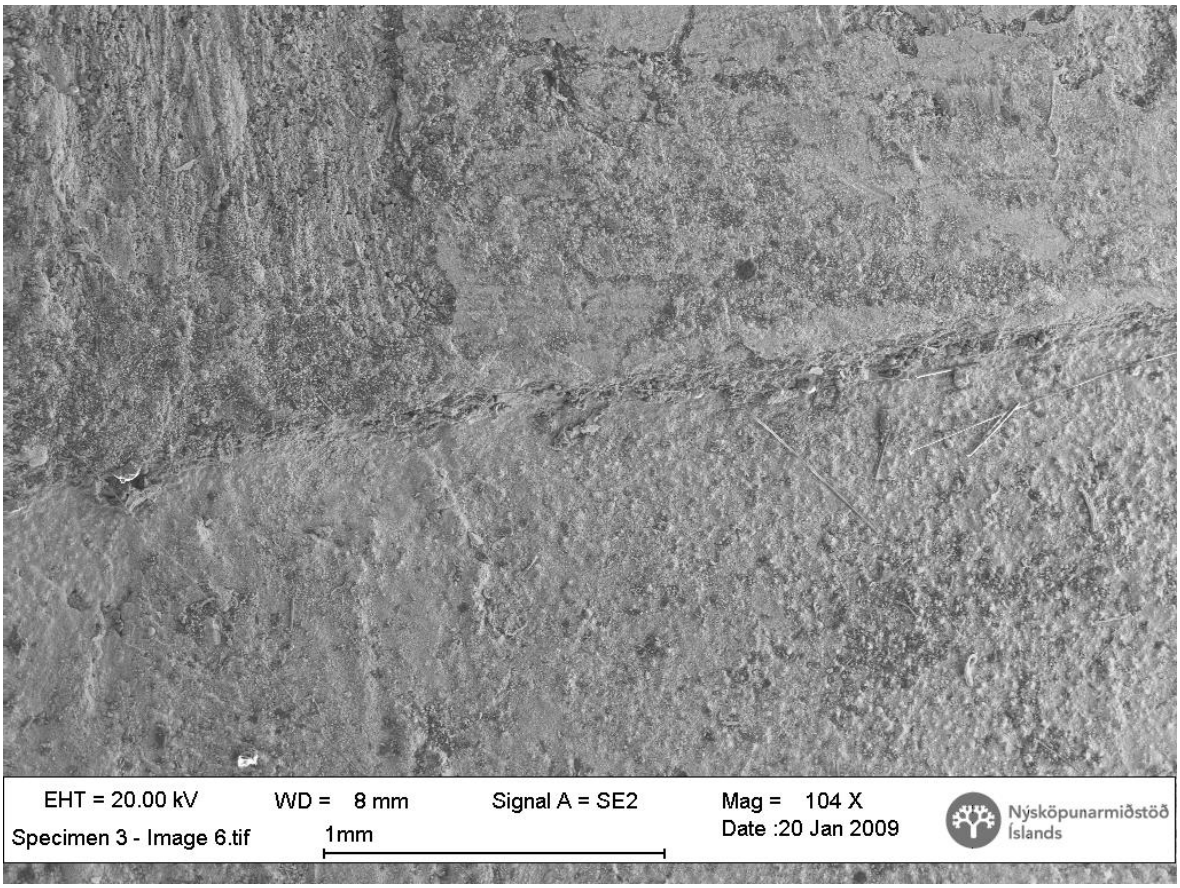

Figure 22. Area 2 of sample 3 can be seen in the bottom half of the image. Running horizontally through the middle of the image is the step structure and in the upper right corner is a filiform channel (area 1).

The compositional analysis is shown in the Table 8. For ease of comparison the results of the analysis outside the channel from area 1 are repeated and shown in the table as well. Neither the region analyzed outside of the channel in area 1 nor area 2 show signs of filiform corrosion. Furthermore, without the aide of magnification or analysis both appear to be covered by the same black corrosion products.

Table 8. Sample 3, area 2 and for comparison, sample 3 area 1 outside the channel.

	Area 2 Analysis		*Outside Channel*	
Element	Weight%	Atomic%	Weight%	Atomic%
C K	35	56.47	32.7	56.02
O K	22.97	27.83	20.48	26.34
Na K	0.31	0.26		
Mg K				
Al K	1.43	1.03	0.2	0.16
Si K	0.87	0.6	0.34	0.25
S K	0.22	0.14	0.2	0.13
Cl K			0.12	0.07
Ca K	0.26	0.13	0.12	0.06
Cr K	2.53	0.94	2.99	1.18
Mn K			0.34	0.13
Fe K	34.98	12.14	42.5	15.66
Ni K	1.44	0.47		
Mo L				
P K				
Totals	100		100	

Discussion of sample 3, area 2 analysis and results

Comparing the micrographs of area 2 (Figure 225) and the outside channel region of area 1 (Figure 21) it can be seen that area 2 has a much rougher appearance. The composition of the two is also different; area 2 has significantly more aluminum, less iron and has nickel. Neither aluminum nor nickel are believed to be part of the composition of the steel in the retaining ring.

The height of the step is about half a millimeter. The depth of the corrosion penetration into the metal of the ring and the amount of material lost shows that under operating conditions the corrosion products must be able to come free from the underlying metal, perhaps flaking off.

Sample 3, area 3 analysis and results

Area 3 is a pit on the opposite end of sample 3 from area 1. A micrograph is shown in

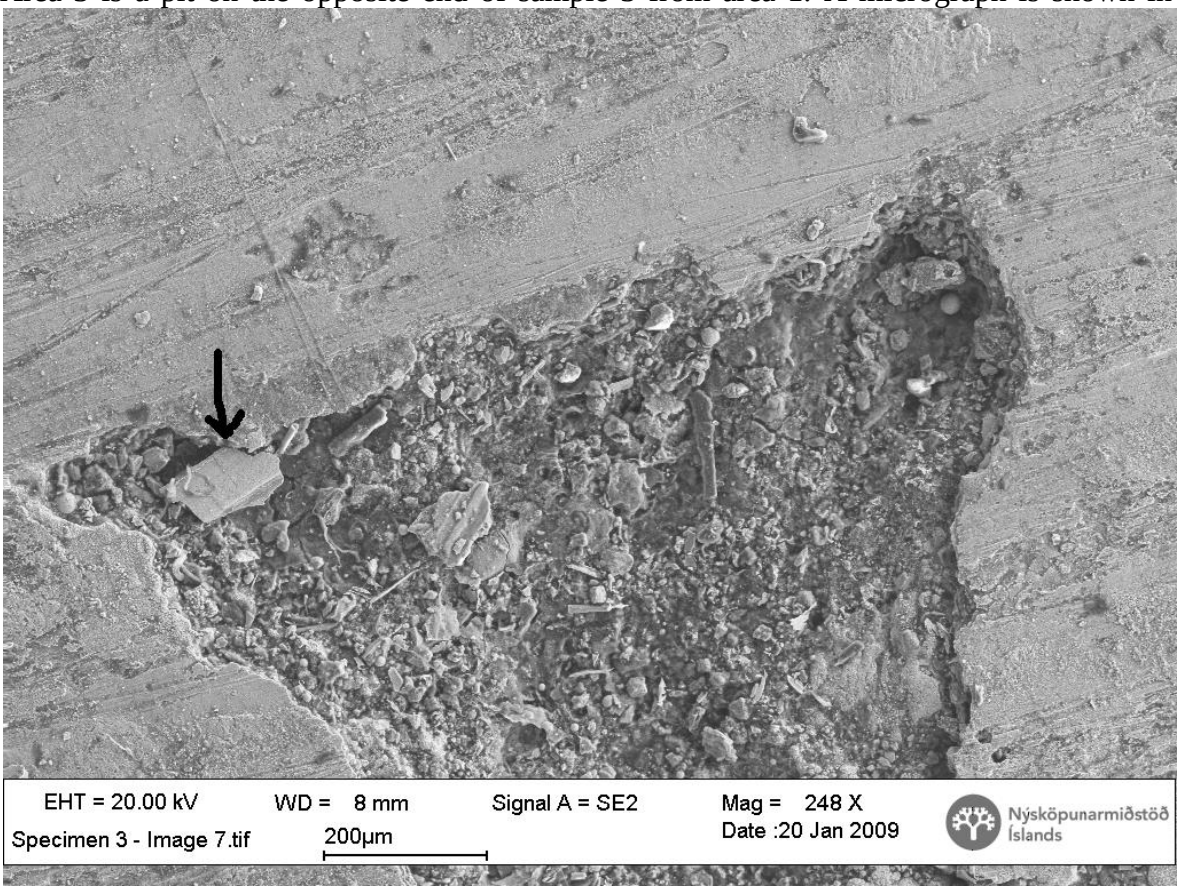

6. The area 3 pit is located at the end of a filiform channel.

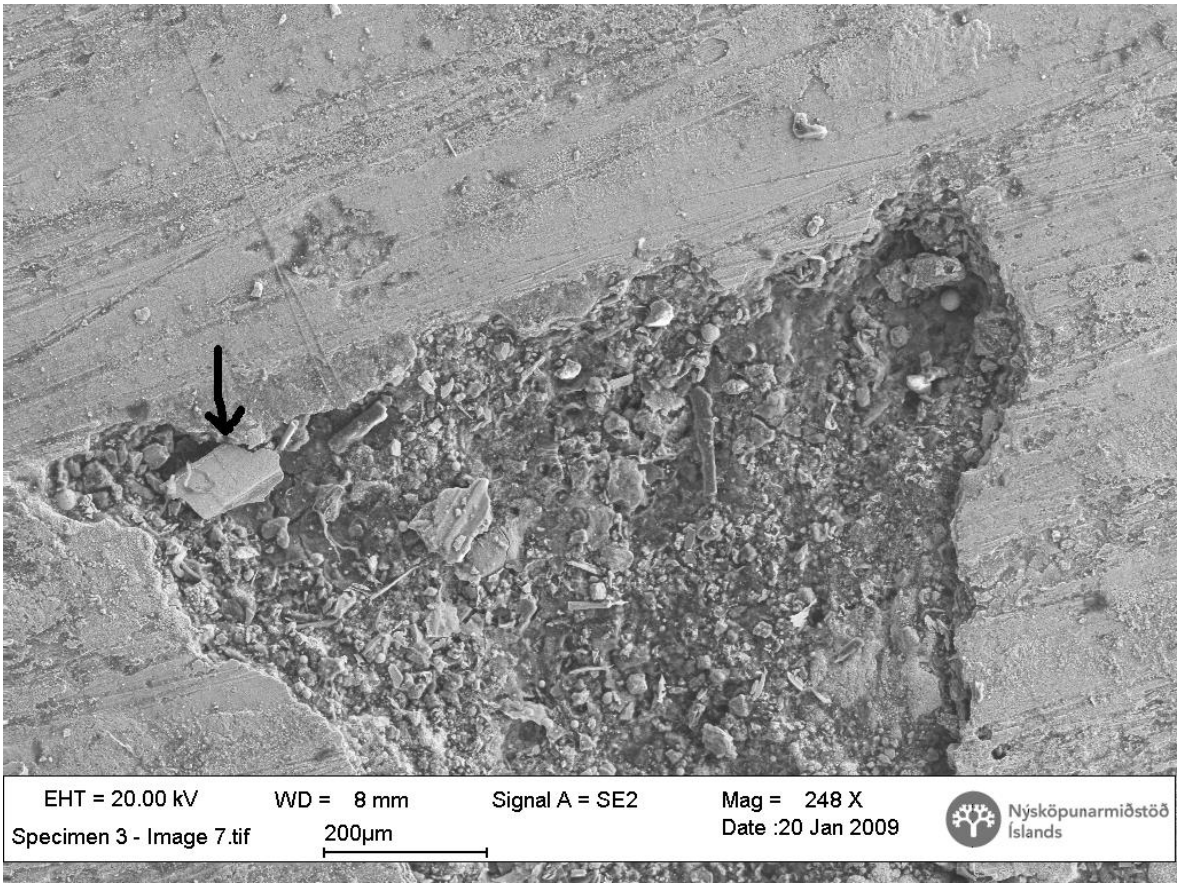

Figure 23. Sample 3, area 3 a pit at the end of a filiform channel at 248X magnification. A particle, analyzed for composition, is marked by the arrow.

X-ray EDS analysis was performed on the area of the pit and on the particle in the pit indicated by the arrow in the image above. The results are given in Table 9 and the analysis of the pit in area 1 is repeated for comparison.

Discussion of sample 3, area 3 analysis and results

In the image above it can be seen that the particle is at the leading edge of the pit and that the surface of the sample appears to nearly overhang the particle. From this it is speculated that the particle had only just broken free of the surface and is relatively unaltered by corrosion or covered by corrosion products. This speculation is supported by the material analyses – the pit analysis did not include the particle but examined the material in the center of the pit, which has much less iron and chromium than the particle. The area 3 pit also has many minor constituents that would not be expected to be alloying elements in the steel of the retaining ring – including magnesium, chlorine, calcium, potassium and copper. It is known that ammonia dissolves copper, alkali and alkaline metals (Maxwell, 2005). It is unclear where in the plant these metals could have been dissolved from and their concentrations are low enough to flirt with the detection limit of the instrument; still it is remarkable to find so many of the metals that are ammonia soluble in one place.

Comparing between the pits of area 1 and area 3, the former is less oxidized and has significantly more iron and chromium, while the latter has more trace elements. It is

unclear why this should be, as they are both pits formed in the same piece of metal under what should be identical conditions.

Table 9. Composition of the pit and large particle in sample 3 area 3 and comparison with the pit in sample 3, area 1.

	Area 3, Pit		*Area 3, Particle*		*Area 1, Pit*	
Element	Weight%	Atomic%	Weight%	Atomic%	*Weight%*	*Atomic%*
C K	51.26	67.72	29.76	51.04	44.32	67.68
O K	24.19	23.99	24.68	31.78	16.5	18.92
Na K	0.5	0.34	0.23	0.21		
Mg K	0.18	0.12			0.15	0.11
Al K	0.94	0.55	0.27	0.21	0.28	0.19
Si K	1.65	0.93	0.58	0.43	0.46	0.3
S K	0.64	0.32			0.44	0.25
Cl K	0.28	0.13				
Ca K	0.67	0.26			0.34	0.15
Cr K	0.5	0.15	1.09	0.43	2.73	0.96
Mn K	0.26	0.07	0.34	0.13	0.63	0.21
Fe K	18.21	5.17	42.38	15.63	34.15	11.22
Ni K						
Mo L			0.66	0.14		
K K	0.37	0.15				
Cu K	0.36	0.09				
Totals	100		100		100	

Sample 3, area 4 analysis and results

Area 4 is a corner of the sample that was filed down to bare metal just before being placed in the SEM. Analysis of this area and comparison with the corrosion products from the first 3 areas of sample 3 will help to establish the mobility, or lack thereof, of corrosion products in the turbine section of the power plant. Two micrographs of area 4 are shown in Figure 24. They show the regions analyzed for composition.

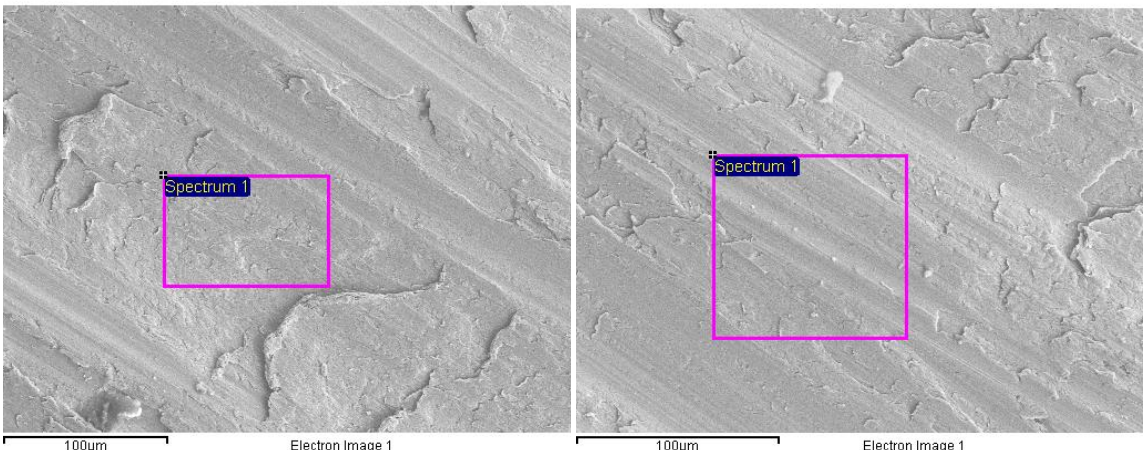

Figure 24. Sample 3, area 4, bare metal exposed by filing away the corrosion products prior to analysis. Images show the areas over which two analyses for composition were carried out.

The results of the compositional analysis are given in

Table 10 along with the composition of the particle in area 3, to substantiate or negate the earlier suggestion that it is of nearly unaltered metal and the composition of the area 3 pit to illustrate the migration of corrosion products.

Table 10. Sample 3, area 4, composition of the base metal of the retaining ring.

	Area 4, Analysis 1		*Area 4, Analysis 2*		*Area 3, Particle*		*Area 3, Pit*	
Element	Weight%	Atomic%	Weight%	Atomic %	Weight%	Atomic %	Weight%	Atomic %
C K	5.82	22.29	2.15	9.23	29.76	51.04	51.26	67.72
O K					24.68	31.78	24.19	23.99
Na K					0.23	0.21	0.5	0.34
Mg K							0.18	0.12
Al K					0.27	0.21	0.94	0.55
Si K	0.31	0.51	0.22	0.41	0.58	0.43	1.65	0.93
S K	0.03	0.04	0.14	0.23			0.64	0.32
Cl K							0.28	0.13
Ca K							0.67	0.26
Cr K	1.02	0.9	0.99	0.98	1.09	0.43	0.5	0.15
Mn K	0.5	0.42	0.68	0.63	0.34	0.13	0.26	0.07
Fe K	91.84	75.61	95.64	88.41	42.38	15.63	18.21	5.17
Mo L	0.48	0.23	0.18	0.1	0.66	0.14		
K K							0.37	0.15
Cu K							0.36	0.09
Totals	100		100		100		100	

Discussion of sample 3, area 4 analysis and results

From the analysis it can be seen that the steel of the retaining ring contains about one percent chromium, half a percent of manganese, less than half of one percent of molybdenum and silicon and trace amounts of sulfur. As has been stated before, attempts at explaining the amount of carbon shown by the analysis are deferred to the end of this chapter. The weight percentage for carbon in low alloy steels is normally less than half of one percent.

Looking at the composition of the particle from area 4, it has a similar mass fraction of chromium to the base metal and both the particle and base metals have molybdenum (though in varying amounts) and the corrosion products do not seem to contain molybdenum. Where the molybdenum goes when the metal corrodes is another mystery, given that it is a minor constituent. Perhaps the increase in weight percent of oxygen (and the mysterious carbon) simply pushes molybdenum below the instrument's detection limit. The amount of silicon on the particle is higher than the base metal but lower than in the pit. The base metal has no aluminum or sodium while the particle has amounts greater than zero but less than the amounts found in the pit. It seems likely therefore that the elements

not found in the base metal but found on the particle and all of the trace elements found in the pit must have been transported with the ammonia-water working fluid, either as dissolved ions or as eroded particles.

6.1.4 Discussion of Sample 3

Oxidation along the filiform channels could be consistent with an oxygen concentration corrosion cell. On the other hand the generally accepted theory of acidification at the head of the filiform channel (Ahmed, 2006) is difficult to reconcile with the ammonia working fluid, which is basic and would neutralize any acid produced.

Significant amounts of aluminum and nickel were found below the step (area 2) and neither was a part of the low alloy steel the retaining ring was made from. Aluminum and copper and magnesium were found in the pit in area 3.

When the plant first began operation in June of 2000, the nozzle ring assembly contained an aluminum alloy sealing ring. This ring was the first casualty of the erosion-corrosion problem in the turbine; within a few moths it had all but disintegrated (Figure 25. The aluminum sealing ring, destroyed within a few months of plant operation. Seen here sitting on the nozzle ring assembly.). Aluminum is frequently alloyed with copper with 2xxx series alloys having as much as 6% copper (Liverpool). The aluminum alloy is also a possible source for magnesium. It is known that copper dissolves in ammonia and that aluminum can be etched by high concentrations of ammonia (The Columbia Encyclopedia, Sixth Edition).

Nickel was used to plate the nuts inside the turbine. The nickel plating that remains shows no sign of corrosion but it has flaked off in places suggestive of erosion. Nickel also could have come from the erosion of the 316 stainless steel pacer ring (sample 2). Nickel is not soluble in ammonia.

The transport of aluminum and copper from inside the nozzle ring assembly to crevices formed by the back of the assembly and the retaining ring and nickel from the plating on the nuts or the spacer ring to the shielded side of the retaining ring is suggestive of a violent and complex flow path. It might also be explained by the turbine repeatedly being taken apart and reassembled, with bits of warn material flaking off onto the gloves of the plant operators and then being deposited on other parts of the turbine – but this mechanism of transport seems more likely to lead to larger discrete particles that would have been seen on the micrographs.

Figure 25. The aluminum sealing ring, destroyed within a few months of plant operation. Seen here sitting on the nozzle ring assembly.

6.1.5 Sample 4

Sample 4 consists of two mild steel cylinders that were placed into the flow stream for several weeks as part of a materials test prior to the current thesis. As pictured in Figure 26, the cylinder on the left, labeled 1, was put in place between the separator and the turbine while cylinder 2, on the right, was placed in the turbine exhaust. Cylinder 1 has developed a hard dark shell of corrosion products typical of most of the piping in the plant while 2 has an uneven, soft, gray surface like the inside of the turbine and the first meters of the turbine exhaust.

Figure 26. Sample 4: 1 is a mild steel cylinder exposed to the conditions between the separator and the turbine, 2 is a cylinder made of the same material but exposed to the conditions of the turbine exhaust.

Sample 4, cylinder 1 analysis and results

The micrographs in Figure 27 show the surface structure of cylinder 1. From the images it can be seen that the surface has bands of flat metal separated by narrow grooves filled with what are probably corrosion products.

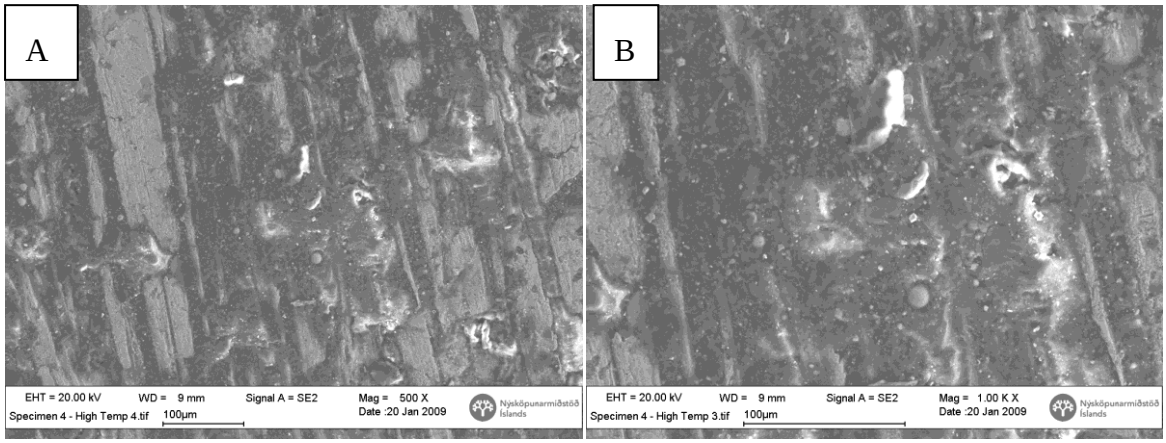

Figure 27. Sample 4, cylinder 1. The two images show that the surface of the cylinder is made up of small bands of flat, exposed metal and narrow grooves filled with material thought to be corrosion products. Image A was taken at 500X magnification while B shows the surface at 1 000X magnification.

Four X-ray EDS analyses were made of cylinder 1. The regions analyzed can be seen in micrographs in **Error! Reference source not found.**. The regions are: A, the exposed etal surface of one of the bands; B, the contents of one of the grooves; C, a crystal found in one of the grooves and D, the background material surrounding the crystal. The results of the analysis can be seen below (Table 11).

Table 11. Surface composition of sample 4, cylinder 1.

	Exposed Metal		*Groove Material*		*Crystal Analysis*		*Background Analysis*	
Element	Weight%	Atomic %	Weight%	Atomic %	Weight%	Atomic %	Weight%	Atomic %
C K	20.07	41.42	55.65	70.39	7.5	17.07	50.94	74
O K	20.63	31.96	23.1	21.93	30.89	52.76	11.6	12.65
Na K	0.35	0.38	1.81	1.19			1.63	1.24
Mg K			0.21	0.13			0.5	0.36
Al K			0.47	0.26			0.34	0.22
Si K	0.14	0.13	1.22	0.66			0.91	0.56
P K			0.18	0.09			0.2	0.11
S K			0.52	0.24			0.22	0.12
Cl K			1.68	0.72			0.58	0.29
K K			1.22	0.47			0.61	0.27
Ca K			0.81	0.31			0.26	0.11
Ti K			0.24	0.08				
Mn K	0.83	0.37	0.24	0.07	2.26	1.12	0.38	0.12
Fe K	57.99	25.74	12.66	3.44	59.35	29.04	31.83	9.94
Totals	100		100		100		100	

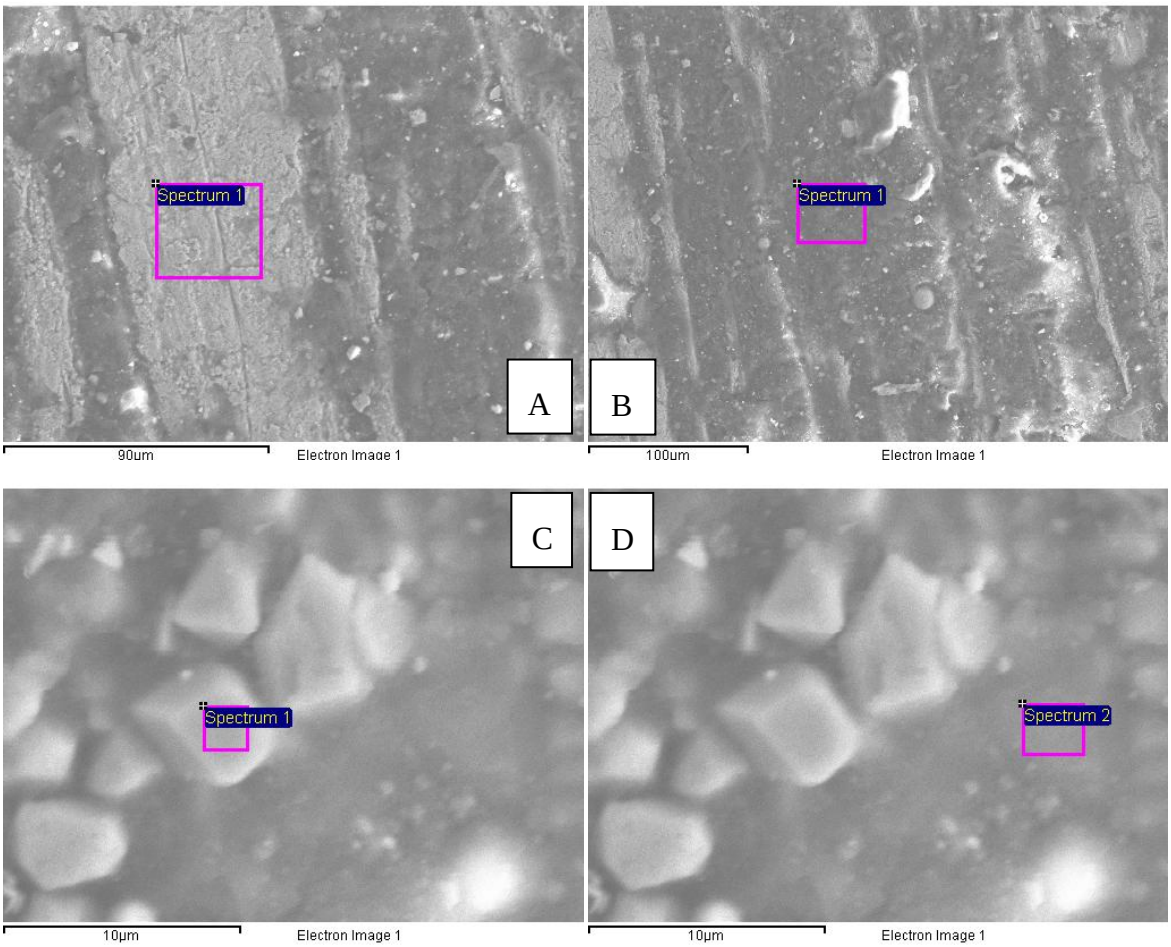

Figure 28. The four regions analyzed by X-ray EDS on sample 4, cylinder 1.

Discussion of sample 4, cylinder 1 analysis and results

From the micrographs it can be seen that two different conditions exist on the surface of cylinder 1: flat bands on which corrosion does not seem to be having an effect and narrow grooves which are filled with material not present on the flat bands. It is unclear what caused these grooves. They may be from the machining of the cylinder and simply formed a place for corrosion to begin. In any case the corrosion does not seem to be damaging to the cylinder, instead the corrosion products have formed a sort of film (from a macroscopic perspective) over the entire cylinder.

The compositional analysis shows that the flat bands are mostly iron and iron oxide. Manganese and silica are probably alloyed in the steel cylinder while the sodium is probably a contaminant and not from the base metal. The material in the groove is far more diverse in composition as all of the contaminants seem to be concentrated there – it is possible that this is related to the drying process. As the film of ammonia and water evaporated from the surface, the raised flat surfaces would have been the first to dry and the liquid film would have pulled back into the grooves where it would have taken longer to dry, being less exposed to the atmosphere. If the contaminants were dissolved in the liquid as the edges of the film receded into the grooves, the ions would have become concentrated there.

In micrographs C and D of Figure 28, crystals can be seen that are very similar to the crystals found on sample 2, area 1 (Figure 14). However the composition of crystals is somewhat different. The crystals found on sample 1 had a significant amount of chromium while the crystals on cylinder A had no chromium and a greater amount of manganese. In both cases however the crystals were mainly iron oxides.

Sample 4, cylinder 2 analysis and results

Cylinder 2 is made of the same metal as cylinder 1 but was installed on the low pressure side of the turbine and exposed to the exhaust. From talking with the plant manager, it is believed that the exhaust contained 6 to 7 percent liquid. Micrographs of cylinder 2 are shown in Figure 29.

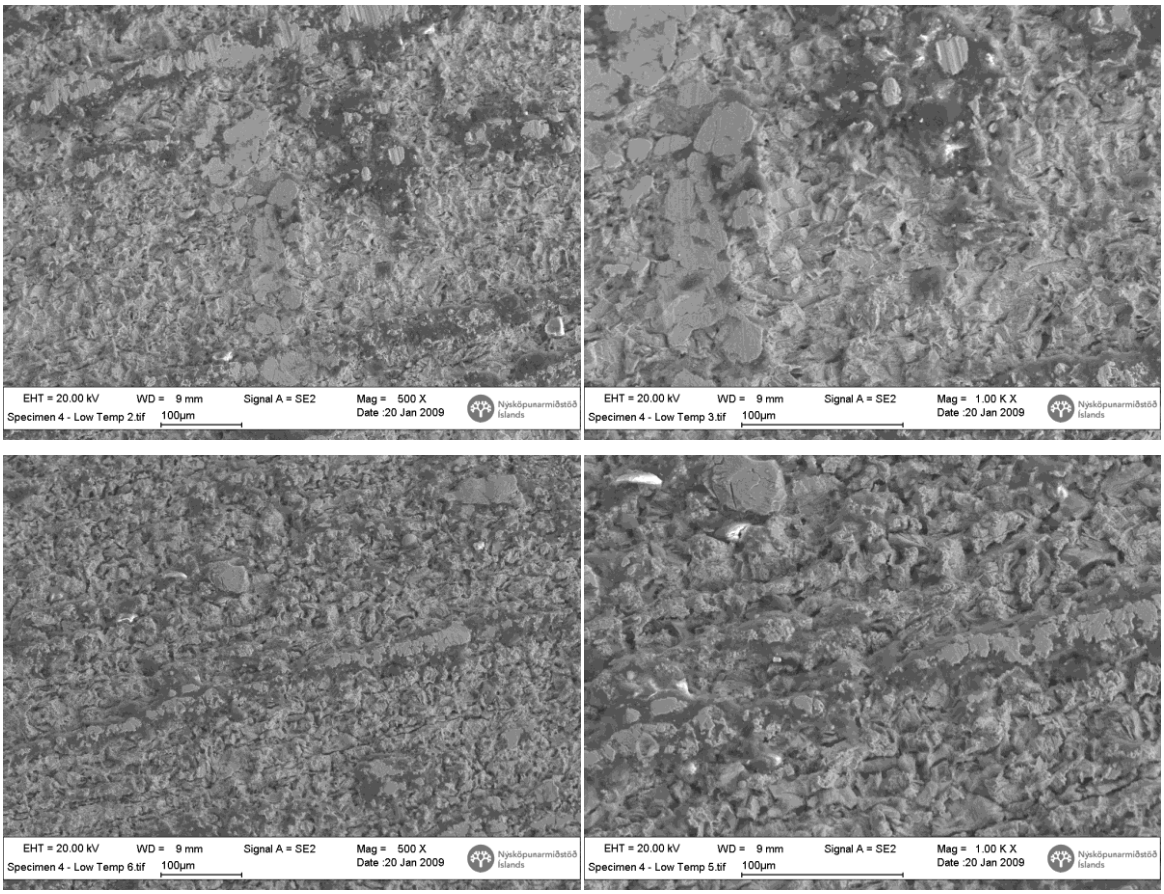

Figure 29. Sample 4, cylinder 2. Micrographs A and C show different regions of the cylinder at 500X magnification. B and D show the same regions as A and C respectively but at 1000X magnification.

Two analyses were made of different regions on cylinder 2 by X-ray EDS, the results are reported in Table 12. No specific structures on the surface were targeted by the analysis and both are averaged compositions taken of regions several hundred microns across. The

composition of the exposed metal from cylinder 1 and the material in the grooves of that cylinder are included for comparison.

Table 12. Surface composition of sample 4, cylinder 2 and compositions of the exposed metal and groove material of cylinder 1 for comparison.

	Cylinder 2, Analysis 1		*Cylinder 2, Analysis 2*		*Cylinder 1, Groove*		*Cylinder 1, Metal*	
Element	Weight %	Atomic%	Weight %	Atomic%	Weight %	Atomic%	Weight %	Atomic %
C K	29.88	58.42	26.06	55.24	55.65	70.39	20.07	41.42
O K	10.96	16.09	9.04	14.39	23.1	21.93	20.63	31.96
Na K					1.81	1.19	0.35	0.38
Mg K					0.21	0.13		
Al K	0.22	0.19	0.42	0.47	0.47	0.26		
Si K	0.63	0.52	0.19	0.18	1.22	0.66	0.14	0.13
P K					0.18	0.09		
S K	0.21	0.16	0.51	0.46	0.52	0.24		
Cl K	0.36	0.24	0.19	0.15	1.68	0.72		
K K	0.21	0.12	0.31	0.22	1.22	0.47		
Ca K	0.54	0.32	0.16	0.1	0.81	0.31		
Cr K	0.21	0.09	0.37	0.23				
Ti K					0.24	0.08		
Mn K	0.53	0.23	0.61	0.28	0.24	0.07	0.83	0.37
Fe K	55.66	23.4	61.22	27.91	12.66	3.44	57.99	25.74
Cu K	0.61	0.23	0.93	0.37				
Totals	100		100		100		100	

Discussion of sample 4, cylinder 2 analysis and results

In the micrographs it can be seen that the surface of cylinder 2 is much rougher than cylinder 1 and also that it seems to have less of the corrosion products attached to it. The flat bands of metal on cylinder one seem to have broken off leaving an irregular surface behind.

The X-ray EDS analyses of cylinder 2 show that both of the regions analyzed have the same composition with only slight variations that might be as much a matter of instrument error as true differences in composition.

In comparison with the material in the grooves of cylinder 1, cylinder 2 has less foreign material present including no sodium, magnesium, phosphorous or titanium and significantly less potassium and chlorine. The biggest difference is in the amount of iron

between the two; the groove having dramatically less, with oxygen and carbon taking its place.

Comparison between the metal bands on cylinder 1 and the surface composition on cylinder 2 show similar amounts of iron but only half as high a concentration of oxygen on cylinder 2. Possibly unoxidized iron is exposed on the surface of cylinder 2 or the breaking off of the corrosion products has left a thinner oxide layer.

6.1.6 Discussion of Sample 4

Sample 4 is important because it was only exposed to the conditions in the plant for a few weeks. It shows how the corrosion and possibly erosion in the case of cylinder 2 begin.

Cylinder 1 illustrates what happens on the high pressure side of the turbine – corrosion seems to begin and be most intense in the grooves. It is unclear if these grooves are from machining or from the corrosion itself. The increased intensity of corrosion in the grooves might be because any liquid condensate forming on the cylinder would be pushed toward the grooves by the flowing vapor stream and, depending on the angle of contact between the liquid and the metal (a liquid-metal interaction dependent property), wetting the groove might allow the liquid to minimize the energy related to surface tension on a free surface. Contaminants also seem to accumulate in the groves, though what roll, if any, they play in the corrosion is unknown. It is known that over longer periods of time the corrosion products form a thick black film in the region as seen in the photo below of the turbine inlet (Figure 30). One hypothesis is that corrosion starts in grooves and defects already existent in the metal surface and spreads from there. It is also possible that the grooves are themselves products of the corrosion process.

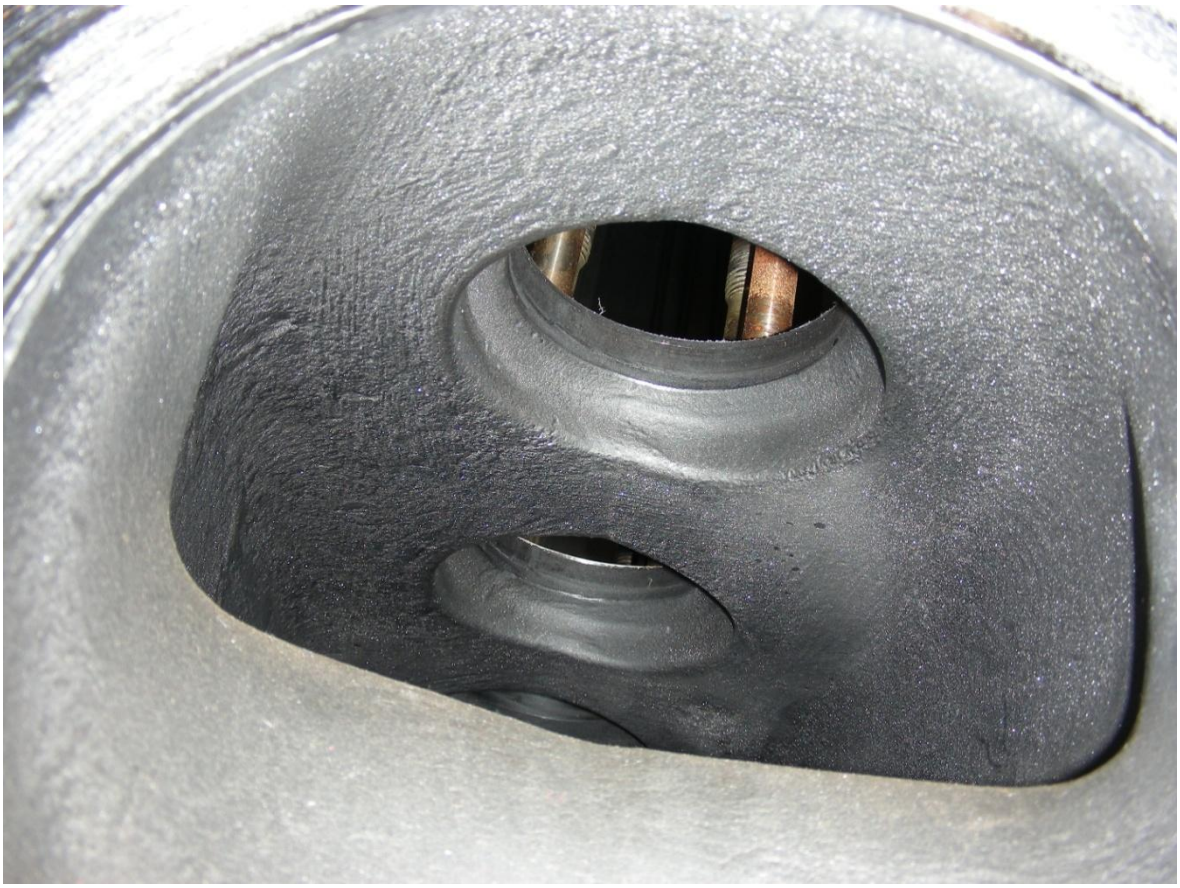

Figure 30. Inlet to the turbine housing coated with black corrosion products.

Cylinder 2 illustrates how the erosion of material begins in the turbine and in the turbine exhaust. Comparing the images of cylinder 1 to cylinder 2 (Figure 27 & Figure 29), on the second cylinder the well defined structure of grooves and flat bands is missing and so is the buildup of corrosion products they contained. Again comparing the surface compositions of the two cylinders, the surface or surface corrosion products of cylinder 2 seem to break off before they can reach the same level of oxidation as cylinder one, or possibly the oxide grains break off soon after forming, thus offering no protection from further corrosion.

6.1.7 The Duplex Steel Pin from Sample 1

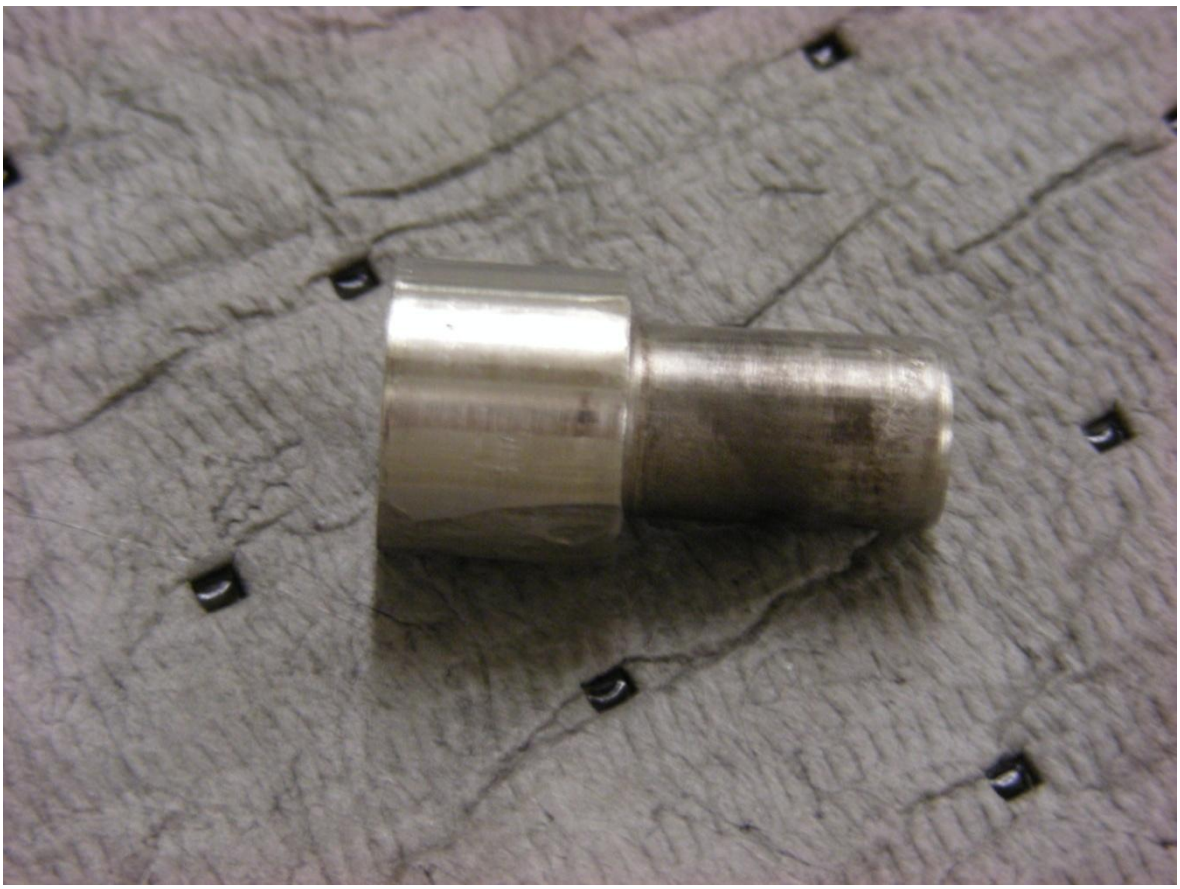

Figure 31. The pin from sample 1, the nozzle vane for the GE-Rotoflow turbine.

The duplex steel pin (Figure 31) is from sample 1, the nitronic 60 nozzle vane of the newer GE-Rotoflow turbine. Sample 1 was too big to put under the microscope but the pin gives an example of a material from the new turbine that did not have corrosion problems. A micrograph on the following page shows the surface of the pin and the region analyzed by X-ray EDS (Figure 32).

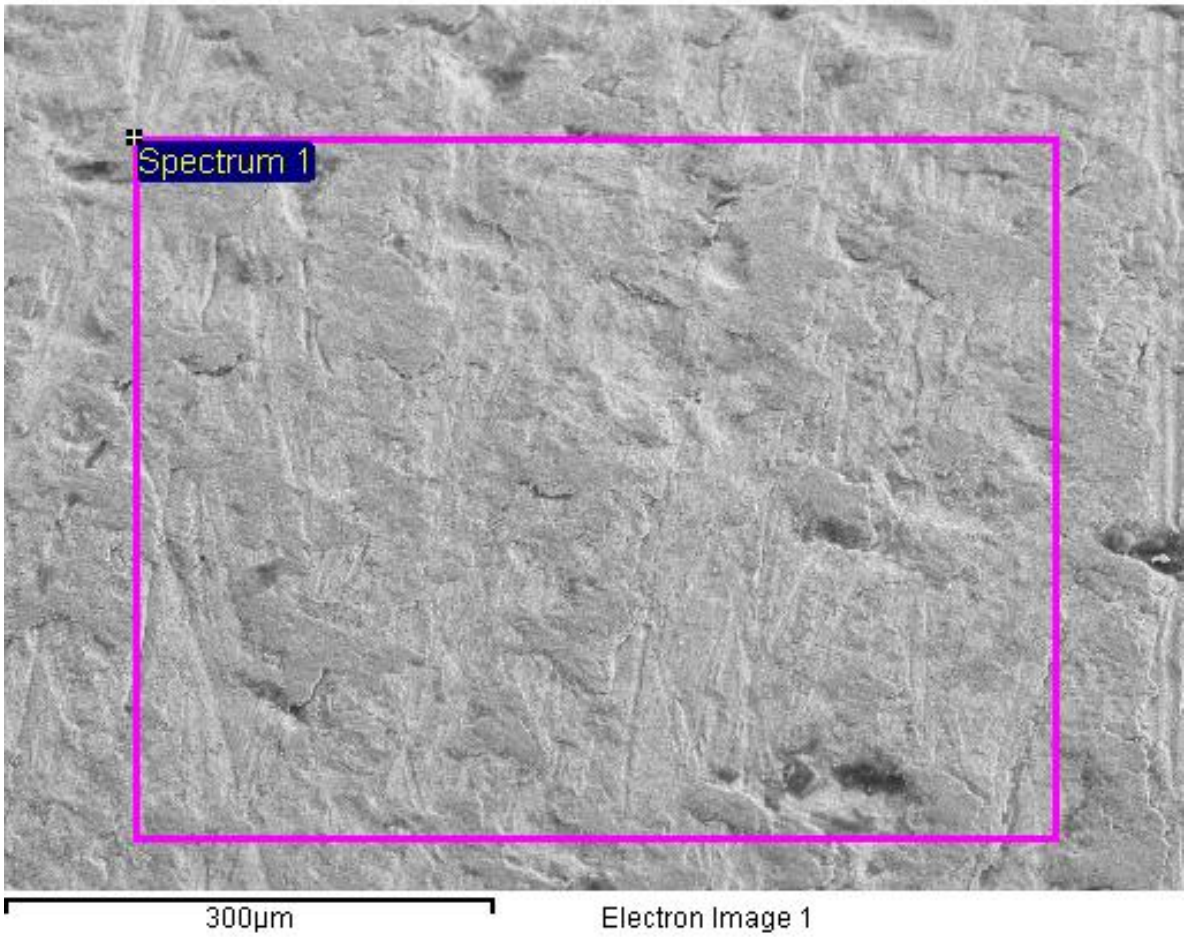

Figure 25. Figure 32. Surface of the duplex steel pin at 500X magnification. Defects in the surface can be seen but the black corrosion products are absent.

The results of the X-ray EDS are presented in Table 13. Additionally the results of the analyses for the 316 stainless steel exposed in the channel of sample 2, area 2, the bare metal of sample 3, area 4 and the metal flat metal band of sample 4, cylinder 1 are presented for comparison.

Table 13. Surface composition of the duplex steel pin and other metals from the system for comparison. The other metals are 316 stainless steel from sample 2, area 2, bare metal from sample 3, area 4 and metal from a flat exposed band on sample 4, cylinder 1.

	Duplex Pin Analysis		*316 SS Analysis 1*		*Bare Metal Analysis*		*Metal Band Analysis*	
Element	Weight%	Atomic%	Weight%	Atomic%	Weight%	Atomic%	Weight%	Atomic%
C K	20.7	42.36	13.46	36.73	5.82	22.29	20.07	41.42
O K	20.3	31.17	8.42	17.24			20.63	31.96
							0.35	0.38
Si K	0.69	0.6	0.48	0.56	0.31	0.51	0.14	0.13
S K					0.03	0.04		
Cr K	14.68	6.94	16.15	10.18	1.02	0.9		
Mn K	2.01	0.9	1.14	0.68	0.5	0.42	0.83	0.37
Fe K	37.88	16.67	49.01	28.75	91.84	75.61	57.99	25.74
Ni K	2.46	1.03	9.18	5.12				
Mo L	1.28	0.33	2.16	0.74	0.48	0.23		
Totals	100		100		100		100	

6.1.8 Discussion of Duplex Steel Pin

This pin was not directly exposed to the flow of the working fluid, unlike for instance the 316 stainless steel spacer ring of sample 2. However, as seen from the example of sample 3, the retaining ring, the surfaces not exposed to flow were still subject to corrosion and the duplex pin, the nitronic 60 nozzle vane it was attached to and the nozzle ring they were both mounted on all could have been sites for crevice or filiform corrosion, but no sign of this is present.

Like sample 4, cylinder 1 the duplex steel pin can be seen to have surface defects and grooves from machining (though these grooves are smaller than on cylinder 1). Unlike cylinder 1, these surface features do not appear to have attracted corrosion.

From the compositional analysis it can be seen that the duplex steel is similar in composition to 316 stainless steel but with less nickel and molybdenum and more manganese. As explained in the section on steels in an earlier chapter duplex steel has a different microstructure than 316 stainless steel, which gives it similar corrosion resistance but superior mechanical properties (IMOA, 2001). Though this pin was in a sheltered environment, the superior mechanical properties might also help against erosion.

6.2 Discussion of SEM Results and Analysis

The examination of samples from the turbine has progressed from a sample taken from the inlet side of the turbine (sample 2) to the outlet side (sample 3). Two test cylinders (sample 4) were examined, both made of the same material but one had been exposed to the inlet conditions and the other the conditions in the turbine exhaust. Finally a duplex steel pin from the newer turbine (from sample 1) was examined and found to be free of corrosion.

Sample 4, cylinder 1 and Figure 30 show what happens to low alloy steels in the high, pressure (30 -35 bar), high temperature (115 – 118 °C) environment between the separator and the turbine. A film of black corrosion products forms on the surface of the metal but the metal does not seem to be damaged and there does not seem to be a loss of material.

Because the working fluid is not super heated, what comes out of the separator is an ammonia rich vapor in equilibrium with a liquid dew that is about 53% water. The pipe between the separator and turbine is not a perfect insulator and some heat can be lost through the pipe walls – therefore, at the walls condensation is taking place and a thin film of liquid will be present.

Sample 2 comes from the region of the turbine inlet. The temperature and pressure are nearly the same as in the pipe from the separator but the vapor is being channeled from the larger diameter of the pipe, through the constriction presented by the nozzle vanes. The vanes are shown in Figure 33. Continuity requires a flow, presented with a restriction, to increase in velocity.

On sample 2 there are channels corresponding to the flowing vapor and there are regions in the channels in which there do not appear to be any corrosion products (sample 2, area 2). This suggests that these channels were formed purely by erosion and not by corrosion.

There are also areas on sample 2 that were covered by the nozzle vanes themselves (sample 2, area 1). On the 316 stainless steel spacer ring there does not appear to have been any corrosion in these areas. It is speculated that the corrosion products found there came from the nozzle vanes and in Figure 33 it can be seen that the nozzle vanes do look like they were corroding where they were in contact with the spacer ring. It is very possible, perhaps even probable, that vapor penetrated into the crevice between the spacer ring and nozzles and then condensed on the surfaces there.

Sample 4, cylinder 2 and the back of sample 3 (see Figure 19) seem to have the same sort of corrosion as the turbine, nozzle vanes (particularly the second stage nozzle vanes) and the turbine exhaust pipe. They have a dull grey color and a rough texture. The conditions at this stage of the turbine were cooler and lower in pressure (mid 50's °C and 5.5 – 6.5 bar). Also, significant condensation had taken place during the expansion (about 5-7% liquid).

Based on the micrographs of sample 4, cylinder 2 and the X-ray EDS analysis of the surface, whatever corrosion products that form are breaking off and offer no protection from further corrosion.

Figure 33. The first stage nozzle vanes, which were flush against the spacer ring that sample 2 comes from. Signs of corrosion can be seen on the face of the nozzles.

The step on the shielded face of sample 3 is at odds with the observations made about the corrosion between the separator and the turbine inlet. Both cases involve the same metal and the corrosion products look similar but the existence of the step clearly indicates that material is being removed in one case, while in the other case loss of material is not noticed.

The filiform corrosion seems indicative of an aggressive medium, either an acid or a solution with dissolved oxygen. On the other hand ammonia at such high concentrations would neutralize any acid. There is no reason to believe a significant amount of dissolved oxygen could be present in the system, based on the way in which the plant operates.

As was suggested for the crevice corrosion between the nozzle vanes and the spacer ring, it could be that vapor was penetrating into the crevice between the retaining ring and the nozzle ring assembly and then condensing.

It is unknown if something about the tight confines of the crevice might be conducive to having more water in the liquid phase there. It is found in the literature (Roberge, 2008) that in cases of filiform corrosion of steels, initially pH neutral water can attain a pH of 1-4 at the head of the corrosion channel.

From the duplex steel pin and other materials used in the newer GE-Rotoflow turbine, none of which seem to have corroded significantly, it can be seen that it is possible to select materials that will not corrode in the Kalina cycle environment.

The discussion of carbon in the X-ray EDS analyses has been put off to this point because there is no really satisfying answer. It is known that this type of analysis tends to overestimate the amount of carbon present, usually by a few percent. This can be seen from the analysis of the bare steel from sample 3 in

Table 10. Is also known that in handling the samples dirt and grease can rub off from finger tips to the sample surface and this also might lead to an error of a few percent. Standards were not used during the analysis, which could again add a few percent to the uncertainty of the measurement but some of the measurements showed 30 – 60 wt. % carbon on the surface.

An applications specialist from Oxford instruments (makers of the X-ray EDS instrument) has looked at the project file generated by the SEM and confirmed that the instrument was operating normally. There is no nitrogen present and there is a significant amount of carbon present on the samples.

One hypothesis to explain the carbon is that it is from the metal itself. Steels contain a small amount of carbon, present as cementite as well as interstitial defects and at grain boundaries. In this hypothesis the iron is oxidized to a corrosion product and flakes off, leaving the carbon behind. A possible shortcoming of the hypothesis is that it does not explain why the carbon is found where it is on the samples. If the carbon is from the steel and the iron has oxidized and been removed, the carbon might be expected to be high at metal surfaces and low in the corrosion products, which would be mostly iron oxides. Looking at sample 4, cylinder 1, in Figure 27 and Table 11, it can be seen that the highest concentration of carbon is in the corrosion products in the grooves (56 wt. %) while the metal bands have much lower carbon content (20 wt. %).

One way to test the hypothesis might be to vary the accelerating voltage of the SEM; a higher voltage would penetrate deeper into the sample and have a higher interaction volume. It would be consistent with the hypothesis for a low accelerating voltage (surface scanning) to show more carbon than a high accelerating voltage (deep scan). According to the hypothesis, the iron was lost from the surface, and carbon was left in an enriched percentage.

Another hypothesis might be that a hydrocarbon contaminant (perhaps a lubricant used in one of the pumps or bearings) got into the system and coated the surfaces. Ammonia is a good solvent but after the ammonia was drained from the turbine and pipes some of it would be left clinging to the surface and when it evaporated anything in the ammonia, like a dissolved lubricant, would be left on the surface.

A way to test this hypothesis might be to try to desorb the hydrocarbon (if it is there) from the surface with a solvent – similar to liquid chromatography. The solvent could then be filtered and analyzed.

7 CONCLUSIONS

- Based on photographs of the plant and talking with the plant manager, corrosion happens everywhere in the plant but in most places the corrosion products form a protective film, inhibiting further corrosion. Only in the turbine and turbine exhaust sections of the plant is material loss observed.
- Ammonia-water fluid can be quite aggressive despite being quite basic, as seen in the filiform corrosion of sample 3.
- Why the working fluid is aggressive is unknown and requires further investigation

7.1 Recommendations for the further study of why the working fluid is aggressive:

- Analyze the fluid for dissolved oxygen (there should not be any but it would explain aggressive corrosion under basic conditions) and dissolved CO_2 which could alter the chemistry of the working fluid and be a source of carbon.
- Find or create a Pourbaix diagram (potential-pH diagram) for steel at the temperatures present in the plant.
- More precise analysis of corrosion products.

7.2 Hypotheses

Several hypotheses attempting to explain the material loss in the turbine section have been suggested, including stray current corrosion, selective dissolution, galvanic corrosion, crevice corrosion, erosion corrosion and uniform corrosion.

7.2.1 Stray current corrosion and magnetically induced current corrosion

It is observed that the loss of material due to corrosion occurs only in the turbine and in the first meter or two of the turbine exhaust pipe. In the absence of any other explanation for corrosion problems, it was hypothesized that in this specific area a stray current from the nearby generator may have been responsible for the corrosion.

This has been previously investigated (Ögmundsson, 2003) with inconclusive results. The investigator, a consulting electrical engineer named Lúðvík Ögmundsson, reported that some of the corrosion/erosion reminded him of something he had seen in hydrogen electrolysis, which he described as "galvanic erosion". In the course of the investigation it was determined that the KK&K turbine wheel was magnetically polarized.

A time variant magnetic field would lead to induced current in conductive materials like the turbine housing and exhaust pipe according to Faraday's law of induction

Equation 31

$$E = -\frac{d\varphi_B}{dt}$$

Where E is the electromotive force (induced voltage) and the derivative is the rate of change of the magnetic flux through a surface.

A magnetic field would also act upon charged particles (ions) in the electrolyte solution. It is known that water can deprotonate and that ammonia can take up protons to form ions

Equation 32

$$H_2O \leftrightarrow OH^- + H^+$$

$$NH_3 + H^+ \leftrightarrow NH_4^+$$

It is these ions that make the ammonia water solution capable of conduction electricity as an electrolyte.

It has been observed (Valdimarsson, 2009) that the steel which corroded in the turbine and in the turbine exhaust was ferritic and not austenitic. This observation lead to the hypothesis that the corrosion might be related to magnetic interactions between steel and the ions in solution and or magnetically induced current.

It is concluded that stray current, induced current and magnetism are not causes for corrosion in the turbine and turbine exhaust.

- Stray current would follow the path of least electronic resistance. That would be transported through the metal of the turbine housing (a Faraday cage). There is no reasonable path to completing a circuit that would include current passing through the metal surfaces inside the turbine housing, into or out of the electrolyte.
- Current induced by the magnetic turbine wheel would likewise stay in the turbine housing, not crossing out of the surface. It is true that magnetic fields can cause the migration of ions in solution and this has been investigated with respect to corrosion (Sueptitz, Koza, Uhlemann, Gebert, & Shultz, 2008). However the rate of migration is very slow in comparison to the rate at which the turbine was spinning (over 10,000 rpm) and the effect of the rapidly alternating direction of the magnetic field on ionic transport should therefore be nil.
- With respect to the corrosion only occurring on material capable of ferromagnetism, it is noted that nickel is also a ferromagnetic metal but the nickel plating did not appear to be corroding.

7.2.2 Selective dissolution

It is known that steel is heavily recycled and this can lead to unexpected micro-constituents in the parts per million range. If an ammonia soluble constituent, like copper, were present in the steel of the turbine it would be selectively leached out, leaving the steel weakened and susceptible to erosion. This could be tested by dissolving a section of the turbine in acid and analyzing by ICP-AES.

It is concluded that selective dissolution is not responsible for the material loss in the turbine.

- Carbon steel is used with ammonia in other industries and no reports can be found of selective dissolution.
- Within the plant at Húsavík the loss of material was constrained to certain areas: the turbine, turbine housing, nozzles and rings and part but not all of the exhaust pipe. It would be conceivable that one part, the turbine for instance, was made of a steel which was contaminated with a micro-constituent that then dissolved in the ammonia-water working fluid. It is inconceivable that all of the turbine section was made of contaminated steel but nothing else in the plant.

- The hypothesis also fails to explain why only part of the exhaust pipe lost material while the remainder formed a scale.

7.2.3 Galvanic corrosion

In the turbine housing there were nickel plated nuts and later 316 stainless steel nuts as well as the spacer ring that could have formed galvanic couples with the mild steel. Furthermore it is known that the same type of steel can form a galvanic couple with itself (Ahmed, 2006) if one piece had a passivating film while the other did not. It was observed that the surface leading up to the turbine inlet and away from the turbine exhaust did have a film. Polarization measurements could be made as in (Yin, Yan, Bai, Zhao, & Zhou, 2008) with different couples being compared.

It is concluded that galvanic corrosion was present in the turbine housing but not the fundamental cause of material failure.

- In the examination of the 316 stainless steel spacer ring (sample 2) it was shown that corrosion products were present on the surface of the ring. The corrosion products came from the nozzle vanes, which were made of mild steel. Mild steel is anodic to stainless steel, therefore a galvanic couple existed.
- In the theory section describing the corrosion of nickel, the possibility of forming hexamine nickel (II) in ammonia was discussed. The nickel plating on the turbine nuts did not appear to have corroded or dissolved by complexing with ammonia. It was therefore protected by a galvanic couple with the mild steel.
- Though galvanic corrosion was undoubtedly present, the extent of corrosion was over a large area – much of it remote from the nickel and stainless steel pieces and the material loss was very uniform. Therefore though galvanic corrosion was present it was not a major cause of failure.

7.2.4 Crevice corrosion

Crevice corrosion is generally associated with concentration cells. Often oxygen concentration cells but no oxygen or very little oxygen should have been present in the system. Also, these sorts of cells have been observed to become acidic at the heads but the working fluid had a pH greater than 12. Examination of the retainment ring (sample 3) showed unmistakable crevice and filafom corrosion; therefore though the mechanism of the corrosion cell is unresolved, crevice corrosion was present in the turbine.

It is concluded that while crevice corrosion was present in the turbine it was not a significant cause of failure.

- Most of the corrosion occurred not in crevices but on the exposed faces of the turbine housing, turbine wheel, nozzle vanes, rings and the exhaust pipe.
- The examples of crevice corrosion found on the retaining ring had a comparatively small amount of corrosion products nearby, in comparison to the amount of material that appeared to have been removed.

7.2.5 Erosion-corrosion

It has been shown in this thesis that the channels in the stainless steel spacer ring (sample 2) were most likely caused by erosion due to high flow velocity and possibly liquid entrainment. By the turbine exhaust 5-7% of the mass is in the liquid phase. Erosion by the entrained liquid could remove the passive film leading to further corrosion. It is difficult to test this hypothesis directly but a study could be made of two-phase flow and a computational fluid dynamics study could be carried out to see if turbulent flow or vorticity could account for loss of material outside the direct path of flow (the back of sample 3 for instance).

It is concluded that erosion might play a significant role in material loss.

- Pure erosion in the absence of corrosion has been observed on both the 316 stainless steel spacer ring of the KK & K turbine and on the nozzle vanes of the GE-R turbine, therefore some level of erosion is present in the system.
- Two phase flow might explain why material loss occurs only in the first part of the turbine exhaust. Possibly the vapor moves swiftly enough through the turbine to keep a significant part of the liquid entrained, but as it passed through the exhaust pipe, the liquid hit the pipe wall, at first eroding it but as more and more liquid hit the wall forming a protective annulus of flow.
- Two phase flow does not explain the loss of corrosion products at the protected crevice corrosion sites.

7.2.6 Uniform corrosion

The potential-pH diagram for iron (Figure 7) shows that at sufficiently high pH, as might be present in a system with ~20 M ammonia in water, there is a region of corrosion potential in which soluble corrosion products form ($HFeO_2^-$). This would explain the uniform material losses. This could be tested by directly measuring the pH and using linear polarization to measure the potential.

It is concluded that uniform corrosion might be the cause of failures in the turbine section.

- Soluble corrosion products would explain the loss of material from the crevice corrosion sites (sample 3) and from the test cylinder put into the turbine exhaust (sample 4).
- There is no explanation for why the pH and potential would favor soluble corrosion products in only the turbine section and not elsewhere in the plant. In particular the change from material loss to scale formation in the exhaust pipe seems unexplainable by this hypothesis

7.3 Materials selection for Kalina cycle plants

- In the newer GE-Rotoflow turbine there were no observed problems associated with corrosion of the turbine, nozzle vanes or housing. Therefore it is suggested that 304 stainless steel, duplex steel (the pin from sample 1), Nitronic 60 and titanium are all suitable materials. Further it was shown in the thesis that the 316 stainless steel spacer ring was damaged by erosion but not corrosion, so this material is also recommended.
- The erosion on the spacer ring shows that not only must the appropriate materials be used but flow velocity and erosion must also be taken into account in the turbine design.

7.4 Further Research

Two hypotheses have been presented for the observed material loss from the turbine section of the Húsavík Kalina cycle power plant when it was running a KK & K turbine made of mild steel. Neither hypothesis completely explains all the observations. Testing the pH of the fluid and polarization testing the steel would substantiate the hypothesis of uniform corrosion and these tests should be carried out in the future.

8 BIBLIOGRAPHY

Agency for toxic substance and disease registry. (n.d.). *4. Chemical and Physical Information.* Retrieved February 7, 2009, from Agency for toxis substance and disease registry: http://www.atsdr.cdc.gov/toxprofiles/tp126-c4.pdf

Agrawal, A. K., & al., e. (1994). *Patent No. 5,342,578.* USA.

Ahmed, Z. (2006). *Principles of Corrosion Engineering and Corrosion Control.* Oxford: Elsevier.

Ásgeirsson, S. D. (2008, October 14). Húsavík Power Plant Corrosion and Erosion Experience. (P. Whittaker, Interviewer)

Birk, J. P. (2001, December 4). *Iron*. Retrieved February 18, 2009, from General Chemistry with Qualitative Analysis: http://www.public.asu.edu/~jpbirk/qual/qualanal/iron.html

Chen, C. C., Chen, J. H., Chao, C. C., & Say, W. C. (2005). Electrochemical characteristics of surface of titanium formed by electrolytic polishing and anodizing. *Journal of Materials Science vol. 40* , 4053-4059.

Chumbley, P. S. (n.d.). *Scanning Electron Microscopy*. Retrieved January 23, 2009, from Iowa State University Materials Science and Engineering Department: http://mse.iastate.edu/microscopy/home.html

Electron Guns. (2000). Retrieved January 23, 2009, from University of Liverpool - Matter: http://www.matter.org.uk/tem/electron_gun/electron_sources.htm

Georgsson, L. S., Sæmundsson, K., & Hjartarson, H. (2005, April). *Exploration and Development of the Hveravellir Geothermal Field, N-Iceland.* Retrieved January 3, 2009, from Orkuveita Húsavíkur: http://www.oh.is/skrar/File/Skyrslur_og_greinar/Enskar/Exploration_and_Development_of_the_Hveravellir_Geothermal_Field_NIceland.pdf

Grabke, H. J., Muller-Lorenz, E. M., Straus, S., & al, e. (1998). Effects of Grain Size, Cold Working, and Surface Finish on Metal-Dusting Resistance of Steels. *Oxidation of Metals, Vol. 50, Nos. 314* , 241 - 253.

Hjartarson, H. (2002, June 10). *Multiple-use of geothermal energy in Húsavík.* Retrieved January 3, 2009, from Orkuveita Húsavíkur: http://www.oh.is/skrar/File/Skyrslur_og_greinar/Enskar/Multiple_use_of_geothermal_energy_in_Husavik.pdf

Hjartarson, H., Maack, R., & Jóhannesson, S. (2003, September 14). *Húsavík Energy Multiple use of geothermal energy.* Retrieved January 3, 2009, from Orkuveita Húsavíkur: http://www.oh.is/skrar/File/Skyrslur_og_greinar/Enskar/OH_energy_multiple_use_grein_f_radstefnu.pdf

Ibrahim, O. M. (1996). Design Considerations for Ammonia-Water Rankine Cycle. *Energy* , 835-841.

IMOA. (2001). *Duplex Stainless Steel*. Retrieved January 31, 2009, from International Molybdenum Association: http://www.imoa.info/moly_uses/moly_grade_stainless_steels/duplex_stainless_steel.html

Kruger, J. (2001, April). *Electrochemistry of Corrosion*. Retrieved February 18, 2009, from Electrochemistry Encyclopedia: http://electrochem.cwru.edu/ed/encycl/art-c02-corrosion.htm

Liu, F., Tang, J. E., Jonsson, T., & al, e. (2006). Microstructural Investigation of Protective and Non-Protective Oxides on 11% Chromium Steel. *Oxidation of Metals, Vol 66, Nos. 5/6* , 295 - 319.

Liverpool, E. A. (n.d.). *aluSelect Alloy Composition Details*. Retrieved January 29, 2009, from Matter.org.uk: http://aluminium.matter.org.uk/aluselect/06_composition_browse.asp

Making X-rays. (2000). Retrieved January 23, 2009, from University of Colorado, Department of Physics: http://www.colorado.edu/physics/2000/xray/making_xrays.html

Mansfield, F. B., & Sun, Z. (2001). *Patent No. WO/2001/029285.* World Intellectual Property Organisation.

Maxwell, G. R. (2005). *Synthetic Nitrogen Products.* New York: Kluwer Academic Publishers.

Ögmundsson, L. B. (2003). *Húsavík Stray Current Investigation.* Unpublished.

Roberge, P. R. (n.d.). *Aluminum E-pH diagram*. Retrieved February 18, 2009, from Corrosion Doctors: http://corrosion-doctors.org/Corrosion-Thermodynamics/Potential-pH-diagram-aluminum.htm

Roberge, P. R. (2008). *Corrosion Engineering - Principles and Practice.* New York: McGraw-Hill.

Secondary Electrons. (n.d.). Retrieved January 2009, 2009, from The University of Michigan Electron Microbeam Analysis Laboratory: http://www.emal.engin.umich.edu/courses/semlectures/se1.html

Shaik, H., Rao, R. V., George, R. P., Anita, T., & Katack, H. S. (2003). Corrosion Failures of AISI type 304 Stainless Steel in a Fertilizer Plant. *Engineering Failure Analysis vol. 10, no. 3* , 329-339.

Siemens. (2004). *Húsavík Inspection Report.* Unpublished.

Sivaprasad, S., Narang, S. K., & Singh, R. (2006). Failure of high pressure ammonia line in a fertilizer plant - A case study. *Engineering Failure Analysis vol. 13, no. 6* , 867-875.

Srinophakun, T., Laowithayangkul, S., & Ishida, M. (2000). Simulation of Power Cycle with Energy Utilization Diagram. *Energy Conversion and Management* , 1437 - 1456.

Sueptitz, R., Koza, J., Uhlemann, M., Gebert, A., & Shultz, L. (2008). Magnetic field effect on the anodic behavior of a ferromagnetic electrode in acidic solutions. *Electrochimica Acta* , In press.

Sukumaran Nair, M. P. (2001). Control corrosion factors in ammonia and urea plants. *Hydrocarbon Processing* , January issue 85-100.

Talbot, J., & Talbot, D. (1998). *Corrosion Science and Technology.* Boca Raton: CRC Press.

The Columbia Encyclopedia, Sixth Edition. (2008). New York: Columbia University Press.

Valdimarsson, P. (2009, February 11). Personal Communication. *Unpublished* . Akureyri, Iceland.

Wall, G., Chuang, C.-C., & Ishida, M. (1989). Exergy Study of the Kalina Cycle. *Analysis and Design of Energy Systems: Analysis of Industrial Processes* (pp. 73-77). New York: American Society of Mechanical Engineers.

Wittke, J. H. (2006, January 18). *Moseley's Law*. Retrieved January 23, 2009, from Northern Arizona University, Department of Geology: http://www4.nau.edu/microanalysis/microprobe/xray-moseleyslaw.html

Yin, Z. F., Yan, M. L., Bai, Z. Q., Zhao, W. Z., & Zhou, W. J. (2008). Galvanic corrosion associated with SM 80SS steel and Ni-bassed alloy G3 couples in NaCl solution. *Electrochimica Acta* , 6285-6292.